Enhanced Diffusion in Latex Films Induced by Oligomers and Characterized by Pyrene Excimer Fluorescence

by

Zehou You

A thesis

presented to the University of Waterloo

in fulfilment of the

thesis requirement for the degree of

Master of Science

in

Chemistry

Waterloo, Ontario, Canada 2019

© Zehou You 2019

Author's Declaration

I hereby declare that I am the sole author of this thesis. This is a true copy of the thesis, including any required final revisions, as accepted by my examiners.

I understand that my thesis may be made electronically available to the public.

Abstract

Pyrene excimer fluorescence (PEF) was used to investigate the effects that the presence of low molecular weight oligo(*n*-butyl methacrylate) (OBMA) have on the diffusion of high molecular weight poly(*n*-butyl methacrylate) (PBMA) in latex films. In this project, a high molecular weight PBMA latex labeled with 1.9 mol% pyrene (Py-PBMA, M_w = 410 kg/mol, PDI = 2.0) was mixed with nine non-fluorescent latex particles which needed to be prepared. Among these nine particles, two unlabeled latexes (M_w = 360 kg/mol, PDI = 1.8 and M_w = 420 kg/mol, PDI = 1.9) were prepared without oligomers. Their molecular weight distribution (MWD) was slightly different from that of Py-PBMA. Four latex dispersions that incorporated four different weight fractions of an OBMA with an M_n of 3.0 kg/mol were prepared from a PBMA seed latex, whose MWD (M_w = 350 kg/mol, PDI = 1.9) was close to one of the unlabeled latex particles prepared without OBMA. Three more latex dispersions with three weight fractions of OBMAs with an M_n of 5.0 kg/mol were prepared from a PBMA seed latex, whose MWD (M_w = 460 kg/mol, PDI = 2.4) was similar to the other unlabeled latex polymerized without OBMA.

Several blends of latex particles constituted of 5 wt% of Py-PBMA and 95 wt% of the non-fluorescent PBMA latex with or without oligomers were prepared and latex films were cast from these mixtures. The films were annealed at different temperatures and the fluorescence spectra of the films were acquired as a function of annealing time. They were analyzed to retrieve the fraction of mixing (f_m), representing the molar fraction of Py-PBMA chains having diffused out of the Py-PBMA latex. In turn, the diffusion coefficients reflecting the diffusion of the polymer chains during film annealing were calculated from the f_m values at each temperature and for different annealing times. Diffusion of the Py-

PBMA chains was much enhanced upon mixing the Py-PBMA latex with the PBMA latex that contained a larger weight fraction of a same OBMA or a shorter OBMA at a same weight fraction. Master curves of the diffusion coefficient as a function of f_m could be generated by determining the shift factors (a_T). A plot of $Ln(a_T)$-*vs*-$1/T$ yielded the activation energy for the diffusion of the Py-PBMA chains, which was found to equal 163 ± 9 kJ/mol, regardless of the OBMA content or chain length. The efficiency (β) of OBMA as a plasticizer was determined as a function of oligomer length using the Fujita-Doolittle model. In addition, the temperature dependence of the efficiency was studied. The results showed that the plasticizer efficiency of the 3.0 kg/mol oligomer was larger than that of the 5.0 kg/mol at all temperatures studied, but that the difference in plasticizer efficiency between the two oligomers decreased for decreasing temperatures. The higher plasticizer efficiency of the 3.0 kg/mol oligomer was confirmed from a plot of T_g as a function of oligomer weight fraction, showing that T_g decreased more markedly with the 3.0 rather than the 5.0 kg/mol oligomer.

In summary, this project further demonstrated the validity and robustness of the procedure based on pyrene excimer formation (PEF) to probe polymer chain diffusion in latex films.

Acknowledgements

First, I would like to thank my supervisor, Prof. Jean Duhamel, for giving me the opportunity to work on this project. I also want to thank him for creating and maintaining a friendly lab environment that allowed me to grow into a skilled researcher. Next, I would like to thank my committee members Prof. Mario Gauthier and Prof. Alexander Penlidis for reviewing my thesis and sharing their constructive advice. Then, I would like to thank graduate student Remi Casier in our group for providing pyrene-labeled latex particles and guiding me patiently when I was a beginner. I would like to thank my best friend Weize Yuan for giving me continuous support and suggestions for my research and pulling me through the hard times. I would like to thank other members in the Duhamel and Gauthier's groups for their kind help when I met troubles. I would like to thank my family for supporting me financially and mentally. At last, I would like to thank NSERC for funding.

Table of Contents

Lists of Figures

Lists of Tables

Lists of Schemes

Abbreviations

a.u.	Arbitrary units
Abs	Absorbance
$[Acc]_{loc}$	Local acceptor concentration
a_{oligo}	Shift factor with respect to weight fraction of oligomer
AOT	Sodium dioctyl sulfosuccinate
APS	Ammonium persulfate
a_T	Shift factor with respect to temperature
B_1	Molar fraction of donors that undergo FRET
B_2	Molar fraction of donors that dos not undergo FRET
BMA	*n*-Butyl methacrylate
C	Concentration
C_{XA}	Chain transfer constant
D	Apparent diffusion coefficient
D_0	Apparent diffusion coefficient at a reference temperature
D_h	Hydrodynamic diameter
DIW	Deionized water
DLS	Dynamic light scattering
DRI	Differential refractive index
DSC	Differential scanning calorimetry
E_a	Activation energy
f	Fraction of free volume
Φ_{ET}	Energy transfer efficiency

f_m	Fraction of mixing
f_{Py}	Molar fraction of pyrene
FRET	Fluorescence resonance energy transfer
$f_{w,o}$	Weight fraction of oligomer
GPC	Gel permeation chromatography
I_1	Fluorescence intensity of the first peak
I_2	Fluorescence intensity of the second peak
I_3	Fluorescence intensity of the third peak
I_4	Fluorescence intensity of the fourth peak
I_E	Fluorescence intensity of the excimer
I_M	Fluorescence intensity of the monomer
IOMPA	Isooctyl ester of mercaptopropionic acid
IPD	Interparticle polymer diffusion
K	Kilograms per mole or Kelvin
kD	Kilodalton
l	Pathlength
LALS	Low-angle light scattering
M	Monomer
m	Massic polymer concentration
M_0	Molar mass of the structural unit
M_{BMA}	Molar mass of *n*-butyl methacrylate
MC	Master curve
m_d	Mobility of the diluent molecules

MFT	Minimum film formation temperature
M_n	Number-average molecular weight
M_{PyLM}	Molar mass of 1-pyrenebutyl methacrylate monomer
M_w	Weight-average molecular weight
MWD	Molecular weight distribution
NaOH	Sodium hydroxide
OBMA	Oligo(*n*-butyl methacrylate)
P	Parameter proportional to the local acceptor concentration
p	Intercept of master curves
PBMA	Poly(*n*-butyl methacrylate)
PDI	Polydispersity index
PEF	Pyrene excimer fluorescence
Py	Pyrene
$[Py_{inter}]_{loc}$	Local pyrene concentration (excimer is formed intermolecularly)
$[Py_{intra}]_{loc}$	Local pyrene concentration (excimer is formed intramolecularly)
PyLLPs	Pyrene-labeled latex particles
r	Distance between an arbitrary point and the center of the particle
R	Ideal gas constant
RALS	Right-angle light scattering
R_L	Radius of latex particles
R_S	Radius of a spherical particle
SSF	Steady-state fluorescence
T_0	Reference temperature

t_{an}	Annealing time
T_g	Glass transition temperature
THF	Tetrahydrofuran
UV-Vis	UV-Vis spectrophotometer
VOC	Volatile organic compound
X_0	Number-average degree of polymerization without chain transfer agent
XA	Chain transfer agent
X_n	Number-average degree of polymerization
β	Plasticizer efficiency
ε	Molar extinction coefficient
η	Viscosity
λ_{Py}	Pyrene content
τ_D	Lifetime of donor
φ	Volume fraction of oligomer

Chapter 1 – Introduction

1.1 Background

Over the past decades, polymer latex films have played a critical industrial role due to their applications in a wide variety of commercial products and their exceptional performance. For instance, they are used as varnishes or paints to decorate houses, coatings to protect surfaces, or binders or adhesives to bind wood or leather together.[1,2] Since latex films have a large number of applications, they have been the focus of intense research to improve latex film performance. Previous studies have established that latex film formation proceeds in three main steps.[1-8] The first step after applying the latex dispersion onto a surface is the evaporation of water, which enables the latex particles to come in close contact with each other, generating voids between the particles. The second step corresponds to the deformation of the close-packed latex particles. It takes place when the film is held above the minimum film formation temperature (MFT), which is close to or slightly above the glass transition temperature of the polymer. The polymer chains are mobile when the temperature is above the MFT,[4] which allows the deformation of the latex particles into a honeycomb shape, resulting in the disappearance of the voids. The third step involves particle coalescence, where the polymer chains diffuse across the particle boundaries into neighboring particles in a process that generates a homogeneous film. All these processes are illustrated in Figure 1.1.

During film formation, the extent of particle coalescence is associated with latex performance, and it is quantified by the fraction of mixing (f_m), which is a crucial parameter to understand and predict film behavior. For example, a film that is only used for decoration

purposes, like the paint on a wall, does not need to fully coalesce, and its f_m value can be relatively low. However, a film being used for protection must be as homogeneous as possible. Otherwise small molecules such as water, acids, and oxygen can pass through the film, and the film will lose its protective properties.[6]

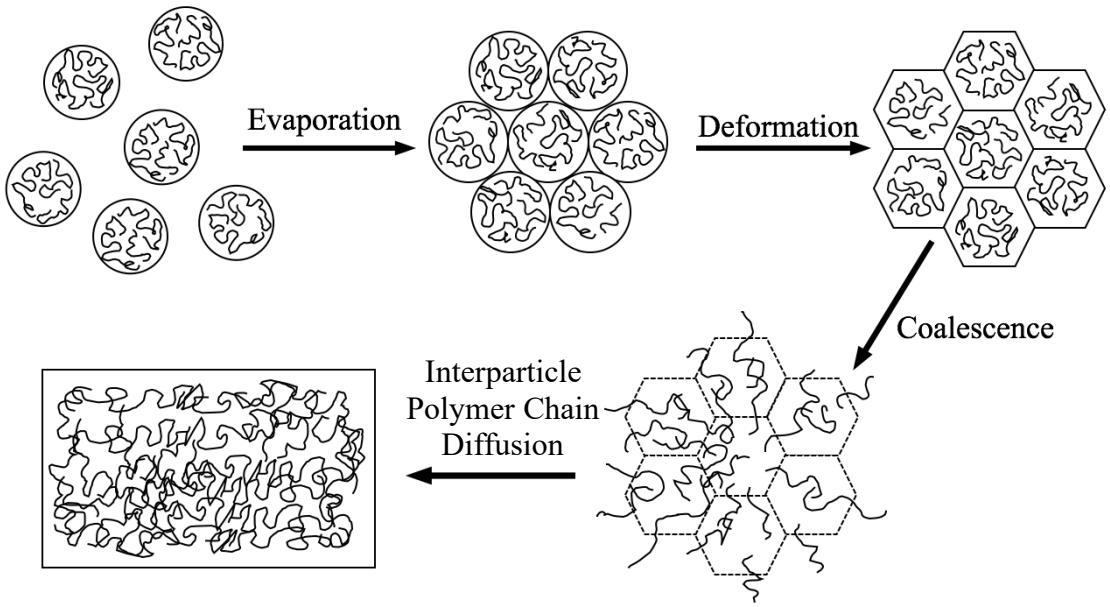

Figure 1.1. Processes involved during film formation.

1.2 Use of a Plasticizer to Promote Film Formation

The importance of particle coalescence to latex performance during film formation led to the implementation of practical procedures that would improve the latex film properties. One of them was the use of a plasticizer. To this end, researchers incorporated a number of coalescing agents into latex films to ease film formation.[7-11] The main goal of a plasticizer is to lower the glass transition temperature (T_g) by creating free volume in the latex film. After the incorporation of plasticizer, the intermolecular interactions are affected by the free volume introduced by the plasticizer at the molecular level. As a result, the monomeric friction coefficient amongst polymer chains decreases, leading to smoother reptation and

therefore an acceleration of the diffusion of polymer chains.[8,9,11] Traditional plasticizers used to be volatile organic compounds (VOCs). Plasticizers soften the latex particles, facilitating their deformation from spherical to a void-free honeycomb structure, and their final coalescence into a homogeneous film.

Unfortunately, evaporation of the plasticizers as VOCs into the atmosphere turns them into airborne contaminants, promoting ground-level ozone formation and contributing to global warming.[10] Therefore, they are environmentally unfriendly and harmful to human health. Their replacement, triggered by governmental regulations demanding a reduction in VOC emissions, required the implementation of new procedures. One of them consisted in adding low molecular weight oligomers to promote interparticle polymer chain diffusion (IPCD).[6,10] To this end, researchers prepared seed particles with a high molecular weight polymer first, and then incorporated low molecular weight oligomers into the particles, forming larger seed-oligomer particles. Taking advantage of the increase in free volume associated with polymer chain ends, a film formed with seed-oligomer particles had more free volume as compared to a film prepared with seed latex particles without oligomers. Consequently, the T_g for the seed-oligomer latex particles was lower than that of the seed latex particles, thus reducing the MFT and enabling the formation of a film with homogeneously distributed polymer chains more quickly upon annealing (Figure 1.2).

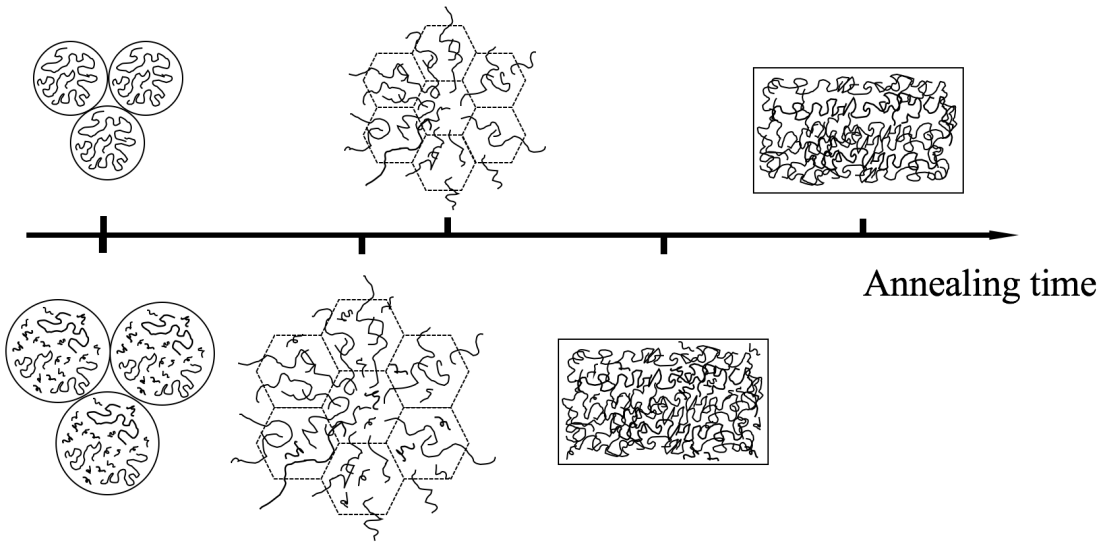

Figure 1.2. Schematic representation of the formation of a film prepared from seed (top) or seed-oligomer (bottom) latex particles

1.3 Methods for Probing Interparticle Polymer Chain Diffusion (IPCD)

1.3.1 Probing IPCD using FRET

Winnik and co-workers have demonstrated that fluorescence resonance energy transfer or FRET is a powerful method to probe IPCD during film formation.[2-5,7,8,10-13] In a FRET experiment, two latex particles are labeled with two different fluorescent dyes, one particle with an energy donor, and the other particle with an energy acceptor. When the donor becomes excited upon absorption of photons and is within a few nanometers of an acceptor, the excess energy of the excited donor is transferred to the acceptor through dipole-dipole interactions in a non-radiative manner. The Winnik Group prepared films made from a latex mixture containing 10 wt% of donor-labeled particles and 90 wt% of acceptor-labeled particles.[10] Before the latex particles deformed and the polymer chains diffused, FRET was relatively weak since it only occurred at the boundary between particles, and the donor

emitted mainly with its natural lifetime τ_D. Upon film annealing, the polymer chains diffused in the films taking along the fluorescence donors and acceptors which were brought closer to each other. As a result, FRET happened more effectively, resulting in faster decay of the donors. The fluorescence decays of the donor could be fitted to Equation 1.1,[8]

$$[D^*]_{(t)} = [D^*]_o \left\{ B_1 \exp\left[-t/\tau_D - P(t/\tau_D)^{1/2} \right] + B_2 \exp(-t/\tau_D) \right\} \quad (1.1)$$

where B_1 represents the molar fraction of donors that undergo FRET, B_2 is the molar fraction of donors that do not undergo FRET, and P is proportional to the local acceptor concentration.

Figure 1.3 illustrates the change in the decay of the donors acquired at different times (t_{an}) during film annealing.[7] Before annealing, the area under the decay curve ($Area(t_{an}=0)$) was the largest since little energy transfer occurred, and $Area(t_{an}=0)$ approached τ_D. As annealing proceeded, the area decreased due to more efficient FRET. Upon full annealing, when a homogeneous film was obtained, the area reached its minimum value.

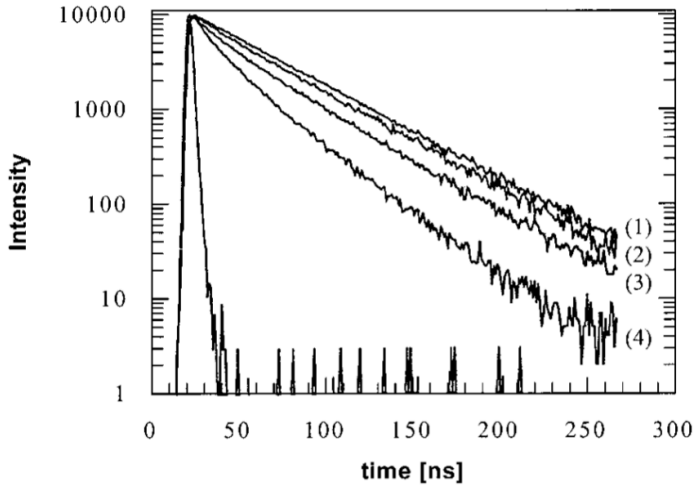

Figure 1.3. Fluorescence decay curves for the donor (1) before annealing and after annealing at 76°C for (2) 30 min, (3) 1000 min, and (4) infinite time, corresponding to a homogeneous film.

After fitting the decays with Equation 1.1, the energy transfer efficiency Φ_{ET} (t_{an}) at a specific annealing time t_{an} was determined from the area ($Area(t_{an})$) under the decay curve as shown in Equation 1.2.[9]

$$\Phi_{ET} = 1 - \frac{Area(t_{an})}{\tau_D} \tag{1.2}$$

Finally, the fraction of mixing at a given annealing time f_m (t_{an}) could be calculated with Equation 1.3, since the area under the curve was proportional to the efficiency of energy transfer.

$$f_m(t_{an}) = \frac{Area(t_{an}) - Area(0)}{Area(\infty) - Area(0)} = \frac{\Phi_{ET}(t_{an}) - \Phi_{ET}(0)}{\Phi_{ET}(\infty) - \Phi_{ET}(0)} \quad (1.3)$$

Equation 1.3 combines the areas under the decay curves acquired at $t_{an} = 0$ before annealing, at intermediate times (t_{an}) during annealing, and at infinite time ($t_{an} = \infty$), when the latex polymer chains are thoroughly mixed in the film.

Although FRET is a powerful method to probe IPCD, it has some drawbacks. First, FRET requires that all the latex particles constituting the film be fluorescently labeled, which precludes its usage to study unlabeled raw latex particles prepared in an industry setting. Second, the acquisition of the fluorescence decays for the FRET donor requires the use of a more specialized time-resolved fluorometer, in comparison to a simpler steady-state fluorometer. Third, the fluorescence decays must be analyzed with a proper model such as the one resulting in Equation 1.1. Fourth, the analysis of the FRET data is complicated by the strong dependence of the FRET efficiency on the sixth power of the distance between each donor and acceptor pair.[12] As a result, the efficiency of energy transfer is not directly proportional to the acceptor concentration in the film, which implies that Equation 1.3 is only an approximation for $f_m(t_{an})$, whose analysis only yields relative diffusion coefficients. Absolute diffusion coefficients can be obtained through Monte-Carlo simulations to generate a distribution of donors and acceptors and finding the distribution of dyes that would yield a theoretical fluorescence decay that would best match the experimental decay. In turn, changes in the distribution of dyes, and thus the FRET efficiency, are related to the diffusion coefficient of the polymer chains in the film, which can be extracted from this analysis. Based on the above, it can be argued that FRET is a powerful method to probe IPCD during film formation, but that its implementation is

mathematically challenging.

1.3.2 Probing IPCD using PEF

A new research venue for probing film formation was introduced two years ago by Casier et al., who first demonstrated that pyrene excimer fluorescence/formation (PEF) could probe polymer diffusion in latex films successfully.[6] The different photophysical processes involved in PEF are shown in Scheme 1 and the resulting fluorescence spectrum is presented in Figure 1.4. Upon absorption of a photon, a ground-state pyrene can become excited. That excited pyrene can either decay to the ground-state through monomer emission, or form an excimer by interacting with another ground-state pyrene monomer. PEF can be measured with a steady-state fluorometer, and the resulting fluorescence spectrum expected for a pyrene-labeled polymer is shown in Figure 1.4. The pyrene monomer emission can be easily identified from its four fluorescence peaks referred to as I_1, I_2, I_3, and I_4 in Figure 1.4, located between 370 and 400 nm. The excimer fluorescence between 400 and 600 nm appears as a broad structureless emission centered at 480 nm in the spectrum. From the fluorescence spectrum, two critical intensities are obtained, namely the monomer (I_M) and excimer (I_E) fluorescence intensity. The former can be calculated by taking the area under the spectrum between 392 and 398 nm, and the latter is obtained from the area under the curve from 500 nm to 530 nm.

$$\mathrm{Py+Py+}h\nu \rightarrow \mathrm{Py^*+Py} \rightarrow \mathrm{(PyPy)^*} \leftarrow \mathrm{(PyPy)+}h\nu$$

$$\downarrow 1/\tau_M \qquad \downarrow 1/\tau_E$$

Scheme 1. Kinetic Scheme Representing Pyrene Excimer Formation.

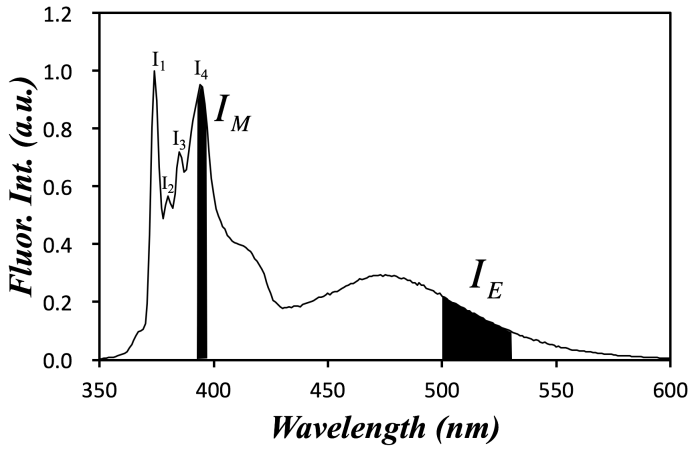

Figure 1.4. Fluorescence spectrum for a pyrene-labeled polymer.

The procedure using PEF to probe IPCD during latex film formation requires that the polymer chains of one latex be randomly labeled with pyrene to yield pyrene-labeled latex particles (PyLLPs). A dispersion is then generated with 5 wt% of PyLLPs and 95 wt% of unlabeled latex particles. The latex mixture is applied to prepare a latex film where the latex particles pack themselves against each other by adopting a honeycomb structure as shown in Figure 1.5.[6] Initially, the PyLLPs are surrounded by many non-labeled latex particles that are present in excess.

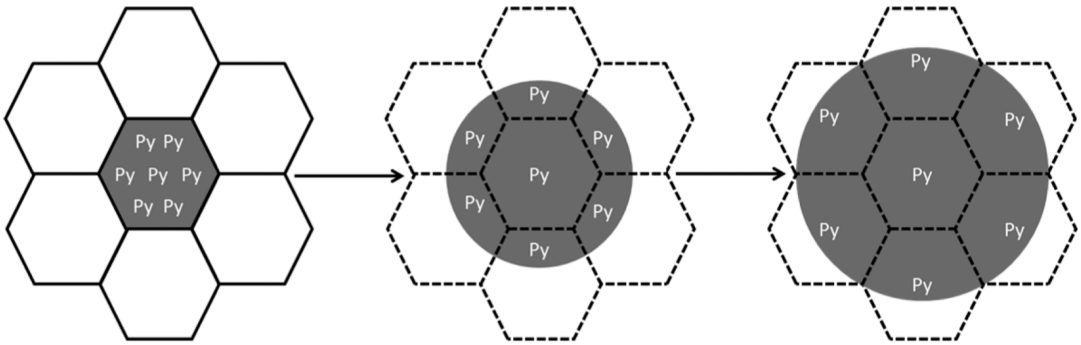

Figure 1.5. Illustration of the change in the local pyrene concentration during latex film formation.[6]

Upon annealing the film, the polymer chains bearing the pyrene labels diffuse out of the PyLLPs, resulting in a decrease in the local pyrene concentration. The formation of pyrene dimers yielding pyrene excimer fluorescence (PEF) is controlled by the equilibrium described in Scheme 2. According to this equilibrium, the concentration ratio of pyrene labels involved in the formation of pyrene dimers over that of pyrene monomers, namely the ratio $[(PyPy)^*]/[Py^*]$, is equal to the product $K\times[Py]$. Based on this relationship, the ratio of the fluorescence intensity of the excimer (I_E) over that of the monomer (I_M), namely the fluorescence intensity ratio (I_E/I_M), is directly proportional to the local concentration ($[Py]_{loc}$) of the ground-state pyrene monomer averaged over the film, as shown in Equation 1.4 where k is a proportionality constant.

$$Py + Py \underset{}{\overset{K}{\rightleftharpoons}} PyPy$$

Scheme 2. Equilibrium controlling pyrene excimer formation in the solid state.

$$\frac{I_E}{I_M} = k \times K[Py] = k \times \frac{[(PyPy)]}{[Py]} = k \times \frac{[(PyPy)^*]}{[Py^*]} \qquad (1.4)$$

The direct proportionality between the I_E/I_M ratio and $[Py]_{loc}$ illustrated by Equation 1.4 offers researchers an opportunity to probe the magnitude of IPCD in a latex film, by analyzing the fluorescence intensity ratio I_E/I_M obtained by steady-state fluorescence. In this case, $[Py]_{loc}$ can be divided into two parts, depending on whether the excimer is formed intra- ($[Py_{intra}]_{loc}$) or inter- ($[Py_{inter}]_{loc}$) molecularly as shown in Equation 1.5.[6]

$$\left(\frac{I_E}{I_M}\right)_{(t_{an})} = k \times \{[Py_{intra}]_{loc} + [Py_{inter}]_{loc}\} \tag{1.5}$$

During film annealing, the diffusion of the pyrene-labeled polymer chains out of the PyLLPs reduces $[Py_{inter}]_{loc}$, the equilibrium in Scheme 2 shifts to the left, and $(I_E/I_M)(t)$ decreases toward its minimum value ($(I_E/I_M)(t \to \infty)$) as shown in Equation 1.6. At that point, all the pyrene-labeled chains have diffused out of the PyLLPs and are embedded in a polymer matrix constituted of mainly unlabeled polymers, resulting in $[Py_{inter}]_{loc}$ being equal to zero. We note that at infinite annealing times, the ratio $(I_E/I_M)(t \to \infty)$ cannot equal zero despite the large excess of unlabeled chains, due to the non-zero $[Py_{intra}]_{loc}$ generated by the pyrene labels on a single polymer chain.

$$\left(\frac{I_E}{I_M}\right)_{(t_{an} \to \infty)} = k \times [Py_{intra}]_{loc} > 0 \tag{1.6}$$

Combining Equations 1.5 and 1.6 provides a mathematical means to calculate $[Py_{inter}]_{loc}$ as shown in Equation 1.7.

$$[Py_{\text{inter}}]_{loc}(t_{an}) = (1/k) \times \left[\left(\frac{I_E}{I_M} \right)_{(t_{an})} - \left(\frac{I_E}{I_M} \right)_{(t_{an} \to \infty)} \right] \tag{1.7}$$

The fraction of mixing (f_m), defined as the relative change of $[Py_{\text{inter}}]_{loc}$ over time with respect to its initial value at time t_{an}=0, can be calculated with Equation 1.8, and can be determined experimentally using Equations 1.6 and 1.7 for the concentrations $[Py_{\text{intra}}]_{loc}$ and $[Py_{\text{inter}}]_{loc}$ as shown in Equation 1.9. Therefore, f_m is obtained experimentally by monitoring the change in the fluorescence intensity ratio I_E/I_M.

$$f_m(t_{an}) = \frac{[Py_{\text{inter}}]_{loc}(t_{an}=0) - [Py_{\text{inter}}]_{loc}(t_{an})}{[Py_{\text{inter}}]_{loc}(t_{an}=0)} \tag{1.8}$$

$$f_m(t_{an}) = \frac{\left(\frac{I_E}{I_M} \right)_{(t_{an}=0)} - \left(\frac{I_E}{I_M} \right)_{(t_{an})}}{\left(\frac{I_E}{I_M} \right)_{(t_{an}=0)} - \left(\frac{I_E}{I_M} \right)_{(t_{an} \to \infty)}} \tag{1.9}$$

As compared to FRET, PEF possesses several advantages. First, PEF can be used to probe IPCD with a non-labeled latex, since 95 wt% of the latex film is constituted of non-labeled latex particles. This feature increases the appeal of a PEF-based approach for the characterization of latex particles produced industrially, since they simply have to be mixed with the PyLLPs.[6] Second, PEF employs a steady-state fluorometer, which is much simpler to operate than a time-resolved fluorometer. Third, the experimental determination of the

I_E/I_M ratios from steady-state fluorescence, a mere fluorescence intensity ratio, to calculate f_m according to Equation 1.9, is more straightforward than the much more complex mathematical treatment required when using FRET. Fourth, since I_E/I_M is directly proportional to the local pyrene concentration, the Monte Carlo simulations required to determine the local acceptor concentration in a FRET experiments are not needed in a PEF experiment.

The difference between the ways f_m is calculated in a PEF or FRET-based approach comes from the very nature of the photophysical processes at play. Because PEF occurs only upon contact in a way similar to an on-off switch, there is no distance dependency on the I_E/I_M ratio, which is directly proportional to $[Py]_{loc}$. In contrast, the FRET efficiency (Φ_{ET}) is a function of the local acceptor concentration ($[Acc]_{loc}$), that is complicated by the 6^{th}-power dependency of the distances separating every donor and acceptor pair. Using Φ_{ET} in Equation 1.3 only yields an approximate value of f_m, which has nevertheless been shown to satisfyingly represent IPCD during latex film formation. Presently, an absolute measure of f_m can be obtained either by applying PEF or by conducting Monte Carlo simulations on the Φ_{ET} values obtained in a FRET study of film formation. Consequently, it can be argued that PEF allows the determination of an absolute f_m value in a simpler manner than FRET.

However, it must be also acknowledged that despite its many advantages, PEF is also plagued by a number of problems. The main problem associated with PEF is that it is restricted to the use of pyrene. Many other dyes such as perylene or naphthalene also form excimer, but pyrene is much superior to other excimer-forming dyes because it forms excimer much more efficiently than naphthalene, and its monomer and excimer fluorescence are much better separated spectroscopically than for perylene. Consequently,

if the polymer matrix interferes with pyrene excimer formation or quenches pyrene emission, PEF cannot be a viable method to probe IPCD of a polymer, and it will be difficult to substitute pyrene with another dye. In this case, FRET, and one of the many dye pairs available for FRET,[13] could be selected to circumvent a given spectroscopic issue that would forbid the use of PEF.

1.4 Diffusion Coefficient (D) Determined from f_m

Once f_m has been determined through PEF or FRET experiments, a Fickian model can be applied to determine the diffusion coefficient of the polymer chains in the film from the f_m values.[2-6,8,10,11] Approximating the PyLLPs as spheres of radius (R_L), which can be determined by dynamic light scattering measurements, Equation 1.10 can be employed to predict the concentration profile ($C(r, t_{an})$) of the pyrene-labeled chains located at a distance r from the center of a PyLLP after annealing the film for a time t_{an}. We note that the $C(r, t_{an})$ profile depends solely on the diffusion coefficient (D), since t_{an} and R_L are known experimentally and C_o, which is the initial concentration of pyrene labels in the PyLLPs, is eliminated in the derivation of f_m.

$$C(r,t_{an})=\frac{C_o}{2}\left[erf\left(\frac{R_L+r}{2\sqrt{Dt_{an}}}\right)+erf\left(\frac{R_L-r}{2\sqrt{Dt_{an}}}\right)\right]-\frac{C_o}{r}\sqrt{\frac{Dt_{an}}{\pi}}\left\{\exp\left[-\frac{(R_L-r)^2}{4Dt_{an}}\right]-\exp\left[-\frac{(R_L+r)^2}{4Dt_{an}}\right]\right\} \quad (1.10)$$

The fraction f_m, representing the fraction of pyrene-labeled chains that still remain in the PyLLP after annealing the film for a time t_{an}, can be calculated by integrating $C(r,t_{an})$, given by Equation 1.10, as shown in Equation 1.11. The optimal D value can be obtained by inputting different D values until f_m calculated with Equation 1.11 matches the f_m value

determined experimentally from the analysis of the fluorescence spectra with Equation 1.9.

$$f_m(t_{an}) = 1 - \frac{\int_o^{R_L} C(r, t_{an}) 4\pi r^2 dr}{\frac{4}{3}\pi R_L^3 C_o} \tag{1.11}$$

1.5 Thesis Outline

The goals of this thesis are two-fold. It will first aim to demonstrate that PEF is a valid and robust experimental technique to probe the IPCD of long polymer chains during latex film formation when oligomers are introduced in the latex particles as non-volatile plasticizers. Second, it will take advantage of the simplicity of PEF to probe the effect that temperature has on the plasticizer efficiency. The PyLLP sample used in this thesis was prepared earlier by Remi Casier, a graduate student in the Duhamel Laboratory. Latex particles were prepared from a latex seed, where the polymer chains had a molecular weight distribution similar to the PyLLPs, in which a small weight fraction of oligomers was introduced. Two different oligomer lengths were used, and four different weight fractions of a same oligomer were introduced into the latex seeds. The synthesis and characterization of the latex particles is discussed in Chapter 2. Chapter 3 describes how the films were prepared and annealed, the I_E/I_M ratios were determined through the analysis of the steady-state fluorescence spectra, and the fraction of mixing and diffusion coefficients were estimated from the I_E/I_M ratios. The activation energy and the plasticizer efficiency of the oligomers were calculated and compared to the results obtained in previous research.[6,10] Finally, Chapter 4 summarizes all the results reached in this thesis and suggests future work.

Chapter 2 – Latex Synthesis and Characterization

2.1 Latex Synthesis

2.1.1 Materials

Deionized water (DIW) was obtained from a Biopure Series 4400 single pass reverse osmosis system. Sodium dioctyl sulfosuccinate (AOT, 98%), sodium hydroxide (NaOH, 97%), ammonium persulfate (APS, 98%), isooctyl ester of mercaptopropionic acid (IOMPA, 99%), and tetrahydrofuran (THF, 99%) were supplied by Sigma-Aldrich and were used as a received, as was the tetrahydrofuran (distilled in glass, inhibitor-free), purchased from Caledon. The hydroquinone inhibitor in *n*-butyl methacrylate (BMA, Sigma-Aldrich, 99%) was removed by mixing BMA thoroughly with an equal volume of 2 mol/L NaOH.

2.1.2 Latex Seed Synthesis

The latex particles were prepared in a three-neck glass reactor equipped with a rotor and a condenser capped with a rubber septum, as shown in Figure 2.1. DIW (116 mL) and the AOT surfactant (104 mg, 0.23 mmol) were added to the reactor, and the reaction mixture was stirred at 550 rpm to dissolve the AOT. The AOT solution was purged with a gentle flow of nitrogen through needle “B” in Figure 2.1 to remove oxygen. After 30 minutes, the nitrogen line was removed from needle “B”, which was capped with an air-tight syringe to withdraw latex samples during the emulsion polymerization. The nitrogen line was switched to a needle inserted into the rubber septum capping the condenser on the other side of the reactor in Figure 2.1, to keep the reaction under nitrogen atmosphere. The 1 mL air-tight plastic syringe capping needle “B” also prevented the solution inside the reactor

from leaking out due to the positive nitrogen pressure. When the temperature inside the reactor had stabilized at 80 ^{o}C, the APS initiator (8.2 mg, 36 μmol) dissolved in 1 mL DIW was introduced into the reactor through needle "A". To ensure that all the APS was added into the reactor, an additional 1 mL of DIW was used to wash the vial, the syringe, and the long needle that contained the APS solution, and this wash was injected into the reactor. Meanwhile, an emulsion of DIW (1 mL), AOT (34.5 mg, 78 μmol), the BMA monomer (3.8 g, 27 mmol), and IOMPA (0.53 mg, 2.6 μmol) was prepared by mixing vigorously on a vortex mixer. This turned the clear phase-separated feed to a milky white viscous liquid. After five minutes the homogeneous mixture was fed to the reactor with a syringe pump through needle "A" over 1.5 hours. After all the feed was loaded into the reactor, an extra 1 mL DIW was passed through the syringe to wash residues left in the syringe. After 10 additional minutes the set up was dismantled and the emulsion was poured out of the reactor through a Whatman #4 filter paper, to filter the seed latex and verify whether a coagulum had formed during the reaction. No coagulum was ever observed in all the reactions conducted for this project.

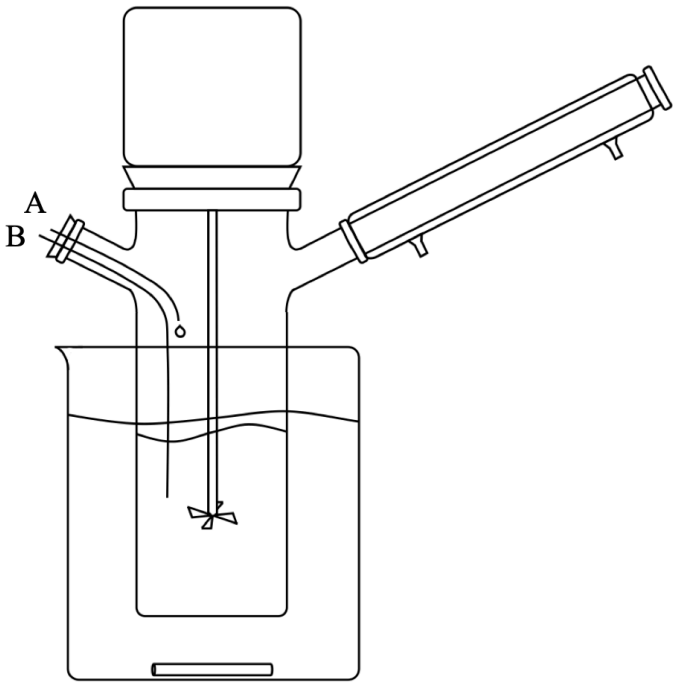

Figure 2.1. Reaction setup for emulsion polymerization

2.1.3 Oligomer Incorporation

After the seed latex had been prepared, a second feed containing the same concentration of BMA, DIW, and AOT, but with a much higher concentration of the chain transfer agent IOMPA, was loaded through needle "A" to synthesize the oligomer. The same synthetic strategy was applied to all oligomers. The incorporation of 3.0 K oligomer is described in detail hereafter. After the synthesis of the seed latex was completed, a glass syringe was connected to needle "B" to extract 1 mL of product. The water was removed by lyophilization, the remaining solids were dissolved in THF and the polymer was characterized by gel permeation chromatography (GPC) analysis to determine the molecular weight of PBMA in the seed latex.

After confirmation that the required molecular weight of the PBMA in the seed latex

had been obtained, APS (4.4 mg, 19 μmol) was introduced into the reactor according to the procedure described in the previous section. After 5 minutes a mixture of DIW (0.4 mL), AOT (15.8 mg, 36 μmol), the BMA monomer (1.73g, 12 mmol), and IOMPA (128 mg, 0.58 mmol), vigorously mixed beforehand, was fed into the reactor with a syringe pump over 30 minutes. During that period, the syringe pump was turned off when 50%, 75%, and 90% of the second monomer feed had been transferred to the reactor. After the pump was turned off, the mixture was allowed to react for 5 minutes, after which a gas-tight glass syringe was used to withdraw ca. 5 mL aliquots from the reactor through needle "B" and transfer them immediately to 7 mL vials. Then, the nitrogen line that was connected to the condenser in Figure 2.1 was transferred to needle "B" to flush the remaining emulsion inside needle "B", at which point needle "B" was capped with a 1 mL air-tight plastic syringe. The nitrogen line was connected back to the condenser. This process was applied three times to withdraw three samples of latex particles containing different weight fractions of oligomer having the same chain length. Ten minutes after the addition of the second monomer feed to the reactor was completed, the syringe was rinsed with 1 mL of DIW. After this was done, the fourth latex sample, containing the highest weight fraction of oligomer, was filtered through Whatman #4 paper to ensure that no coagulum had formed during the reaction. Since no coagulum was observed by the end of the polymerization reaction, it is assumed that all samples were coagulum-free.

2.1.4 Vigorous Mixing of Monomer Feed

Before the aqueous dispersion of monomer, surfactant, and chain transfer agent was fed into the reactor, it was important that it be fully homogenized. A homogeneous monomer

feed was obtained by mixing the dispersion vigorously on a vortex mixer. The vigorous mixing helped the dissolution of AOT, whose solubility limit in water at 25 ^{o}C has been reported to equal 15 g/L or 33 mM. For the seed synthesis, the AOT surfactant (0.23 mmol) was impossible to dissolve in 1 mL water, and the following addition of IOMPA (2.6 μmol) did not help either. However, after adding BMA into the mixture and mixing vigorously for 10 seconds, the feed turned into a milky white viscous liquid and the mixture appeared homogeneous. As described earlier, the feed for preparation of the oligomer required the dissolution of 46 μmol AOT and 0.63 mmol IOMPA in 0.6 mL of DIW. The much lower AOT concentration (77 mM for the oligomer synthesis versus 230 mM for the seed synthesis) made it easier to obtain a homogeneous mixture with AOT. After addition of the monomer the mixture was vigorously shaken on the vortex mixer to obtain a milky viscous homogeneous emulsion, which was fed into the reactor. While oligomers were produced in decent yield, the final weight fraction ($f_{w,o}$) of oligomer was always lower than theoretically expected because the feed was too viscous and adhered to the walls of the vials where it had been prepared, resulting in less liquid being actually transferred to the syringe. Consequently, to obtain a $f_{w,o}$ value of 0.27 necessary for the experiments, a larger quantity of feed needed to be added to the reaction mixture to generate the oligomer emulsion. It must also be pointed out that manually shaking the monomer feed yielded an unstable mixture that would phase separate within seconds, resulting in drifting in the molecular weight distribution of the oligomer as a function of the polymerization time.

2.2 Latex Characterization

2.2.1 Instrumentation

Steady-State Fluorescence (SSF): All the fluorescence spectra were obtained with a

steady-state fluorometer from Photon Technology International. Films were cast on a quartz plate mounted on a front-face geometry holder, where the angle between the excitation beam and the quartz plate was adjusted to 160 ° to minimize stray light from reaching the detector. The excitation wavelength was set to 344 nm, and the emission wavelength was scanned at a rate of 10 nm/s from 350 to 600 nm in 1 nm increments. The excitation and emission slit widths were set to 0.6 and 0.5 nm. The fluorescence intensity of the excimer (I_E) was calculated by taking the area under the spectrum from 500 to 530 nm, and the fluorescence intensity of the monomer (I_M) was determined from the area under the 4th peak in the monomer fluorescence spectrum, by integrating the fluorescence intensity 3 nm before and after the 4th peak maximum located at 394 or 395 nm, depending on the fluorescence spectrum.

Lyophilizer: Aqueous latex dispersions (0.4 g) were placed in 7 mL vials capped with Kimwipes secured with rubber bands before they were frozen at −80 ˚C inside a freezer. After 20 minutes the fully frozen samples were lyophilized overnight in a LABCONCO FREEZONE 6 lyophilizer at a pressure that was lower than 0.133 mPa. Around 10 mg of white powder or sticky material was obtained.

Gel Permeation Chromatography (GPC): The lyophilized samples were dissolved at a concentration of 2 mg/mL in 5 mL THF. The solutions were filtered with a 0.22 μm Teflon filter to remove any dust or coagulum. The filtered samples were injected into a Viscotek VE 2001 GPC instrument equipped with a UV detector model 2600, a differential refractive index (DRI) detector, as well as a right-angle (RALS) and a low-angle (LALS) light scattering detectors. The polymer solution was eluted at a flow rate of 1 mL/min through a series of three PolyAnalytik SupeRes mixed bed columns at 35 ºC. The DRI, RALS, and

LALS detectors were used to obtain the absolute molecular weight of the seed latex, after calibration with a 72.2 kg/mol polystyrene standard (PDI=1.02). The characterization of the oligomers incorporated into the seed latex was based on a series of 8 polystyrene standards, whose molecular weights ranged from 1.3 to 17.5 kg/mol, employed to build a calibration curve that yielding apparent molecular weight.

Dynamic Light Scattering (DLS): DLS was used to measure the hydrodynamic diameter (D_h) and particle size dispersity (PSD) of each latex sample. The emulsion used for the DLS measurements was prepared by mixing 1 drop of 27 g/L latex emulsion and 7 g of DIW, thus resulting in a 0.04 g/L dispersion. The autocorrelation function of the scattering signal acquired for the aqueous latex dispersions was obtained with a Brookhaven 90Plus Particle Size Analyzer instrument at 25 ˚C. The detector was set to an angle of 90 º relatively to the incident beam. The diameter of the particles was calculated from the effective diameter based on the light scattering intensity.

UV-Vis Spectrophotometer (UV-Vis): Absorption measurements were conducted on a Cary 100 Bio UV-Visible spectrophotometer. It was used to determine the pyrene content (λ_{Py}) of the PyLLPs, expressed in mole of pyrene per gram of polymer. Solutions were prepared with distilled in glass THF and added to a UV cell with a 1 cm-pathlength (l = 1 cm). The absorbance (Abs) at 344 nm of a solution of known massic polymer concentration (m) was measured. The pyrene content was obtained from the ratio $Abs/(\varepsilon \times m)$, where ε is the molar extinction coefficient of the pyrenemethoxy group in THF, found to equal 42,700 $M^{-1}.cm^{-1}$ at 344 nm.

Differential Scanning Calorimetry (DSC): A TA Q20-2528 DSC was used to measure the T_g of each sample. To this end, a small amount (3 mg) of the lyophilized latex sample was

loaded in an aluminum pan and sealed with an aluminum lid. The samples were equilibrated for 5 minutes at −70 ºC and the temperature was ramped from −70 to 110 ºC at a rate of 40 ºC/min.

2.2.2 Characterization of PyLLPs

To probe the IPCD of the latex film by PEF, it was necessary to remove free pyrenyl derivatives from the latex dispersion since their presence would interfere with the fluorescence measurements. Dialysis was used to remove all small-molecule impurities still present in the latex dispersions. Spectra/Por 7 dialysis tubing with a 50 kg/mol molecular weight cutoff was placed in a 500 mL beaker filled with DIW to presoak thoroughly and remove toxic azide compounds. After 15 minutes one end of the tubing was folded and sealed with a plastic clamp. Then, 10 g of the PyLLPs aqueous dispersion was added to the tubing, and the other end of the tubing was sealed with another clamp, with around 10 cm^3 of air inside to enable the tube to float. This provided some space of swelling of the latex dispersion during dialysis, thus preventing the expansion of the solution and explosion of the tubing. The tubing was placed in a 1 L beaker filled with 600 mL DIW, 150 mL reagent ethanol, and the same concentration of AOT (1.2 g, 2.7 mmol) as the latex solution. A large piece of aluminum foil was used to cover the beaker, to minimize solvent evaporation and pyrene degradation due to the light. The dialysate was replaced after 4 hours. According to previous research,[6] the amount of unbound pyrene in the latex dispersion decreased to negligible levels after 19 dialysis cycles.

GPC analysis yielded the molecular weight of the polymer in the PyLLPs and the trace from the UV-Vis detector was used to ensure that all free pyrenyl derivatives had been

removed from the dispersion. To this end, the dialyzed latex dispersion was lyophilized. The dry residual solids were dissolved in THF and injected into the GPC. The GPC analysis yielded an M_w value of 407 kg/mol and a PDI of 2.3 for the polymer in the PyLLPs. As seen in Figure 2.2, the good overlap between the DRI and UV traces demonstrates that the polymers constituting the PyLLPs were labeled with pyrene, while the flat baseline obtained for the UV trace at high elution volumes (ca. 33-34 mL) confirms that no free pyrene remained in the latex dispersion, as had been established earlier.[6]

For the pyrene content determination of the PyLLPs, the polymer needed to be separated from other small molecules that might be present in the sample, including BMA, AOT, and unbound pyrene labels. Repeated precipitations were used to purify the PyLLPs. A 1 mL latex dispersion sample was frozen and lyophilized to remove the water. Then, a minimum amount of THF (around 8 drops) was used to completely dissolve the latex powder, followed by the addition of 6 mL methanol. Vigorous shaking of the mixture yielded a pale-yellow precipitate of PyLLPs. This procedure was repeated four times to fully eliminate the small molecules. Finally, the polymer precipitate was placed in a vacuum oven overnight at room temperature to evaporate the THF. A mass of 0.19 g of PyLLPs was obtained.

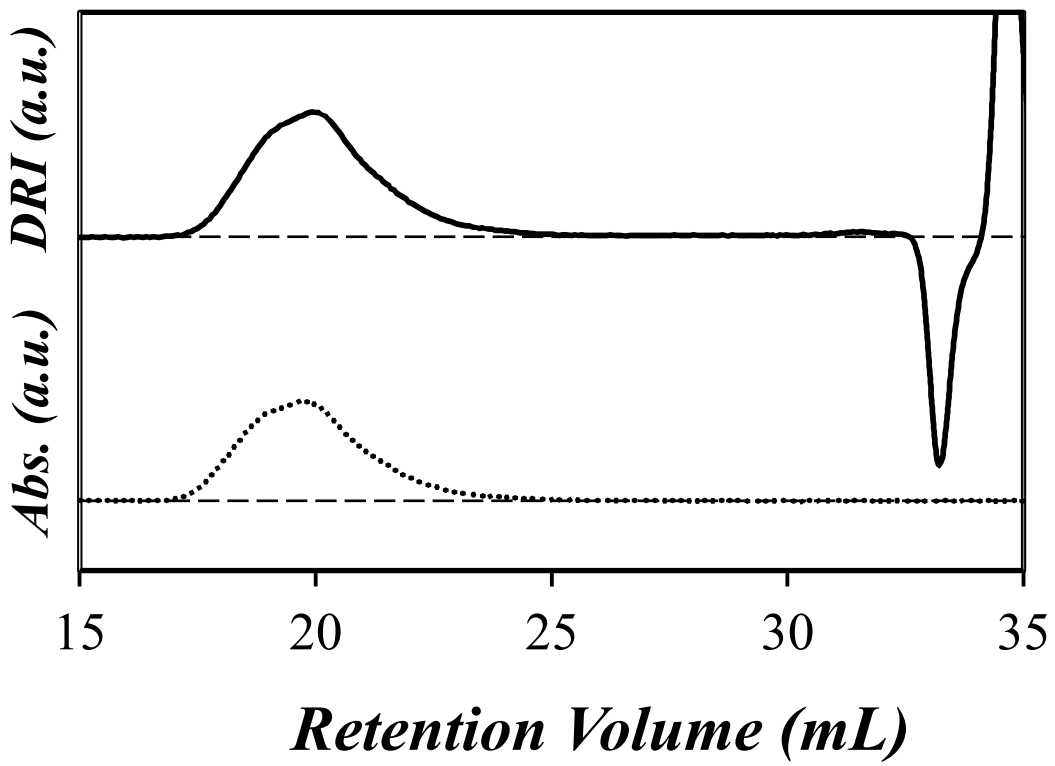

Figure 2.2. DRI(—) and UV(•••) traces for PyLLPs

After the pyrene content (λ_{Py}) of the PyLLPs had been determined by UV-Vis spectrophotometry, the molar fraction (f_{Py}) of pyrene labeled monomers in the PyLLPs was determined according to Equation 2.1.

$$f_{Py} = \frac{M_{BMA}}{1/\lambda_{Py} + M_{BMA} - M_{PyLM}} \tag{2.1}$$

In Equation 2.1, M_{BMA} and M_{PyLM} are the molar masses of *n*-butyl methacrylate (142 g.mol^{-1}) and the 1-pyrenebutylmethacrylate monomer (342 g.mol^{-1}), respectively. In these experiments, f_{Py} was found to equal 1.6 mol%.

DLS was used to determine the size distribution of the PyLLPs latex particles. An average hydrodynamic diameter of 125 nm was obtained with a particle size dispersity of 0.02. All the results are summarized in Table 2.1. The parameters reported for the PyLLPs latex in an earlier publication,[6] and those obtained in this thesis for the freshly dialyzed PyLLPs latex, were sufficiently similar that the PyLLPs latex could be used in the experiments presented in this thesis.

Table 2.1. Comparison between the parameters obtained in this thesis for the characterization of the PyLLPs and those reported in an earlier publication.[6]

Samples	f_{Py} (mol %)	M_w (kg/mol)	PDI	Diameter (nm)	PSD	I_E/I_M
PyLLPs[6]	1.9	360	1.8	123	0.01	0.119
PyLLPs	1.6	407	2.3	125	0.02	0.116

2.2.3. Characterization of Native Latex

The molecular weight distribution (MWD) of the polymers constituting the seed and seed-oligomer latex particles was characterized by GPC analysis, while DLS was employed to determine the size distribution of the latex particles. Table 2.2 lists the relevant parameters for the characterization of all the seed and seed-oligomer latex particles used in this project. Seed-3K and Seed-5K are two seed latex particles prepared individually without oligomers, whose molecular weight distribution is similar to that of the polymers constituting the PyLLPs. The seed latex particles extracted before the incorporation of oligomers are identified as 3K-0, and 3K-0.12, 3K-0.17, 3K-0.19, 3K-0.27, representing the seed-oligomer latex particles prepared with an OBMA having an M_n of 3.0 kg/mol (3.0 K) incorporated in the latex at four different weight fractions ($f_{w,o}$) of 0.12, 0.17, 0.19, and

0.27, respectively. The same nomenclature was applied to the sample prepared with an OBMA having an M_n of 5.0 kg/mol, whereby 5K-0 is the seed latex particles obtained before incorporation of the 5.0 K oligomer, and 5K-0.10, 5K-0.16, 5K-0.23 represent the seed-oligomer latex particles whose weight fraction of 5.0 K oligomers equaled 0.10, 0.16, and 0.23, respectively. The GPC traces obtained with the DRI detector are shown in Figures 2.3 and 2.4. The excellent overlap observed for the peak eluting at 20 mL demonstrates that the molecular weight of the PBMA seed was identical for a same series of seed-oligomer latex particles, and the second peak with a lower molecular weight appearing at 27 mL reflected the successful incorporation of different $f_{w,o}$ of short OBMA oligomers in the seed-oligomer latex particles. In addition, a run with pure THF solvent was conducted to ensure that the peak eluting at 33 mL was from the solvent peak rather than a low molecular weight impurity, as shown in Figure 2.3.

Table 2.2. Molecular weight and particle size distribution, and T_g of the seed and seed-oligomer films.

Sample	$[XA]_{seed}$ (mol %)	Absolute MW for Seed (kg/mol)			Apparent MW for Oligomer (kg/mol)			$f_{w,o}$ (%)	$[XA]_{oligo}$ (mol %)	Diameter (nm)	PSD	T_g (°C)
		M_n	M_w	PDI	M_n	M_w	PDI					
Seed-3K	0.009	195	358	1.8	-	-	-	0	-	122	0.02	37
Seed-5K	0.009	215	415	1.9	-	-	-	0	-	127	0.03	39
3K-0	0.008	187	349	1.9	-	-	-	0	-	112	0.01	35
3K-0.12					3.0	4.8	1.6	12	4.6	117	0.01	28
3K-0.17					2.9	4.6	1.6	17		120	0.01	25
3K-0.19					2.9	4.8	1.6	19		122	0.02	24
3K-0.27					3.0	5.0	1.6	27		126	0.01	18
5K-0	0.008	188	464	2.4	-	-	-	0	-	171	0.01	35
5K-0.10					5.0	7.2	1.4	10	3.1	178	0.05	32
5K-0.16					4.9	7.1	1.4	16		181	0.03	29
5K-0.23					5.0	7.2	1.4	23		184	0.03	27

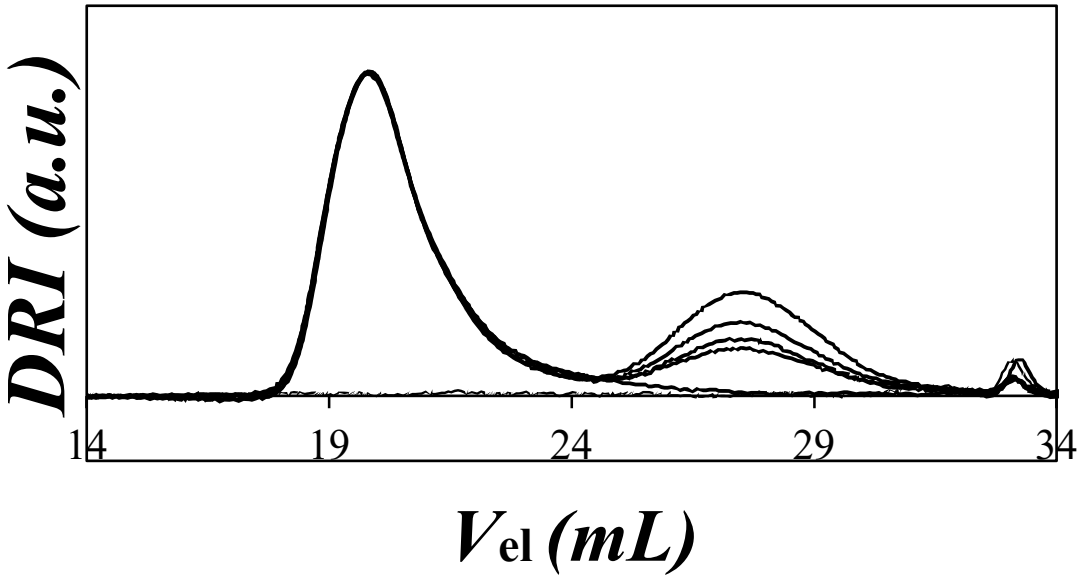

Figure 2.3. GPC traces for the seed (3K-0) latex particles, seed-oligomer latex particles with 3.0 kg/mol OBMA, and pure THF solvent. From bottom to top: THF, 3K-0, 3K-0.12, 3K-0.17, 3K-0.19, 3K-0.27.

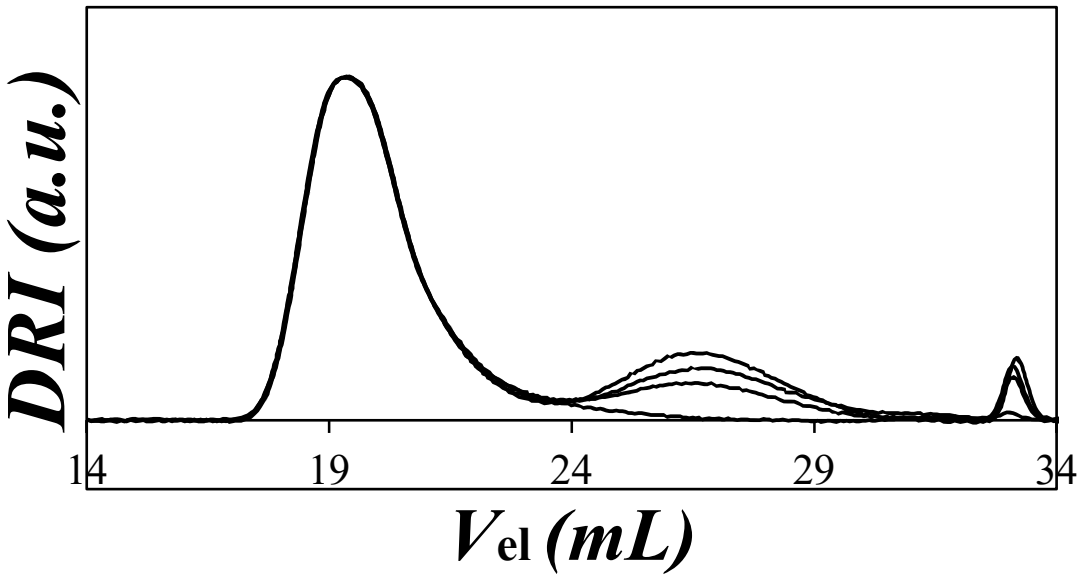

Figure 2.4. GPC traces for the seed (5K-0) latex particles and the seed-oligomer latex particles with 5.0 kg/mol OBMA. From bottom to top: 5K-0, 5K-0.10, 5K-0.16, 5K-0.23.

2.2.4 Molecular Weight Control

According to the Mayo equation and the relationship between the number-average degree of polymerization (X_n) and M_n given in, respectively, Equations 2.2 and 2.3, $1/M_n$ is expected to increase linearly with the concentration of chain transfer agent, [*XA*]. In Equation 2.2, X_0, C_{XA}, and [*M*] represent the X_n value in the absence of chain transfer agent, the chain transfer constant, and the monomer concentration in the polymerization, respectively. M_0 in Equation 2.3 is the molar mass of the structural unit, equal to 142 g/mol for *n*-butyl methacrylate.

$$\frac{1}{X_n} = \frac{1}{X_0} + C_{XA} \times \frac{[XA]}{[M]} \tag{2.2}$$

$$\frac{1}{X_n} = \frac{M_0}{M_n} \tag{2.3}$$

The Mayo equation shown in Equation 2.2 applies to homogeneous polymerizations conducted with a chain transfer agent. The emulsion polymerizations carried out in this study were not homogeneous, and the [*XA*] and [*M*] concentrations represented the local concentration of IOMPA chain transfer agent and BMA monomer in the polymer particles. Nevertheless, since the same emulsion volume and mass of BMA were used in the emulsions, the [*XA*]/[*M*] ratio in the polymer particles was expected to be proportional to the [*XA*]/[*M*] ratio in the reaction vessel, using a proportionality constant that could be included in the chain transfer constant C_{XA}. It was confirmed that this was indeed the case through the linear relationship found by plotting $1/M_n$ as a function of the [IOMPA]/[BMA] ratio, expressed in terms of the overall concentration in the emulsion reactor (Figure 2.5). This linear relationship could be employed to predict the amount of IOMPA needed to

obtain a given molecular weight for a PBMA or OBMA sample. In particular, it was used to prepare seed latex particles made of PBMA chains having a target M_n value of 200 kg/mol, corresponding to a weight-average molecular weight (M_w) of 400 kg/mol when assuming a PDI of 2.0. Based on the results listed in Table 2.2, the M_w value obtained for most seed latex particles approached the 400 kg/mol value, thus demonstrating the validity of the procedure.

Table 2.3. M_n, M_w, PDI (=M_w/M_n) and mol% of IOMPA in the polymers for molecular weight calibration.

Sample	[*XA*]	Absolute Molecular Weight			Apparent Molecular Weight		
	(mol %)	M_n (kD)	M_w (kD)	PDI	M_n (kD)	M_w (kD)	PDI
*XA*01	0	325	695	2.1	234	456	1.9
*XA*02	0	368	646	1.8	218	422	1.9
*XA*03	0	220	390	1.8	147	277	1.9
*XA*04	0	208	508	2.4	134	333	2.5
*XA*1	0.1	101	221	2.2	69	157	2.3
*XA*2	0.23	61	106	1.7	44	85	2.0
*XA*3	0.45	25	51	2.3	23	46	2.0
*XA*4	0.71	23	38	1.7	16	33	2.1

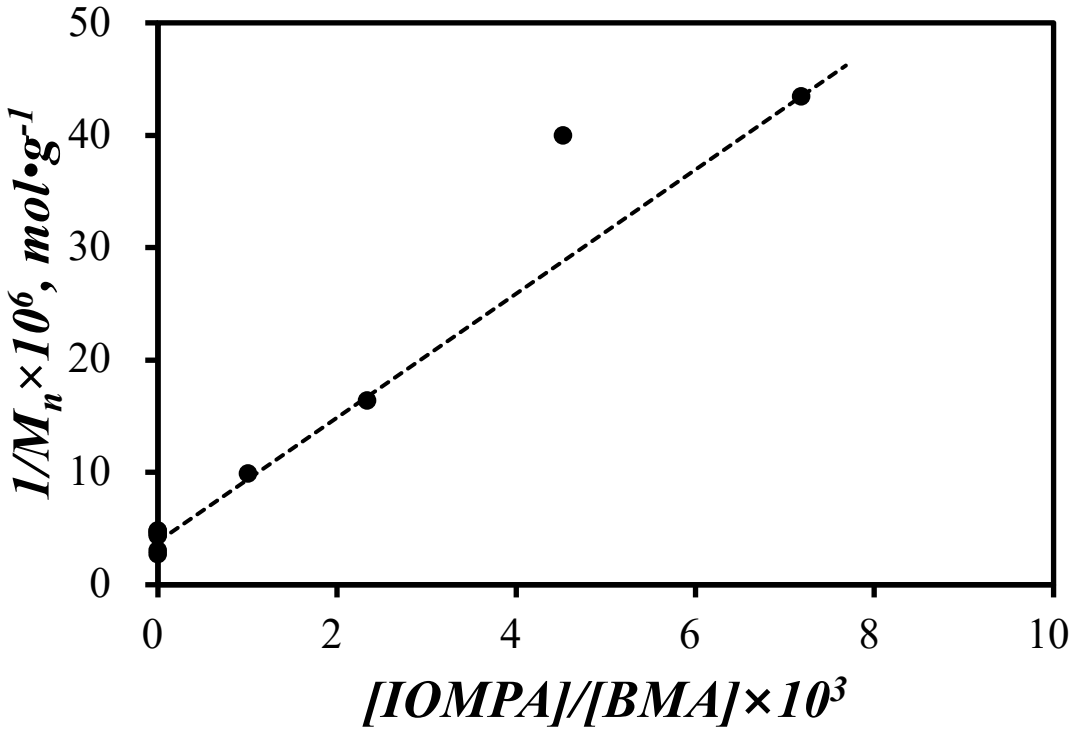

Figure 2.5. Linear relationship between $1/M_n$ and [IOMPA]/[BMA] for the polymers obtained by emulsion polymerization. M_n represents the absolute number-average molecular weight.

The linear relationship shown in Figure 2.5 showed increased scatter in the $1/M_n$ values for higher IOMPA concentrations, corresponding to lower M_n values. The increased scatter in the M_n values was due to the light scattering signal generated by the OBMA samples being too weak for reliable molecular weight analysis.

To circumvent this issue, the apparent number-average molecular weight ($M_{n,app}$) obtained through analysis of the DRI signal was used. Figure 2.6 confirms that $1/M_{n,app}$ increased linearly with increasing [*IOMPA*]/[*BMA*] ratio over the entire range of IOMPA concentrations used in this project.

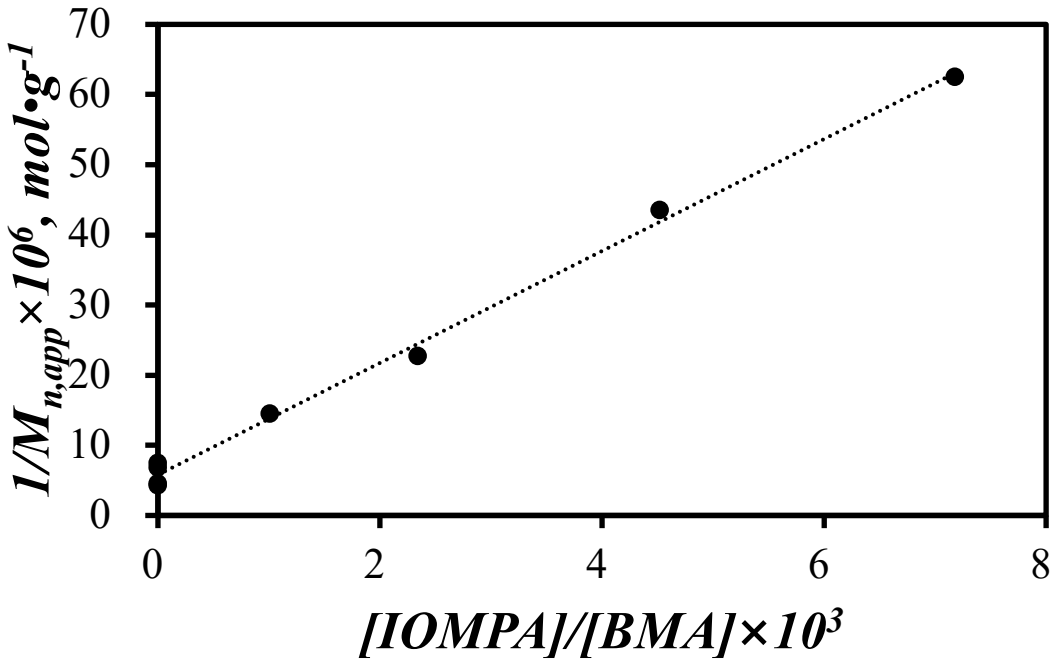

Figure 2.6. Plot of $1/M_{n,app}$ as a function of [IOMPA]/[BMA]. $M_{n,app}$ represents apparent molecular weight obtained from polystyrene standard.

The straight line obtained in Figure 2.6 was extrapolated to higher IOMPA concentrations, to predict the amount of IOMPA needed to generate OBMA samples of desired molecular weights, as shown in Figure 2.7. Even though the $M_{n,app}$ values obtained for the OBMA samples did not fall perfectly on the straight line, this plot was helpful in predicting the quantity of IOMPA needed to synthesize the OBMA samples.

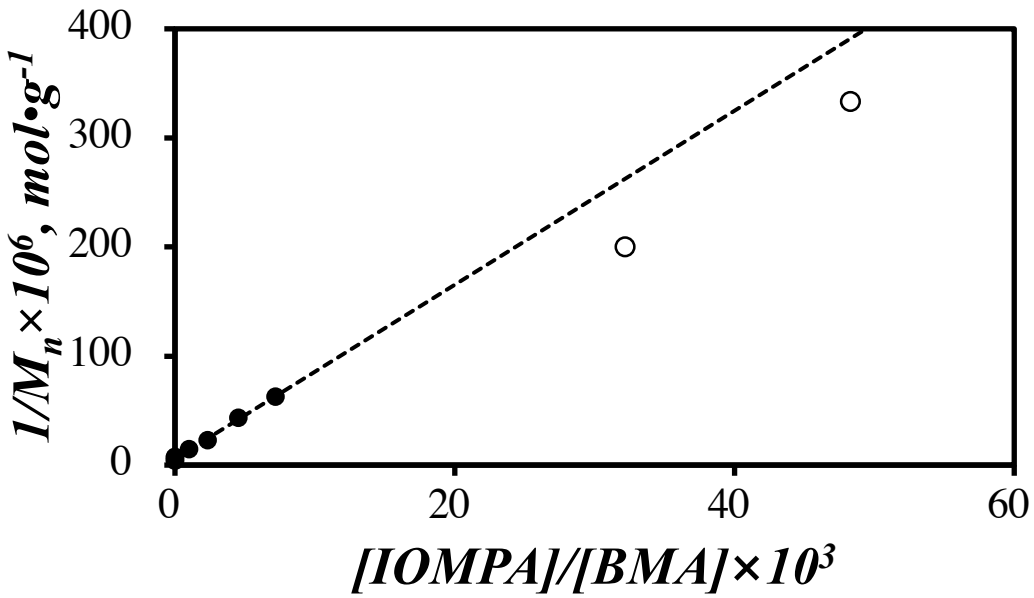

Figure 2.7. Expanded plot of $1/M_{n,app}$ as a function of [IOMPA]/[BMA]. $M_{n,app}$ was obtained with respect to polystyrene standards.

2.2.5 Oligomer Content Measurement

Oligomer incorporation was quantified by determining the weight fraction ($f_{w,o}$) of oligomer in each sample. Gravimetric analysis was applied for this purpose. After water removal by lyophilization, the solid part of the seed latex was constituted of the seed polymer PBMA, surfactant AOT, and initiator APS. Similarly, the solid part of the seed-oligomer latex contained the same ingredients as described previously plus the oligomer OBMA. By calculating and subtracting the mass of AOT and APS contributing to the mass of the lyophilized sample, the mass of pure polymer and/or pure polymer plus oligomer could be determined. The $f_{w,o}$ value was equal to the mass of pure oligomer over the sum of the masses of pure polymer and oligomer. The detailed procedure for determining $f_{w,o}$ gravimetrically is provided in Appendix A.

Another strategy to determine $f_{w,o}$ for the oligomers was to use the area under the DRI

signal in the GPC trace. This procedure took advantage of the direct relationship that exists between the DRI signal and polymer concentration. This procedure assumed as a first approximation that the change in refractive index with polymer concentration (dn/dC) is independent of molecular weight, which is known to be incorrect for shorter chains. It was used nonetheless to obtain an estimate of $f_{w,o}$. The $f_{w,o}$ value for a seed-oligomer latex was calculated with Equation 2.4, where $Area_s$ and $Area_{s,o}$ represent the total area under the GPC trace of the seed and seed-oligomer latex, respectively.

$$f_{w,o} = \frac{Area_{s,o} - Area_s}{Area_{s,o}} \tag{2.4}$$

The $f_{w,o}$ value of a seed-oligomer latex could also be determined by monitoring the change in particle size obtained by conducting DLS experiments. This was based on the assumption that an increase in particle size reflected an isotropic swelling of the particles during oligomer incorporation. Equation 2.5 provided a means to calculate $f_{w,o}$ from the volumes V_s and V_{so} and hydrodynamic diameters $D_{h,s}$ and $D_{h,so}$ of the seed and seed-oligomer latex particles, respectively.

$$f_{w,o} = \frac{V_{s,o} - V_s}{V_{s,o}} = 1 - \frac{D_{h,s}^3}{D_{h,so}^3} \tag{2.5}$$

The weight fractions of oligomers calculated by these three methods are listed in Table 2.4. Even though the three methods yielded similar trends, the procedures based on GPC

and DLS were suspected of being less accurate as compared to the gravimetric analysis. For GPC, the *dn/dC* value for the oligomers was certainly not the same as for the polymer, so that the areas under the GPC traces obtained with the DRI detector did not represent the massic concentrations of the oligomers and the polymers with the same proportionality constant. For DLS, the changes in D_h obtained from the DLS measurements were relatively small, being typically less than 8 %, and the $f_{w,o}$ value had a strong dependence on the 3rd power of the D_h according to Equation 2.5, which could amplify small errors in D_h. As a consequence, the $f_{w,o}$ values retrieved from gravimetric analysis were deemed more accurate and were used to represent the weight fractions of oligomers obtained for the seed-oligomer latex particles studied in this thesis.

Table 2.4. Weight fractions of oligomers determined by gravimetric, GPC and DLS analyses.

	Gravimetric	GPC	DLS
3K-0.12	0.12	0.13	0.13
3K-0.17	0.17	0.18	0.18
3K-0.19	0.19	0.23	0.23
3K-0.27	0.27	0.30	0.30
5K-0.10	0.10	0.12	0.13
5K-0.16	0.16	0.17	0.16
5K-0.23	0.23	0.24	0.21

Chapter 3 – Film Formation

3.1 Introduction

The goal of this chapter was to characterize films of the latex particles prepared in Chapter 2 to study the influence of the length and amount of oligomers incorporated inside a latex particle on film formation. A mixture of pyrene-labeled and unlabeled latex particles was cast on glass plates to form films. As the films were annealed at different temperatures, their I_E/I_M ratio was monitored as a function of annealing time through steady-state fluorescence. The I_E/I_M intensity ratios were used to calculate the fraction of mixing (f_m) according to Equation 1.9, and the diffusion coefficients (D) were obtained from f_m by using a Fickian model (Equations 1.10 and 1.11). The effect that the amount of a 3.0 K or 5.0 K oligomer incorporated into the latex particles had on film formation was assessed by comparing plots of f_m as a function of annealing time, and plots of D as a function of f_m obtained at different annealing temperatures. The diffusion coefficients acquired at different annealing temperatures were then shifted vertically in the D-*vs*-f_m plots according to a shift factor (a_T) with respect to the fraction of mixing to build master curves. A plot of a_T as a function of the reciprocal of the annealing temperature yielded the activation energy (E_a), which is the energy that polymer chains in the films need to overcome to diffuse. Comparison of the E_a values obtained for different films provided a means to probe the effects on E_a of the incorporation of oligomers of different lengths and at different weight fractions ($f_{w,o}$).

In addition, the plasticizer efficiency of the two oligomers was determined as a

function of temperature. To this end, all the master curves obtained for films prepared with a same oligomer but with different $f_{w,o}$ values were normalized to the same reference temperature, combined together in a same plot, and shifted vertically with respect to f_m with a shift factor a_{oligo} using the seed master curve ($f_{w,o}$=0) as reference. Since the molecular weight of the seed used to prepare the 3.0 K seed-oligomer latex (M_w=350 kD) was relatively smaller than that of the 5.0 K seed-oligomer latex (M_w=460 kD), the master curves obtained for the Seed-3K films (M_w=360 kD) and Seed-5K films (M_w=420 kD) were used as reference to build the master curve for the 3.0 K and 5.0 K films, respectively. Then, the a_{oligo} shift factors were used to determine the plasticizer efficiency for an oligomer of a specific length by applying the Fujita-Doolittle model. At last, the plasticizer efficiencies of the 3.0 K and 5.0 K oligomers were compared as a function of annealing temperature, to assess how temperature affected oligoplasticization.

In this project, the range of M_n and $f_{w,o}$ values used for the oligomers in the annealing experiments needed to be assessed. Preliminary experiments showed that, if the M_n of the oligomer was 2 kD, annealing occurred during the drying stage of the latex films so that the initial $(I_E/I_M)_{(tan=0)}$ ratio was too low to obtain reliable f_m and D values. Consequently, M_n for the oligomer had to be larger than 2 kD and M_n values of 3 and 5 kD were selected. It was also found that $f_{w,o}$ values of the oligomer greater than 30 wt% resulted in a non-linear Fujita-Doolittle equation. To take advantage of the Fujita-Doolittle equation to determine the plasticizer efficiency, $f_{w,o}$ values smaller than 30 wt% were employed.

3.2 Film Preparation

Films were prepared from an emulsion (27 g/L solids content) constituted of 5 wt%

pyrene labeled latex and 95 wt% non-labeled latex.[6] A small volume (0.25 mL) of the latex mixture was cast at one end of a 1 cm × 3 cm glass plate. Next, the films were placed in a light-proof box at room temperature under a gentle flow of nitrogen, to accelerate the film-drying process. The end of the glass plate without latex solution was lifted up by 1 mm with a metal bar to generate a small inclination, so that the latex was retained at the other end of the plate. After 3 hours the latex solution became a transparent solid film ready for annealing.

Previously, Casier and coworkers[6] suggested that PBMA latex films with similar specifications needed to be dried overnight to minimize hydroplasticization effects. The latex particles studied in this earlier report did not incorporate any plasticizer. The T_g of these films was slightly above room temperature, and the I_E/I_M ratio of films made of the pyrene-labeled and unlabeled latex mixture after drying retained the same value as a film made solely of the pyrene-labeled latex. This indicated that no IPCD had taken place during drying. In contrast, the present project focused on films where oligomers were purposely added to lower T_g. Such films could enable IPCD during drying before annealing, thus making the characterization of IPCD inaccurate. Drying the films for only 3 hours in the light-proof box was found to prevent IPCD based on the constancy of the I_E/I_M ratio, while ensuring satisfactory water evaporation based on the clear appearance of the films. Furthermore, a study by Winnik et al. on the effect of water for PBMA films suggested that the presence of residual water might not affect IPCD much.[14] Their study showed that as compared to a dry environment, the IPCD of PBMA films at 100% relative humidity was enhanced by a negligible amount, indicating that residual water would not

act as an efficient plasticizer in PBMA films. Consequently, films prepared with oligomers were annealed for only three hours in this study.

3.3 Film Annealing

To investigate film formation, the dried films were annealed at a constant temperature. This was achieved by placing them in two glass tubes and immersing them into an oil bath. The tubes were fitted with rubber stoppers pierced with a needle, to allow a gentle flow of nitrogen and keep the tube under a positive pressure of nitrogen. After a set amount of time the films were taken out and put quickly in contact with an aluminum plate to stop pyrene diffusion. After cooling to room temperature, the films were further characterized by fluorescence.

The calculation of f_m from Equation 1.9 required the determination of the I_E/I_M ratio of a film annealed for an infinitely long time. Such a film was prepared by scraping off the film from the glass plate, redissolving it in 0.1 mL inhibitor-free THF, casting the solution on a glass plate, and evaporating the THF under nitrogen for 20 minutes in the light-proof box. The film was then placed in a glass tube under nitrogen and immersed in an oil bath to anneal for one hour at 120 ºC, to ensure that all the THF had evaporated from the film.

3.4 Steady-State Fluorescence and Fluorescence Intensity Ratios

The steady-state fluorescence spectra for the films were acquired to determine the I_E/I_M

ratio after a given annealing time. The standard deviation of the I_E/I_M ratio was determined by acquiring the fluorescence spectra at three different spots on the films for each annealing time. Figure 3.1A shows some of the fluorescence spectra for the seed film annealed at 86 °C for different annealing times, and Figure 3.1B represents the zoomed-in section of the spectra corresponding to excimer emission between 500 and 530 nm.

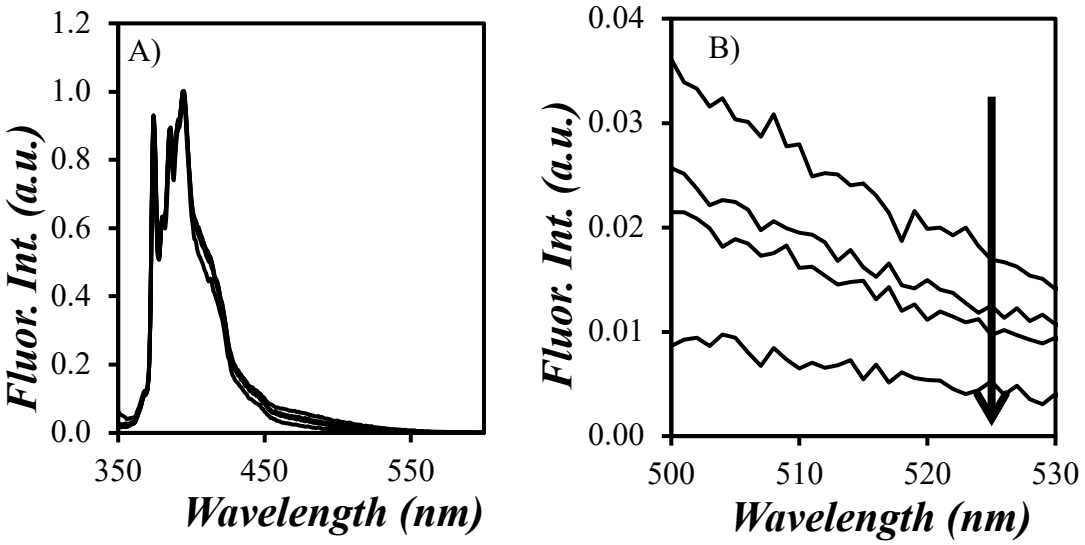

Figure 3.1. Normalized steady-state fluorescence spectra for a film made with the seed latex annealed at 86 °C for different times. B) Zoomed-in section of the normalized fluorescence spectra representing the fluorescence of the excimer between 500 and 530 nm. From top-to-bottom: 0, 30, 120 min, and infinite time.

The four top traces in Figure 3.1B represent the fluorescence spectra scanned before annealing, after annealing for 30, and 120 minutes, and at infinite annealing time. The lowest trace corresponds to the spectrum for the homogeneous film ($t_{an}=\infty$). After normalizing the fluorescence spectra at 395 nm, I_E was found to decrease for increasing annealing times. Although I_E was much lower than I_M, the excimer signal was large

enough to obtain reliable I_E/I_M ratios. Figure 3.2 illustrates how the I_E/I_M ratio varied as a function of annealing time. The dashed line in Figure 3.2 represents the intensity ratio at $t_{an}=\infty$. In this film, the I_E/I_M ratio decreased from 0.115 ± 0.001 to 0.070 ± 0.001, a 50 % change over a 2-hour annealing period, before reaching 0.029 ± 0.001 at infinite annealing time.

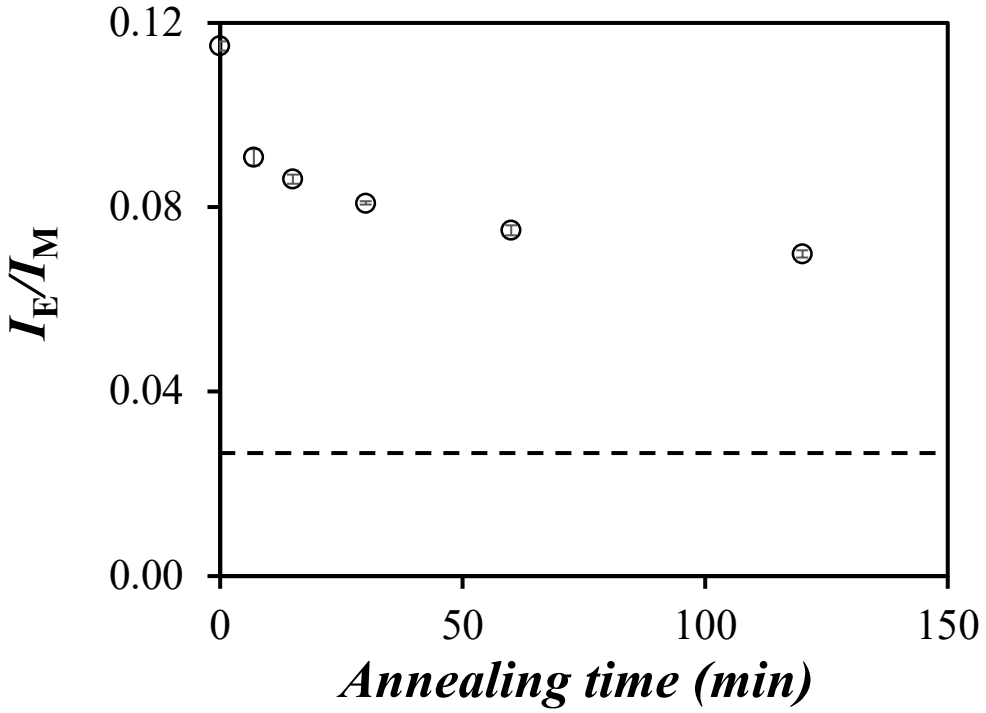

Figure 3.2. Plot of the I_E/I_M ratio for the seed latex film at 86 ºC as a function of annealing time.

3.5 Fraction of Mixing (f_m) and Diffusion Coefficient (D)

Equation 1.9 was used to obtain the fraction of mixing (f_m) from the I_E/I_M ratios. Figure 3.3A shows how the fraction of mixing varied as a function of annealing time for film 3K-0.19 ($f_{w,o}$=0.19) at temperatures ranging from 66 ºC to 103 ºC. All 5 traces followed a same trend upon annealing: f_m increased rapidly within the first 15 minutes of annealing,

before increasing more slowly at longer annealing times. The bimodal behavior observed in the trends shown in Figure 3.3A was attributed to the rapid IPCD experienced by the oligomers at early times, followed by much slower reptation of the longer chains at longer annealing times. These trends match those presented in earlier reports.[2-8,10] The trends also show that for a same annealing time, a higher annealing temperature resulted in a larger f_m value. This outcome was expected, as higher temperatures promote IPCD due to the increased thermal energy.

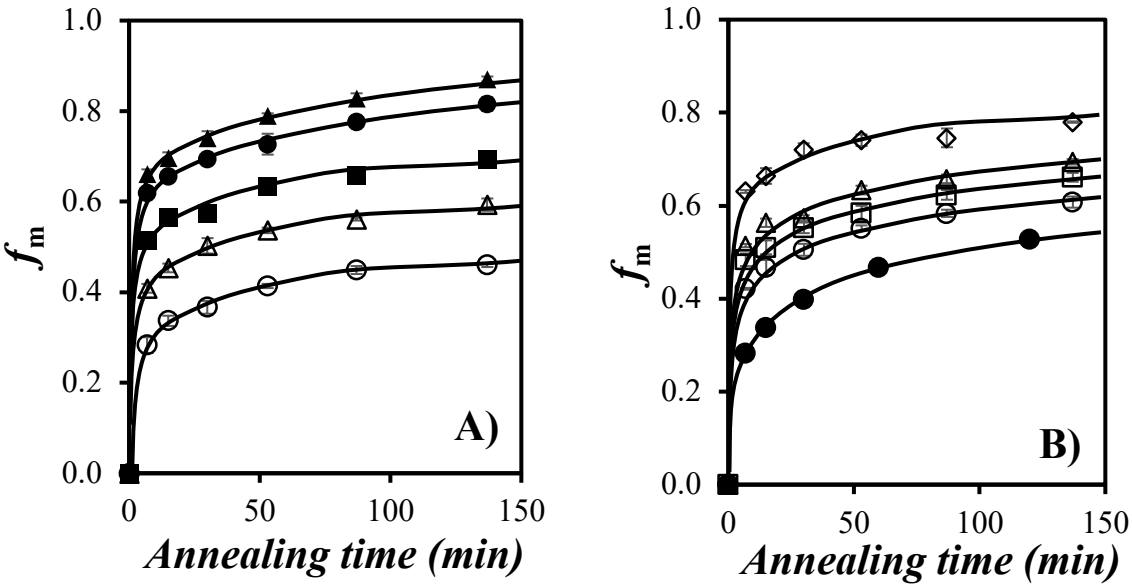

Figure 3.3. Plots of f_m as a function of annealing time for films prepared with A) the seed-oligomer latex 3K-0.19 annealed at (○) 66 ºC, (△) 77 ºC, (■) 86 ºC, (●) 97 ºC, (▲) 103 ºC and B) the seed latex (●) ($f_{w,o}$=0) and the seed-oligomer latex (○) 3K-0.12 ($f_{w,o}$=0.12), (□) 3K-0.17 ($f_{w,o}$=0.17), (△) 3K-0.19 ($f_{w,o}$=0.19), and (◊) 3K-0.27 ($f_{w,o}$=0.27) annealed at 86 ºC.

The profiles obtained for f_m plotted as a function of annealing time for the films prepared with 0 (seed), 12, 17, 19, and 27 wt% of 3.0 K oligomers annealed at 86 ^oC are compared in Figure 3.3B. It must be noted at this point that the samples 3K-0 and 5K-0, which were the actual seeds for the seed-oligomer latex particles, were obtained in too little quantities to conduct the film annealing studies. They were mainly used to determine the MWD of the PBMA seeds and the $f_{w,o}$ values. The samples Seed-3K and Seed-5K, obtained in larger quantities, were used as references in these annealing experiments.

The traces shown in Figure 3.3B are similar to those presented in Figure 3.2. f_m reached a value of 0.34 ± 0.01 after 15 minutes annealing for the films prepared with the seed latex, but it reached a value of 0.47 ± 0.02, 0.51 ± 0.01, 0.56 ± 0.01, and 0.66 ± 0.02 when the seed-oligomer latex contained 12, 17, 19, and 27 wt% of 3.0 K oligomer, respectively. This trend of increasing f_m value with increasing content of 3.0 K oligomer in the seed-oligomer latex is observed at all annealing times in Figure 3.3B. The incorporation of low molecular weight oligomers into the latex films generates more free volume in the films, that reduces T_g, allowing the polymer chains to diffuse more easily in the films and yields a larger f_m value. Therefore, the incorporation of a low molecular weight oligomer in the latex particles facilitates IPCD, and these results agree very well with those obtained in an earlier study based on FRET.[10]

To characterize the IPCD in the films more quantitatively, f_m was used to determine the diffusion coefficient (D) of the PBMA chains by following the protocol described in Chapter 1, based on Equations 1.10 and 1.11. Figures 3.4A and B give plots of the diffusion coefficients obtained from the f_m values presented in Figures 3.3A and B,

respectively. The trends obtained with the diffusion coefficients in Figure 3.4 mimic the trends obtained with f_m in Figure 3.3, whereby the diffusion coefficient increases with decreasing fractions of mixing in Figures 3.4A and B, increasing temperature in Figure 3.4A, and increasing 3.0 K oligomer content in Figure 3.4B. These trends are reasonable since IPCD is larger for low fractions of mixing, higher temperatures, and larger oligomer contents in the films. Other plots are included in Appendix B.

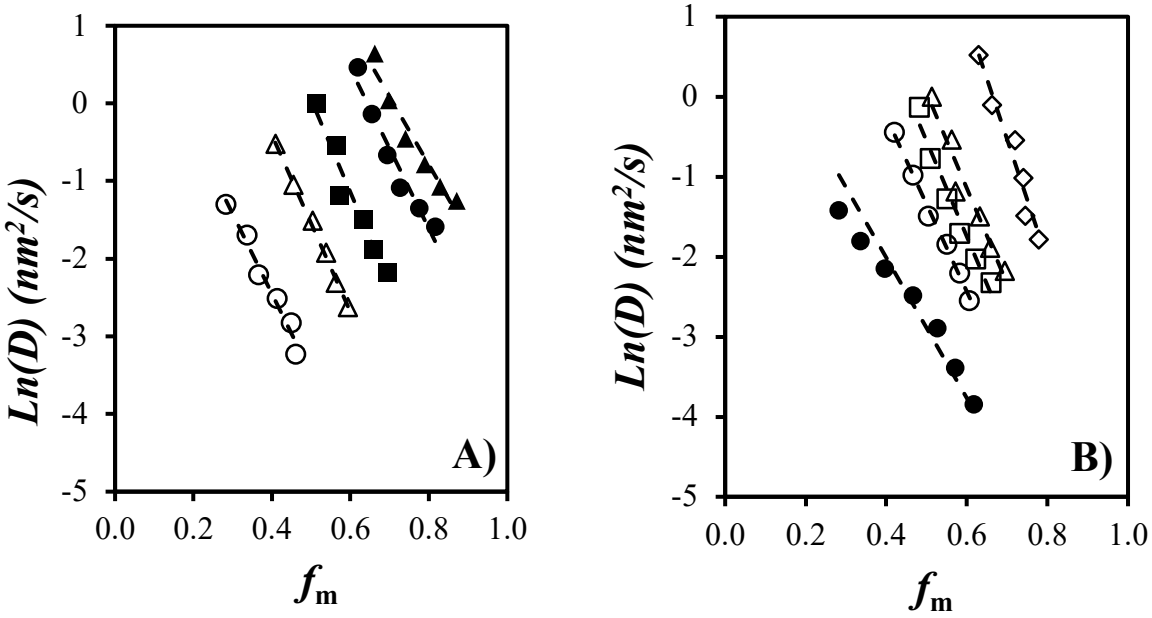

Figure 3.4. Plots of diffusion coefficients as a function of f_m for films prepared with A) the seed-oligomer latex 3K-0.19 annealed at (○) 66 ºC, (△) 77 ºC, (■) 86 ºC, (●)97 ºC, and (▲) 103 ºC and B) the seed latex (●) ($f_{w,o}$=0) and the seed-oligomer latex films (○) 3K-0.12 ($f_{w,o}$=0.12), (□) 3K-0.17 ($f_{w,o}$=0.17), (△) 3K-0.19 ($f_{w,o}$=0.19), and (◊) 3K-0.27 ($f_{w,o}$=0.27) annealed at 86 ºC.

3.6 Shift Factors and Activation Energies

To push the characterization further, the activation energies (E_a) for the diffusion of the pyrene-labeled PBMA in the films prepared with the seed and seed-oligomer latex were calculated. The calculation of E_a is based on an Arrhenius plot of the shift factors (a_T), obtained when building a master curve, by shifting the diffusion coefficients while keeping the fraction of mixing constant as shown in Figure 3.5. A reference temperature (T_o) was selected for the diffusion coefficients (D_o) at T_o, and all other diffusion coefficients (D) obtained at another temperature (T) were translated according to Equation 3.1 by a shift factor (a_T) that was optimized using a linear regression method described in Appendix C. This procedure was applied to align the D-*vs*-f_m trends obtained at different temperatures along a straight line.

$$D = \frac{1}{a_T}\frac{D_o T}{T_o} \tag{3.1}$$

In Equation 3.1, T and T_o are absolute temperatures in Kelvin. This procedure was applied to obtain the master curve shown in Figure 3.5 for the 3K-0.19 films.[6,15] A temperature of 77 ºC was selected as reference for the master curve shown in Figure 3.5.

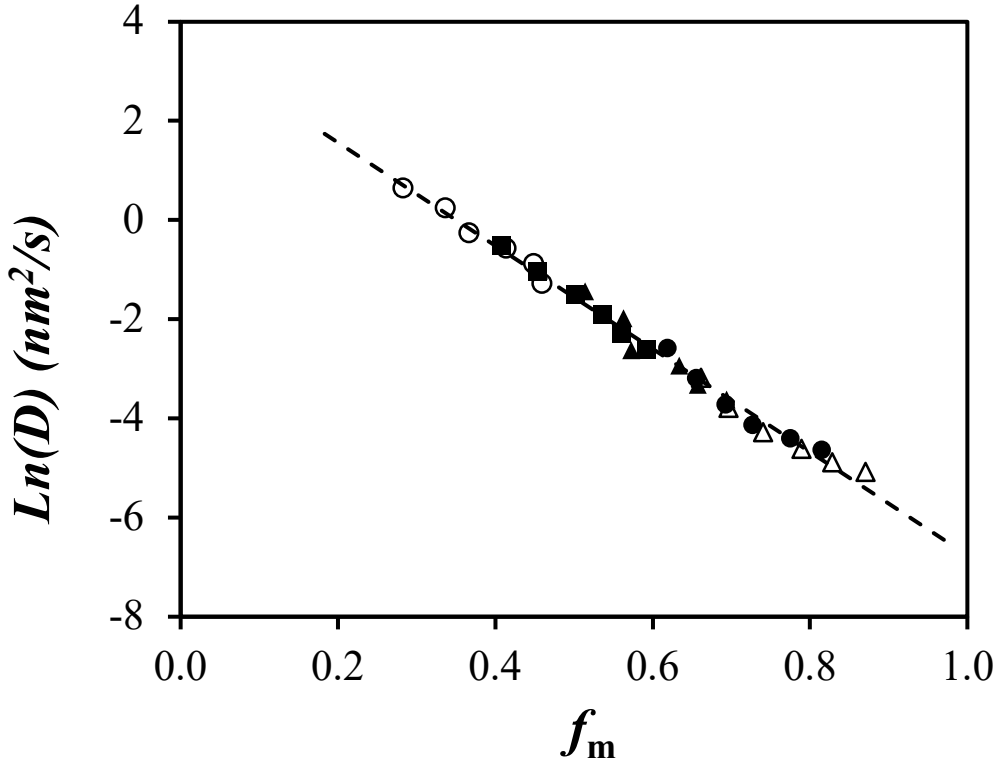

Figure 3.5. Master curve for the diffusion coefficients plotted as a function of f_m for the films 3K-0.19 annealed at (○) 66 ºC, (△) 77 ºC, (■) 86 ºC, (●) 97 ºC, and (▲) 103 ºC. T_o = 350 K (i.e. 77 ºC).

The activation energy for the diffusion of the polymer chains in the latex films was obtained by building an Arrhenius plot with the shift factors.[6] The basis for this procedure is rooted in the exponential dependency of the viscosity with temperature shown in Equation 3.2, and the relationship shown in Equation 3.3 between the diffusion coefficient, the temperature, the radius of a molecule approximated as a sphere of radius R_S, and the viscosity.

$$\eta = A \exp\left(\frac{E_a}{RT}\right) \tag{3.2}$$

$$D = \frac{k_B T}{6\pi\eta R_S} \tag{3.3}$$

Rearranging Equation 3.3 to obtain η as a function of T/D yields the relationships shown in Equation 3.4.

$$\eta \propto \frac{T}{D} \propto \exp\left(\frac{E_a}{RT}\right) \tag{3.4}$$

Taking advantage of the fact that T/D equals $a_T \times (T_o/D_o)$ according to Equation 3.1, the relationship given in Equation 3.4 can be re-written as shown in Equation 3.5.

$$Ln\left(\frac{T}{D}\right) = Ln\left(a_T\right) + const = \frac{E_a}{RT} + const \tag{3.5}$$

Based on Equation 3.5, a plot of $Ln(a_T)$ as a function of $1/T$ would be expected to yield a straight line with a slope equal to E_a/R as shown in Equation 3.6.

$$E_a = R\frac{dLn(a_T)}{d(T^{-1})} \tag{3.6}$$

An example of an Arrhenius plot of $Ln(a_T)$ as a function of T^{-1} is shown in Figure 3.6 for the film 3K-0.19.

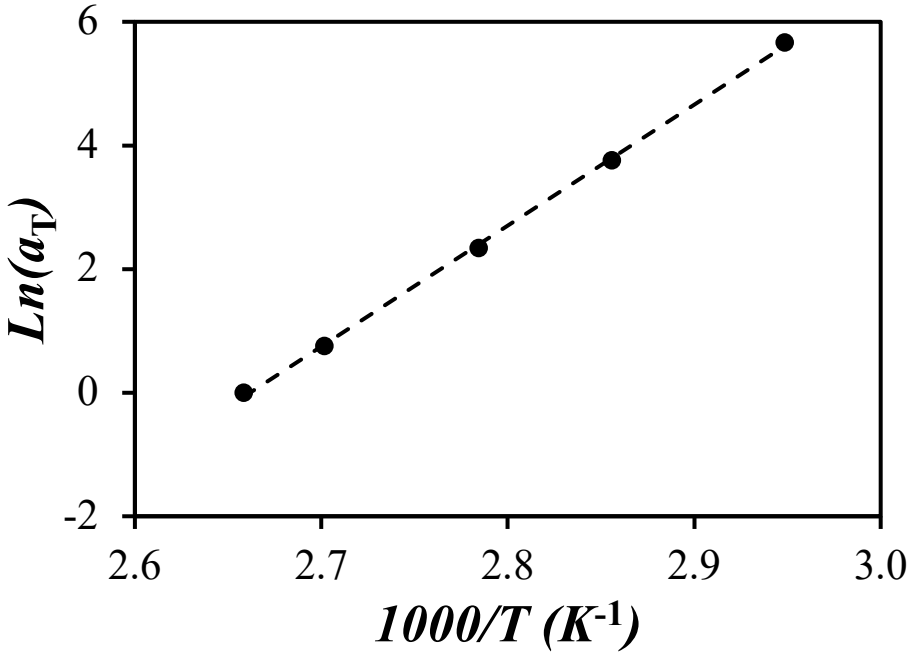

Figure 3.6. Arrhenius plot of $Ln(a_T)$ as a function of T^{-1} for film 3K-0.19.

The E_a values obtained for two films prepared without oligomer and seven films prepared with different oligomer lengths and contents were determined and plotted in Figure 3.7. Within experimental error, the activation energy remained constant and equal to 163 ± 9 kJ/mol, regardless of the type (3.0 or 5.0 K) or amount of oligomer. This result indicates that temperature affected the diffusion coefficient of the pyrene-labeled polymer in the same manner for the films prepared with the seed latex or the seed-oligomer latex. In addition, the E_a value of 163 ± 9 kJ/mol was close to other E_a values reported in the literature to equal 170 ± 9 kJ/mol[6] or 155 kJ/mol.[3,4,16-18] The good agreement found between the different E_a values obtained by applying different techniques suggests that pyrene did not affect the diffusion of the pyrene-labeled PBMA chains.

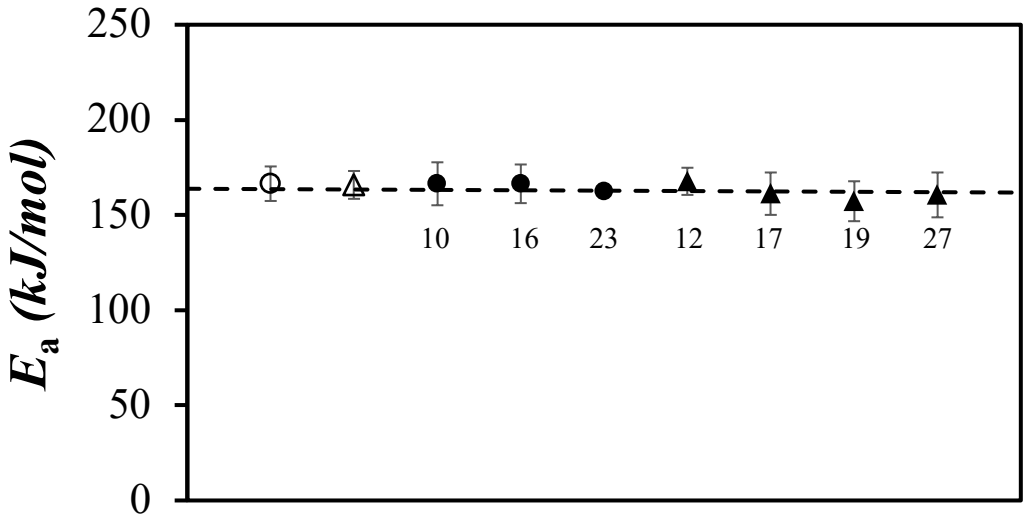

Figure 3.7. E_a for the seed films of Seed-3K (○, 360 kD), Seed-5K (△, 420 kD), and seed-oligomer latex films with (▲) 3.0 K oligomers and (●) 5.0 K oligomers. The values under each point represent the weight fraction (wt %) of oligomers.

3.7 Plasticizer Efficiency

3.7.1 Fujita-Doolittle Model

About 60 years ago, Fujita suggested the existence of a linear relationship between the fractional free volume of a polymer matrix and the volume fraction of plasticizer.[19] This model was widely used in later research to study solvent plasticization, the self-diffusion of liquid diluents in rubber,[20] hydroplasticization,[7] oligoplasticization,[10,11,21] plasticization of a coalescing aid such as Texanol™,[8,22] and surfactant plasticization.[23] Fujita started his derivation using the Doolittle relationship[24,25] between the mobility of the diluent molecule (m_d) and the average fractional free volume of the system (f), as shown in Equation 3.7.

$$m_d = A\exp\left(-\frac{1}{f}\right) \tag{3.7}$$

The mobility of the diluent molecule could be related to the diffusion coefficient and temperature according to Equation 3.8, where R is the ideal gas constant.

$$m_d = \frac{D}{RT} \tag{3.8}$$

Fujita then assumed that the fraction ($f(\varphi,T)$) of free volume in a polymer matrix at temperature T in the presence of a volume fraction (φ) of plasticizer could be described by Equation 3.9, where $f(0,T)$ is the fraction of free volume in the polymer matrix without plasticizer. In this study, φ was taken as the weight fraction of oligomers ($f_{w,o}$) by assuming that the density of PBMA did not change with or without oligomer. The fractional free volume increment experienced by a pure polymer matrix upon addition of a plasticizer at temperature T was accounted for with the parameter $\beta(T)$. Since a large $\beta(T)$ value reflects a large increase in free volume in the polymer matrix, $\beta(T)$ was used as a measure of the plasticizer efficiency.[10]

$$f(\varphi,T) = f(0,T) + \beta(T)\times\varphi \tag{3.9}$$

The combination of Equations 3.7 – 3.9 resulted in Equation 3.10.

$$D(\varphi,T)=RTA\exp\left(-\frac{1}{f(0,T)+\beta(T)\varphi}\right) \tag{3.10}$$

An expression for the diffusion coefficient of the PBMA chains in the polymer matrix without plasticizer was obtained in Equation 3.11, by setting φ to zero in Equation 3.10.

$$D(0,T)=RTA\exp\left(-\frac{1}{f(0,T)}\right) \tag{3.11}$$

Finally, the Fujita-Doolittle Equation was obtained by combining Equations 3.10 and 3.11 into Equation 3.12.

$$[Ln\left(\frac{D(\varphi,T)}{D(0,T)}\right)]^{-1}=\frac{1}{Ln\left(a_{oligo}\right)}=f(0,T)+\frac{f(0,T)^2}{\beta(T)}\times\frac{1}{\varphi} \tag{3.12}$$

The parameter a_{oligo} in Equation 3.12 is a shift factor which normalizes the diffusion coefficients with respect to the weight fraction of oligomer present in the polymer matrix. It is similar to the shift factor a_T which normalizes the diffusion coefficient with respect to temperature, as mentioned in Section 3.5. Since a_{oligo} was equal to D(φ,T)/D(0,T), it could be obtained by shifting vertically the master curves obtained at a same temperature for the seed-oligomer latex films prepared with a same oligomer, but with different $f_{w,o}$ values. The master curve obtained at the same temperature, with the seed latex film for which $f_{w,o}$= 0, was taken as reference in these experiments.[10]

The plasticizer efficiency was determined by plotting $Ln(a_{\text{oligo}})^{-1}$ as a function of φ^{-1}.

A linear relationship would suggest that Equation 3.12 be applied to fit the data, the slope yielding the plasticizer efficiency $\beta(T)$, since the free volume fraction $f(0,T)$ is known to equal $1/(2.303c_1(T))$.[26] The parameter $c_1(T)$ is one of the two constants used in the Williams-Landel-Ferry (WLF) equation, the other being $c_2(T)$, and their values are temperature-dependent. The value of $c_1(T)$ at any temperature was obtained with Equation 3.13, whose derivation is provided in Appendix D.

$$c_1(T) = \frac{c_1(T_o)c_2(T_o)}{c_2(T_o) + T - T_o} \tag{3.13}$$

The c_1 and c_2 values for PBMA have been reported to equal 11 and 170 K at 102 °C, respectively, so 102 °C was used as reference temperature (T_o) in Equation 3.13.[6] After setting $f(0,T) = 1/(2.303c_1(T))$, $\beta(T)$ could be determined from the slope of a plot of $Ln(a_{oligo})^{-1}$-*vs*-φ^{-1} according to Equation 3.12.

3.7.2 Effect of Temperature on Plasticizer Efficiency

To investigate the plasticizer efficiency at any reference temperature, determining the position of the $Ln(D)$-*vs*-f_m master curves at a specific temperature became indispensable, since all the experiments were conducted at slightly different temperatures. The detailed procedure used is described hereafter, taking the data presented in Figure 3.5 as an example. After establishing the master curve shown in Figure 3.8 with empty triangles, using the same reference temperature of 77 °C as in Figure 3.5, other temperatures were selected as reference. As a result, five different master curves could be generated as

illustrated in Figure 3.8.

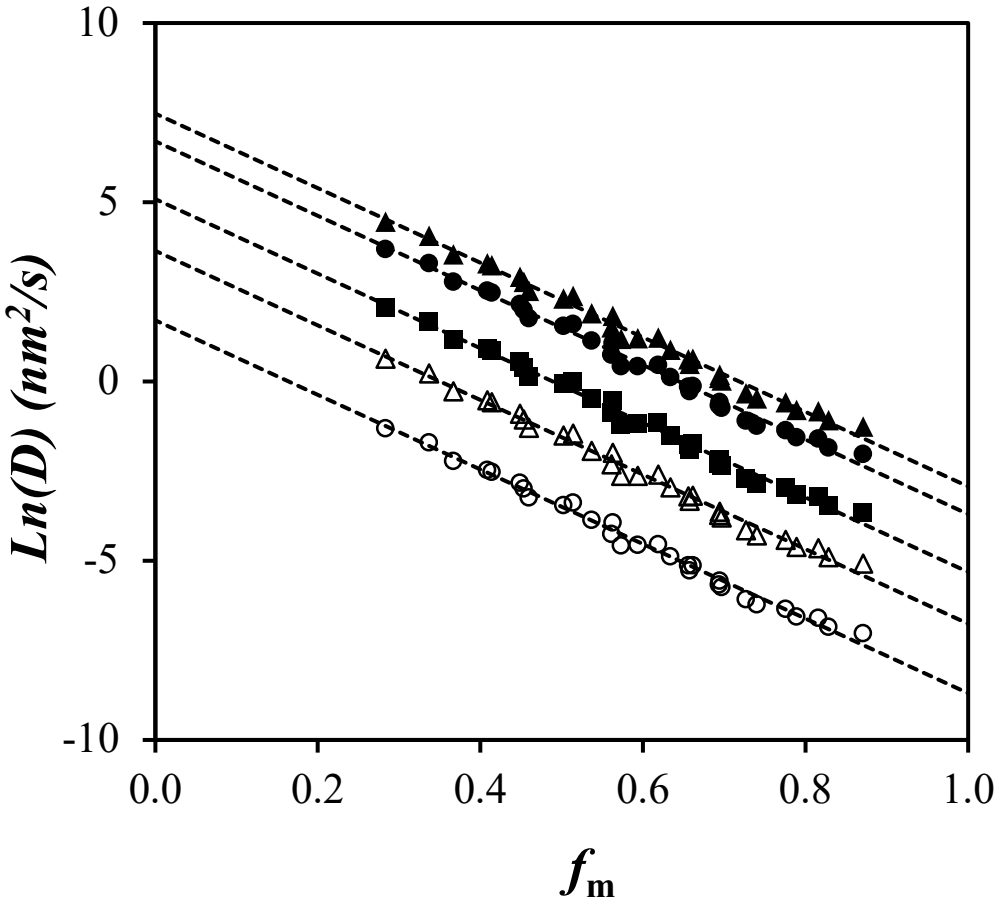

Figure 3.8. Master curves for the diffusion coefficients plotted as a function of f_m for the film 3K-0.19, at reference temperatures of 66 ºC (○), 77 ºC (△), 86 ºC (■), 97 ºC (●), and 103 ºC (▲).

All the master curves (MCs) obtained for a given film annealed at different temperatures shared a same slope of −10.4 ± 0.2 in Figure 3.8, which confirms that the shape of the MCs is independent of the reference temperature. The only difference was their intercept *(p*), which was determined for each MC obtained at different annealing temperature and plotted as a function of T^{-1} in Figure 3.9. A linear relationship was obtained between *p*

and 1/*T*, as predicted in Equation 3.14. With the constant slope and the temperature-dependent intercept given by Equation 3.14, the shift factors a_T could be generated at any temperature as described in Appendix E, so that MCs for the diffusion coefficients could be generated at any temperature.

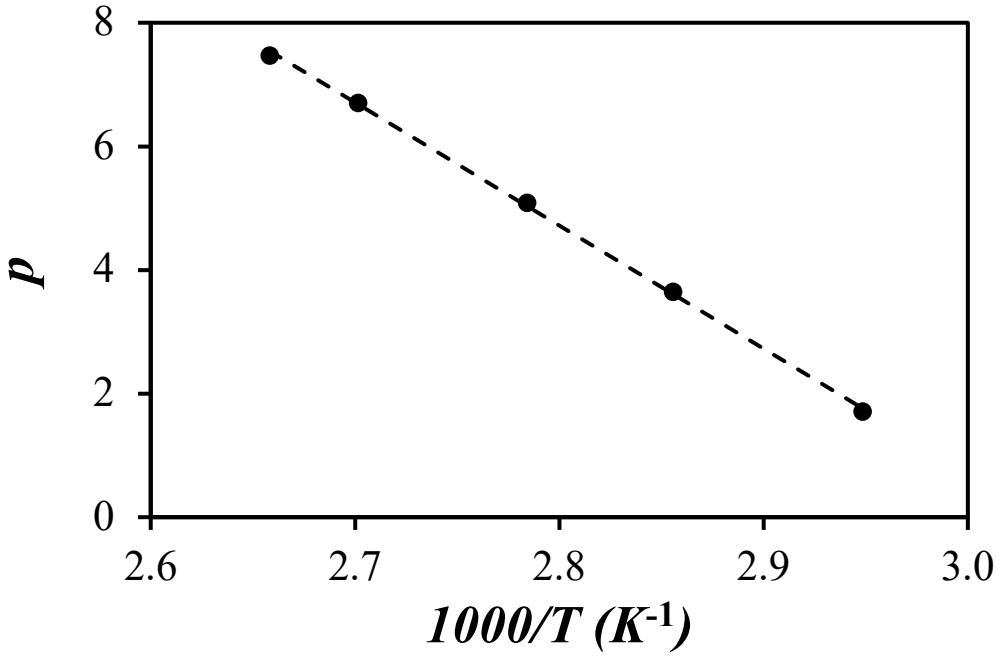

Figure 3.9. Plot of the intercept (*p*) of the master curves in Figure 3.8 as a function of 1000/*T*.

$$p = -19.9\times(1000/T) + 60.5 \quad (3.14)$$

3.7.3 Results and Discussion

According to previous research, the particle size is an important factor that can affect IPCD.[1,27] Although the molecular weight distribution of the Seed-5K latex particles was similar to that of the seed used to prepare the 5.0 K seed-oligomer latex particles, its particle size (127 nm) was smaller than that of the seed latex particles used to prepare the seed-oligomer latex with 5.0 K oligomers (171-184 nm). To ensure that films prepared

with the Seed-5K particles, obtained in much larger quantities for the film annealing experiments, were suitable to use as reference for a MC, a film was prepared from the 5K-0 latex (seed used to prepare the 5.0 K seed-oligomer latex). It was annealed at 90 ºC and the diffusion coefficients obtained during film annealing were plotted in Figure 3.10 with those obtained for the MC of the Seed-5K films normalized to 90 ºC. The perfect overlap between the two sets of data suggested that particle size had a negligible effect in this case, and that the Seed-5K latex could be used as reference.

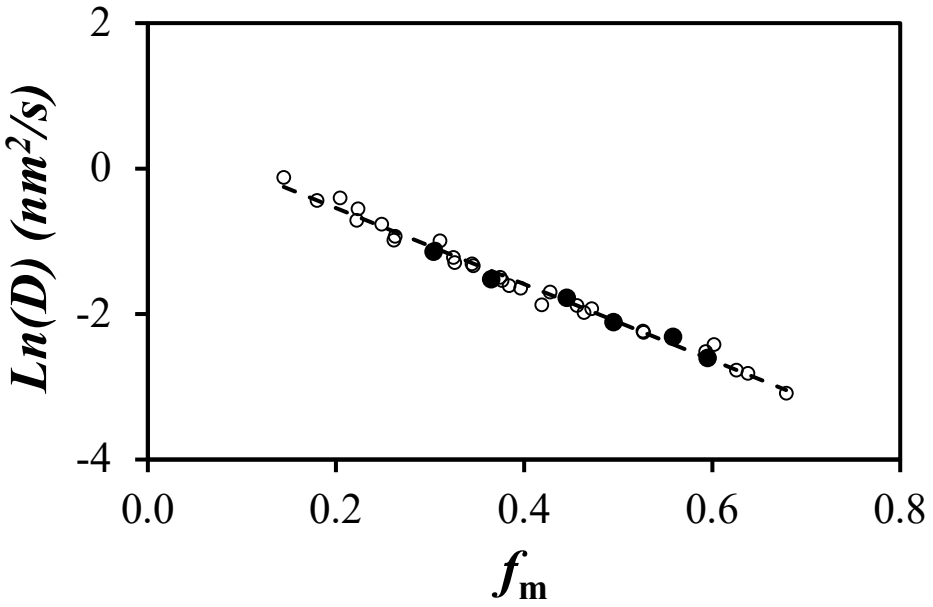

Figure 3.10. Plot of Ln(D) as a function of f_m for 5K-0 film (●) annealed at 90 ºC and the master curve of Seed-5K latex (○) normalized at 90 ºC.

Having demonstrated that the Seed-5K latex could serve as reference for the annealing of films prepared with 5.0 K seed-oligomer latex particles, all the MCs obtained with films having different amounts of a same oligomer were normalized to a same temperature, such as 100 ºC. The MCs built with the films prepared with 3.0 K and 5.0 K oligomers are shown in Figure 3.11A and Figure 3.12A, respectively. The trends shown

in these two plots are similar to those observed in Figure 3.4B. A larger $f_{w,o}$ value results in higher diffusion coefficients for a same fraction of mixing, which reflects stronger IPCD. The MCs presented in Figures 3.11A and 3.12A for a given amount ($f_{w,o}$) of oligomer normalized at the reference temperature, 100 ^{o}C in this case, were shifted with respect to the reference master curve obtained with the seed film using the shift factor a_{oligo}. This led to the creation of new MCs as illustrated in Figures 3.11B and 3.12B for the films prepared with the 3.0 K and 5.0 K oligomers, respectively. The optimization of the shift factors a_{oligo} was based on the same procedure used to obtain the a_T shift factors in Section 3.6, described in Appendix C. A plot of $Ln(a_{oligo})^{-1}$ as a function of φ^{-1} is shown in Figure 3.13. It yielded a straight line, as expected from Equation 3.12 based on the Fujita-Doolittle model.

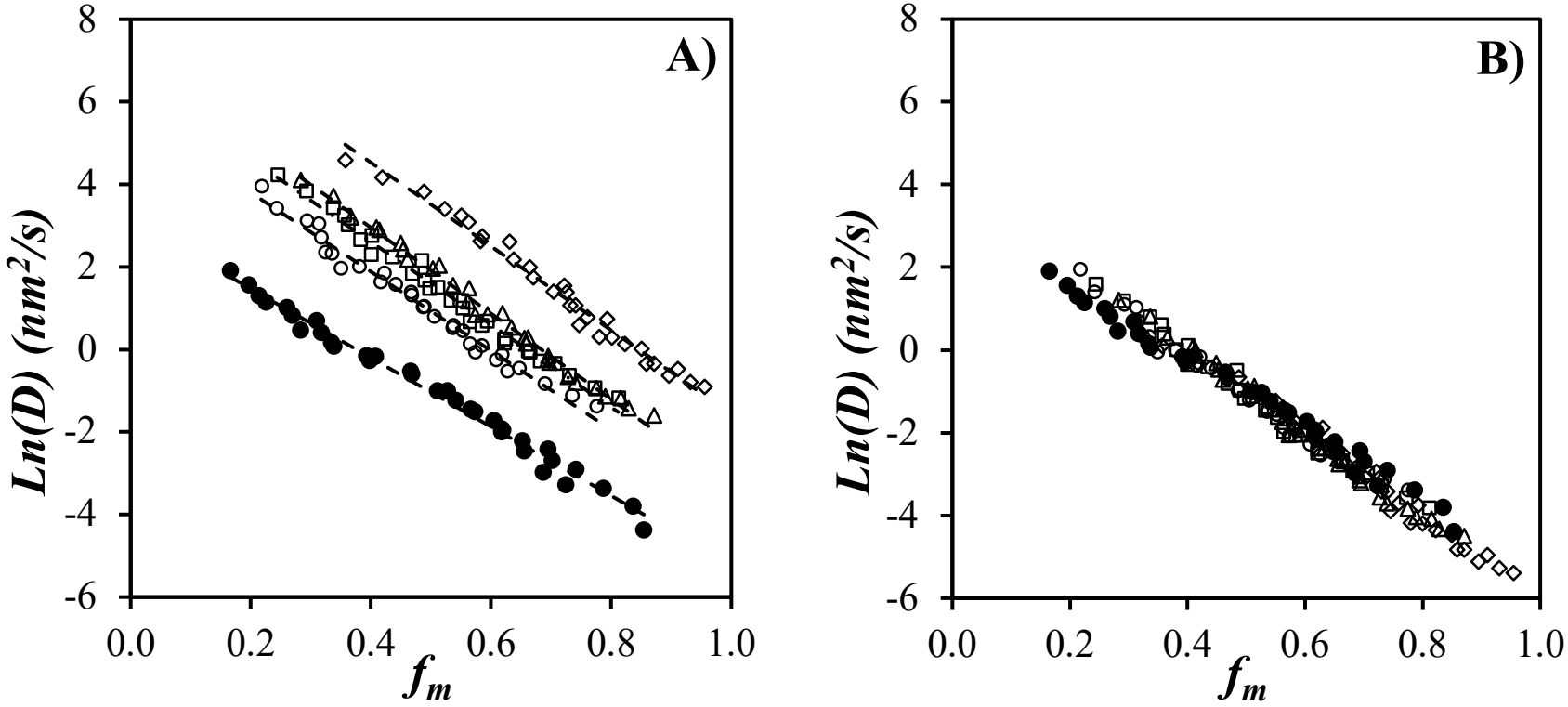

Figure 3.11. Plot of A) the master curves obtained at 100 °C for D as a function of f_m for films prepared with (●) the Seed-3K latex ($f_{w,o}$=0) and the films prepared with the seed-oligomer latex (○) 3K-0.12 ($f_{w,o}$=0.12), (□) 3K-0.17 ($f_{w,o}$=0.17), (△) 3K-0.19 ($f_{w,o}$=0.19), and (◊) 3K-0.27 ($f_{w,o}$=0.27), and B) the master curve obtained at 100 °C using the shift factors a_{oligo} for the 3.0 K oligomer.

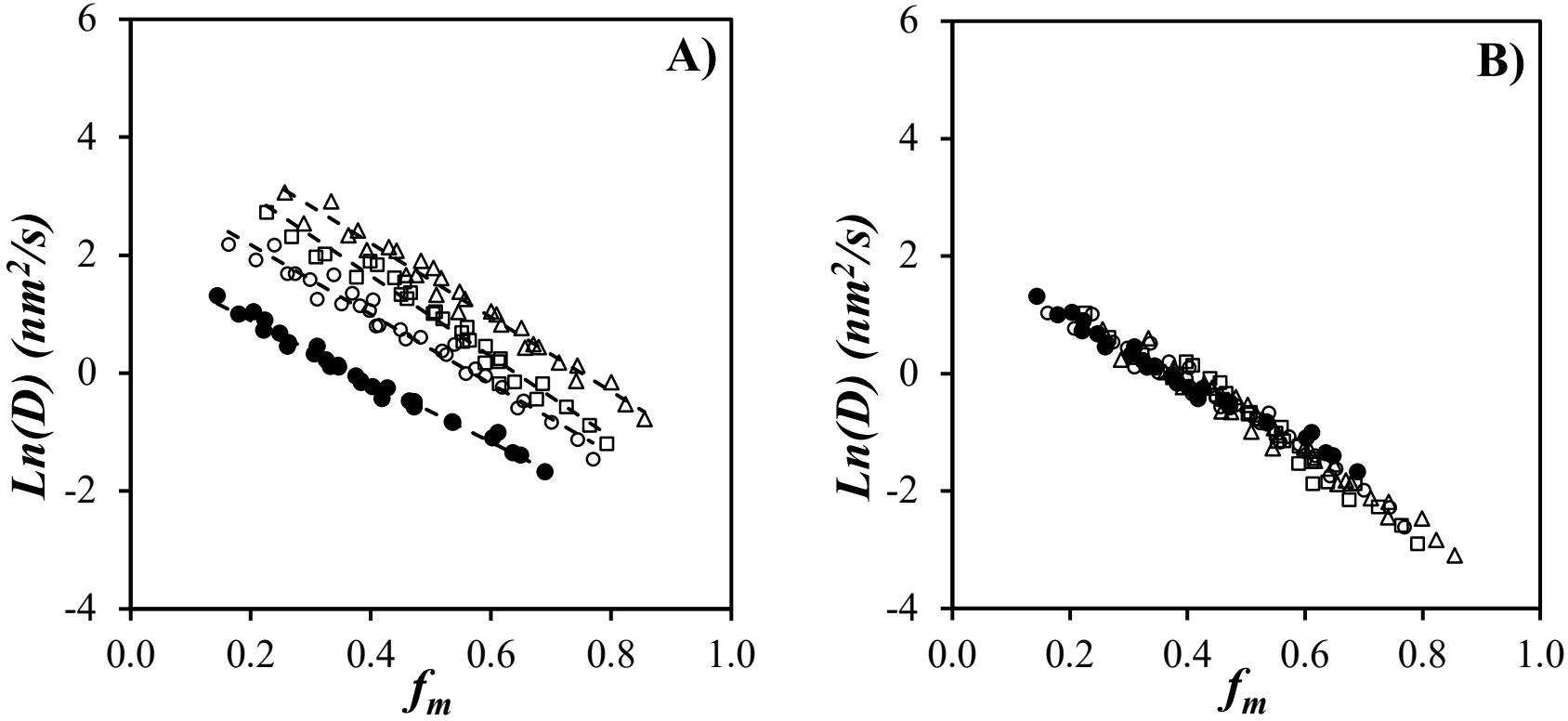

Figure 3.12. Plot of A) the master curves obtained at 100 °C for D as a function of f_m for films prepared with (●) the Seed-5K latex ($f_{w,o}$=0) and the films prepared with the seed-oligomer latex films (○) 5K-0.10 ($f_{w,o}$=0.1), (□) 5K-0.16 ($f_{w,o}$=0.16), and (△) 5K-0.23 ($f_{w,o}$=0.23), and B) the master curve obtained at 100 °C using the shift factors a_{oligo} for the 5.0 K oligomer.

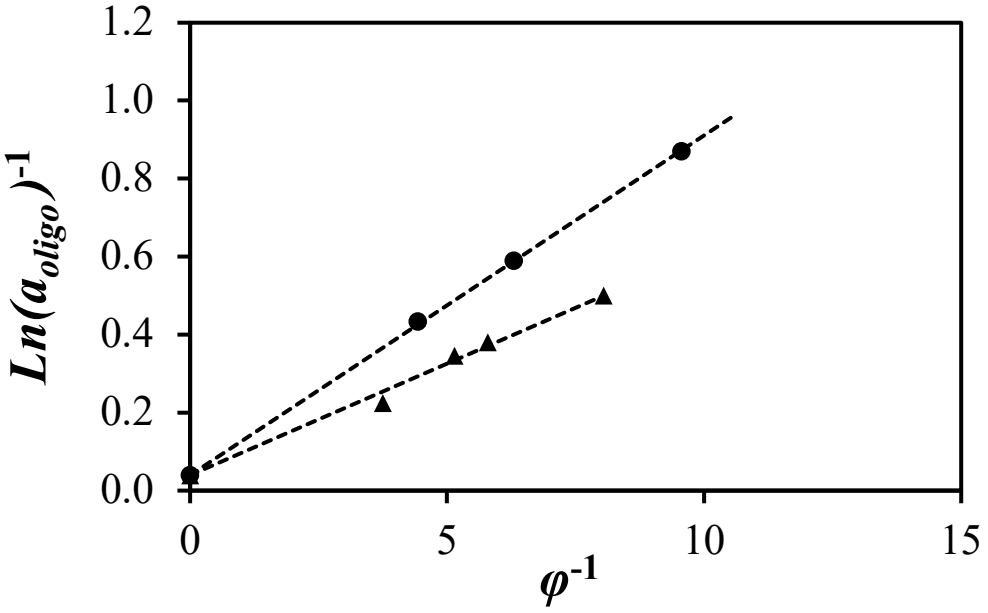

Figure 3.13. Fujita-Doolittle plot of $Ln(a_{oligo})^{-1}$ as a function of φ^{-1} for latex films prepared with the (▲) 3.0 K and (●) 5.0 K oligomers.

Since $f(0,T)$ is the same for both plots in Figure 3.13, the steeper slope obtained for the 5.0 K oligomer reflects a smaller $\beta(T)$ value according to Equation 3.12, indicating that the 5.0 K oligomer was a less efficient plasticizer than the 3.0 K oligomer. This result was reasonable, as the shorter oligomer generates more free volume, which favors polymer diffusion and mixing. This result also agrees with previous research.[10] Based on the trends obtained in Figure 3.13, the β value for the 3.0 K and 5.0 K oligomers at 100 °C was found to equal 0.272 and 0.179 ($\pm$<0.0001), respectively.

To push the analysis further, and taking advantage of the annealing experiments conducted at different temperatures, Fujita-Doolittle plots of $Ln(a_{oligo})^{-1}$-*vs*-φ^{-1} for the films prepared with 3.0 K and 5.0 K oligomers were generated in Figure 3.14 at other reference temperatures such

as 40, 50, 60, 70, 80, and 90 °C. According to these plots, the slopes for the films prepared with the 5.0 K oligomer are always larger than for the films prepared with the 3.0 K oligomer, down to a temperature of 50 °C. This result indicates that the conclusion reached in Figure 3.13 for the data obtained at 100 °C, namely that the β value for the films prepared with the 5.0 K oligomer was lower than that for films prepared with the 3.0 K oligomer, was also valid at temperatures as low as 50 °C.

Interestingly, the difference between the slopes of the straight lines obtained for the 3.0K and 5.0 K oligomers in Figure 3.14 decreased with decreasing temperature until both trends merged in Figure 3.14F. This behavior was also reflected in a plot of β as a function of temperature in Figure 3.15. The 3.0 K oligomer had a larger β value than the 5.0 K oligomer at temperatures greater than or equal to 50 °C. The plasticizer efficiency of both oligomers increased with increasing temperature, increasing more for the 3.0 K oligomer than for the 5.0 K oligomer. The β value of both oligomers seemed to merge at 40 °C, implying that the oligomer size became less important to film formation when the annealing temperature approached the T_g (= 35 °C) of the polymer without oligomers.

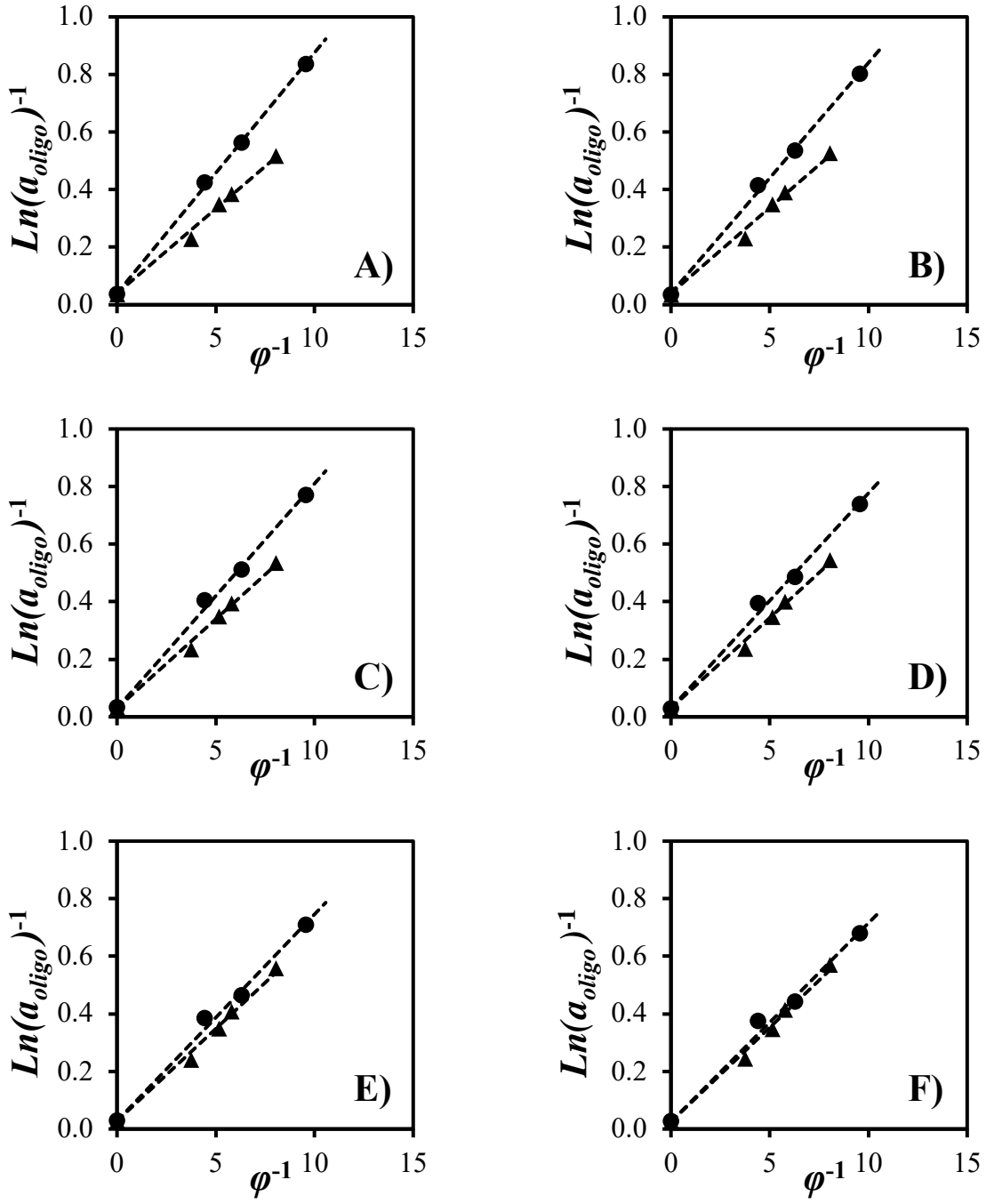

Figure 3.14. Fujita-Doolittle plot of films with the (▲) 3.0 K and (●) 5.0 K oligomers at (A) 90 ºC, (B) 80 ºC, (C) 70 ºC, (D) 60 ºC, (E) 50 ºC, and (F) 40 ºC.

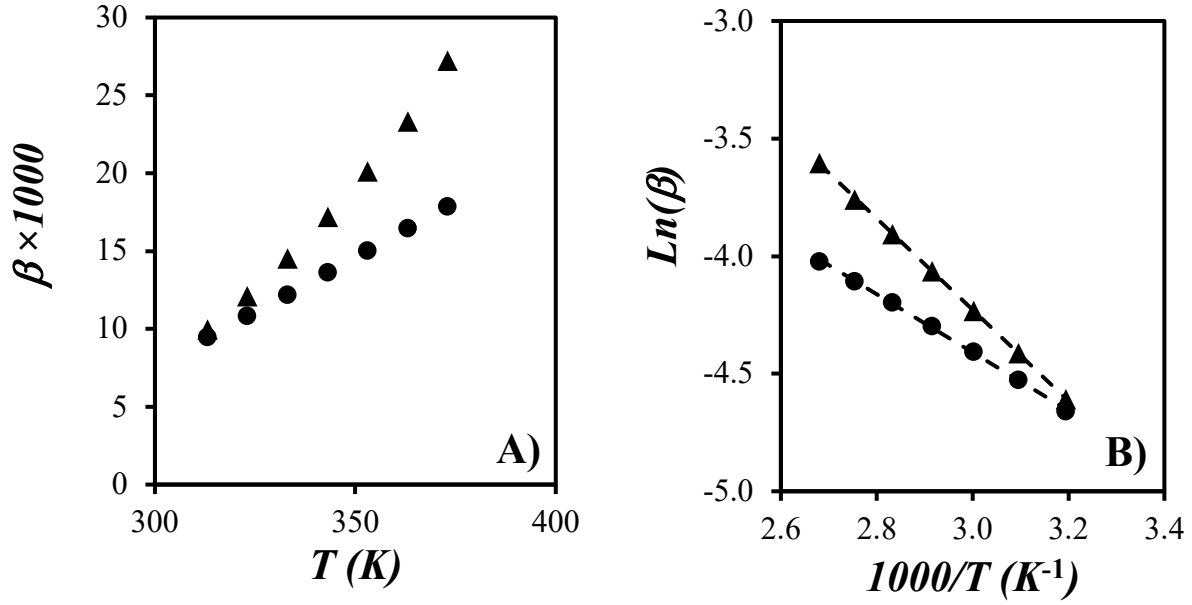

Figure 3.15. Plot of A) plasticizer efficiency (β) as a function of temperature and B) Arrhenius plot representing $Ln(\beta)$ as a function of T^{-1} for films prepared with (▲) 3.0 K and (●) 5.0 K oligomers.

Furthermore, the change in plasticizer efficiency with temperature is well-represented by assuming an Arrhenius behavior, as found in Figure 3.15B, according to Equation 3.15.

$$\beta(T) = \beta_o \exp\left(-\frac{E_a(\beta)}{RT}\right) \tag{3.15}$$

The activation energies obtained from the slopes of the plots shown in Figure 3.15B equal 16 (±<0.1) and 10 (±<0.1) kJ.mol^{-1} for the films prepared with the 3.0 and 5.0 K oligomers, respectively. The larger activation energy found for the films prepared with the 3.0 K oligomers indicate that the plasticizer efficiency of this oligomer was more sensitive to temperature, as

expected from the trends shown in Figure 3.14A. The origin of this difference could be related to the more restricted conformation adopted by the 5.0 K oligomer chains near the boundary of the latex particles compared to the 3.0 K oligomers. The recovery of the conformational space experienced by the 5.0 K chains upon crossing the latex particle boundaries results in the lower activation energy found experimentally for the 5.0 K oligomers.

In addition, Figure 3.16 shows the linear relationship found between T_g and φ for films prepared with different amounts of 3.0 K and 5.0 K oligomers. As the plot illustrates, a steeper slope was obtained for the 3.0 K oligomer, indicating that T_g was affected more strongly than with the 5.0 K oligomer. Therefore, the shorter oligomer decreased T_g more efficiently than the longer oligomer, promoting IPCD in agreement with the conclusions drawn on the plasticizer efficiency determined in Figure 3.15.

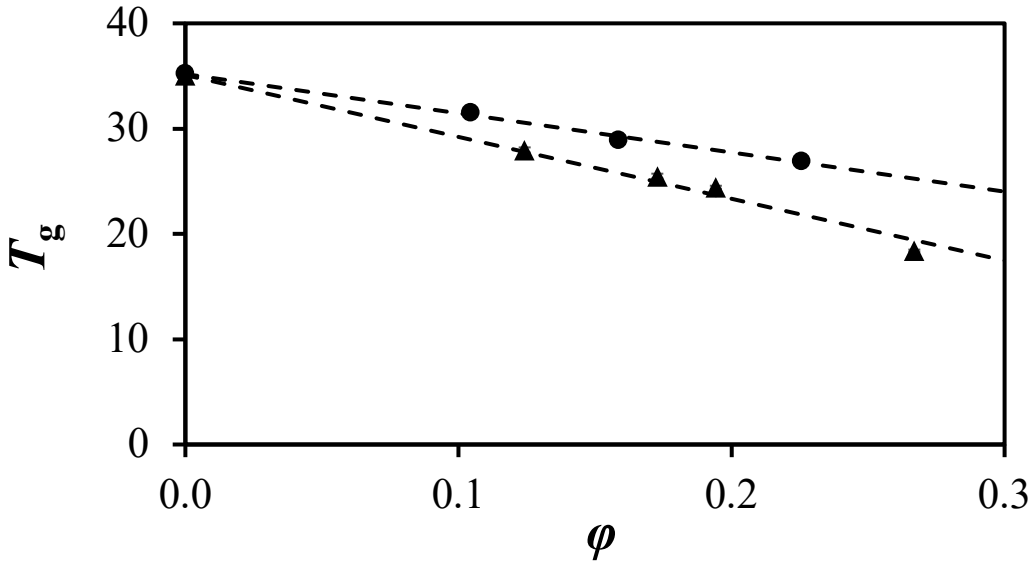

Figure 3.16. Plot of T_g as a function of φ for films prepared with (▲) 3.0 K and (●) 5.0 K oligomers.

3.8 Conclusions

The trends obtained by plotting f_m as a function of t_{an} and D as a function of f_m indicated that diffusion was enhanced when temperature was increased, and when more oligomer was added to the latex particles. Most interestingly, the plasticizer efficiency of the two oligomers was determined as a function of the annealing temperature. The conclusions on the effect of temperature on plasticizer efficiency could be reached thanks to the mathematical protocols established in Appendices A – C. These protocols enabled the transformation of one set of data obtained at a given temperature into another set of data obtained at another temperature, by taking advantage of the predictable temperature-dependent behavior of the shift factors obtained during the generation of MCs with respect to temperature (a_T) or oligomer content (a_{oligo}).

The shift factors a_T obtained during the generation of the MCs built with respect to temperature yielded an activation energy (E_a) for the diffusion of polymers during film formation, that was found to be independent of the oligomer content and length (see Figure 3.7). The plasticizer efficiency shown in Figure 3.15A, obtained for the two oligomers from the Fujita-Doolittle plots, increased with increasing temperature and was larger for the shorter oligomer. By assuming that the β value obeyed an Arrhenius law, a linear relationship between $Ln(\beta)$ and T^{-1} was obtained for the trends obtained with both oligomers. The temperature study conducted on the films prepared with both oligomers showed that the annealing temperature had a much stronger effect on the plasticizer efficiency for the 3.0 K oligomers than for the 5.0 K oligomers.

Chapter 4 – Conclusions and Future Work

In this project, latex particles were prepared by incorporating different weight fractions of oligomers of different lengths. The latex particles were used to study the effects of oligomers on the annealing of latex films, by monitoring pyrene excimer fluorescence (PEF). Nine different PBMA latex particles were successfully synthesized. Two latexes were prepared without oligomers, three with 10, 16, and 23 wt% of 5.0 K oligomer, and four with 12, 17, 19, and 27 wt% of 3.0 K oligomer. A specific molecular weight was achieved for the polymer in the seed and the oligomer in the seed-oligomer latex, by adjusting the amount of the chain transfer agent IOMPA used in the emulsion polymerization. Then the PyLLP, which had been prepared earlier,[6] and nine other latex particles were characterized in terms of their MWD and particle sizes. The parameters retrieved from the characterization of the PyLLP were similar to those established earlier,[6] and the PyLLPs were deemed suitable for use in the experiments conducted in this thesis. The non-fluorescent latex particles were characterized by GPC for molecular weight, DLS for particle size, and DSC for glass transition temperature. Although the non-fluorescent seed and seed-oligomer latex particles showed some differences in terms of molecular weight and particle size distributions, control experiments were conducted that ensured that these differences would not affect the conclusions reached in this thesis.

To determine the effect of oligomers on IPCD, films were prepared by mixing 5 wt% of PyLLP with 95 wt% of non-fluorescent seed and seed-oligomer latex particles. By tracking the I_E/I_M ratio during film annealing, f_m and D could be calculated to generate f_m-vs-t_{an} and D-vs-f_m plots demonstrating that IPCD became more efficient with increasing annealing temperature, larger amounts of oligomers, and the incorporation of shorter oligomers. These conclusions

were reached by building numerous master curves accounting for changes in annealing temperature or oligomer content. The activation energy for the diffusion of the pyrene-labeled PBMA chains (Py-PBMA) was also determined for the seed and seed-oligomer films. The activation energy was similar within experimental error, regardless of the amount and length of oligomers. This result indicates that the annealing temperature affects the diffusion of the Py-PBMA chains in a same manner, independently of the amount or length of oligomer used to prepare the latex films. Then, the plasticizer efficiency of the oligomers was determined by applying the Fujita-Doolittle model. Oligomers with a lower molecular weight were found to promote IPCD, in agreement with expectations and previous research.[10] Finally, the temperature dependence of the plasticizer efficiency was investigated.

While this work has reached some interesting conclusions on the plasticizer efficiency for oligomers used to facilitate latex film formation, it also confirmed the value of a PEF-based procedure to study IPCD. Indeed, while FRET and now PEF have both been used to probe the effects that oligomers have on IPCD during latex film formation, PEF offers several advantages as compared to FRET. PEF obviates many disadvantages inherently linked to FRET, such as the requirements for fluorescently labeling all the latex particles involved in film formation, a proper mathematical model for the analysis of the decays acquired with the FRET donor, and a mathematical procedure that involves Monte Carlo simulations to derive f_m. In contrast, the PEF experiments have a low demand for fluorescently labeled latex (only 5 wt% of the overall latex film, which could be lowered further due to the high sensitivity of fluorescence), short spectrum acquisition times, and simple mathematical derivation to determine f_m.

Another important contribution of this thesis was the introduction of straightforward mathematical procedures enabling the generation of a variety of master curves (MCs) that could

be used to build a library of shift factors as a function of temperature and oligomer content. The mathematical protocols described in Appendices A and B took advantage of the linear relationship found between D and f_m to obtain the shift factors in a manner avoiding any arbitrary interpretation from the operator.

In the future, oligomers with an even lower degree of polymerization could be incorporated into the seed, such as a 7.0 K oligomer. The study of the IPCD in a film with a 7.0 K oligomer as a function of temperature would provide less pronounced effects about the importance of oligomer chain length on IPCD. Second, other industrial plasticizers such as Texanol™, whose β value is known, could be investigated by applying PEF to determine their β value and compare it with previous studies.[22] Third, for the oligomers to serve as non-volatile plasticizers for real latex paints used in daily life, the latex particles prepared with oligomers should avoid the use of IOMPA as chain transfer agent due to its strong smell, especially for shorter oligomers that require larger quantities of chain transfer agent. Therefore, the synthetic procedure can be improved by using a more hydrophobic chain transfer agent, such as 1-dodecanethiol (C_{12}-SH), that is less likely to evaporate upon application of the latex paint and resulting in an odor-free product.[10]

References

1. Ugur, S.; Sunay, M. S. Investigation of Particle Size Effect on Film Formation of Polystyrene Latexes Using Fluorescence Technique. *Colloids Surf. A: Physicochem. Eng. Aspects* **2016**, *510*, 283–292.
2. Juhue, D.; Lang, J. Latex Film Formation in the Presence of Organic Solvents. *Macromolecules* **1994**, *27*, 695–701.
3. Wang, Y.; Winnik, M.A. Polymer Diffusion Across Interfaces in Latex Films. *J. Phys. Chem.* **1993**, *97*, 2507–2515.
4. Zhao, C.; Wang, Y.; Hruska, Z.; Winnik, M. A. Molecular Aspects of Latex Film Formation: An Energy-Transfer Study. *Macromolecules* **1990**, *23*, 4082-4087.
5. Keddie, J. Film Formation of Latex. *Mater. Sci. Eng.* **1997**, *21*, 101–170.
6. Casier, R.; Gauthier, M.; Duhamel, J. Using Pyrene Excimer Fluorescence to Probe Polymer Diffusion in Latex Films. *Macromolecules* **2017**, *50*, 1635-1644.
7. Odrobina, E.; Feng, J.; Winnik, M. A. Effect of Oligomers on the Polymer Diffusion Rate in Poly(Butyl Methacrylate) Latex Films. *J.Polym. Sci. A: Polym. Chem.* **2000**, *38*, 3933–3943.
8. Schroeder, W. F.; Liu, Y.; Tomba, J. P.; Soleimani, M.; Lau, W.; Winnik, M. A. Effect of a Coalescing Aid on the Earliest Stages of Polymer Diffusion in Poly(Butyl Acrylate-Co-Methyl Methacrylate) Latex Films. *Polymer* **2011**, *52*, 3984–3993.
9. Zohrehvand, S.; Nijenhuis, K. T. Film Formation from Monodisperse Acrylic Latices, Part 4: The Role of Coalescing Agents in the Film Formation Process. *Colloid Polym. Sci.* **2005**, *283*, 1305–1312.

10. Soleimani, M.; Khan, S.; Mendenhall, D.; Lau, W; Winnik, M.A. Effect of Molecular Weight Distribution on Polymer Diffusion during Film Formation of Two-Component High-/Low-Molecular Weight Latex Particles. *Polymer* **2012**, *53*, 2652–2663.
11. Soleimani, M.; Haley, J. C.; Lau, W.; Winnik, M. A. Effect of Hydroplasticization on Polymer Diffusion in Poly(Butyl Acrylate-Co-Methyl Methacrylate) and Poly(2-Ethylhexyl Acrylate-Co-Tert-Butyl Methacrylate) Latex Films. *Macromolecules* **2010**, *43*, 975–985.
12. Felorzabihi, N.; Froimowicz, P.; Haley, J. C.; Bardajee, G. R.; Li, B.; Bovero, E.; Frank C. J. M. Van Veggel; Winnik, M. A. Determination of the Förster Distance in Polymer Films by Fluorescence Decay for Donor Dyes with a Nonexponential Decay Profile. *J. Phys. Chem. B* **2009**, *113*, 2262–2272.
13. Felorzabihi, N.; Haley, J. C.; Bardajee, G. R.; Winnik, M. A. Systematic Study of the Fluorescence Decays of Amino-Coumarin Dyes in Polymer Matrices. *J. Polym. Sci. B: Polym. Phys.* **2007**, *45*, 2333–2343.
14. Feng, J.; Winnik, M. A. Effect of Water on Polymer Diffusion in Latex Films. *Macromolecules* **1997**, *30*, 4324–4331.
15. Williams, M. L.; Landel, R. F.; Ferry, J. D. The Temperature Dependence of Relaxation Mechanisms in Amorphous Polymers and Other Glass-Forming Liquids. *J. Am. Chem. Soc.* **1955**, *77*, 3701–3707.
16. Child, W. C.; Ferry, J. D. Dynamic Mechanical Properties of Polyn-Butyl Methacrylate. J. Colloid Sci. **1957**, *12*, 327−341.
17. Ye, X.; Farinha, J. P. S.; Oh, J. K.; Winnik, M. A.; Wu, C. Polymer Diffusion in PBMA Latex Films Using a Polymerizable Benzophenone Derivative as an Energy Transfer Acceptor. *Macromolecules* **2003**, *36*, 8749–8760.
18. Ferry, J. D.; Strella, S. Dielectric Dispersion in Methacrylate Polymers and Its Correlation with Mechanical Properties. *Colloid Sci*. **1958**, *13*, 459–471.

19. Brown, I. M.; Sandreczki, T. C. Motional Correlation Times of Nitroxide Spin Labels and Spin Probes in an Amine-Cured Epoxy Resin: Solvent Dependence. *Macromolecules* **1985**, *18*, 2702–2709.
20. Ferguson, R. D.; von Meerwall, E. Free-Volume Interpretations of Self-Diffusion in Ternary Solutions: N-Paraffin-Hexafluorobenzene-Cis-4-Polybutadiene. *J. Polym. Sci. Polym. Phys. Ed.* **1980**, *18*, 1285–1301.
21. Schroeder, W. F.; Liu, Y.; Pablo Tomba, J.; Soleimani, M.; Lau, W.; Winnik, M. A. Influence of Ethylene Glycol and Propylene Glycol on Polymer Diffusion in Poly(Butyl Acrylate-Co-Methyl Methacrylate) Latex Films. *J. Phys. Chem. B* **2010**, *114*, 3085–3094.
22. Juhup, D.; Wangb, Y.; Winnik, M. A.; Haley, F. Poly(Butyl Methacrylate) Latex Films. **1993**, *349*, 345–349.
23. Kawaguchi, S.; Odrobina, E.; Winnik, M. A. Non-ionic Surfactant Effects on Polymer Diffusion in Poly(Butyl Methacrylate) Latex Films. *Macromol. Rapid Commun.* **1995**, *16*, 861–868.
24. Fujita, H. Diffusion in Polymer-Diluent Systems. *Fortschritte der Hochpolym.* **1961**, *3*, 1–47.
25. Doolittle, A. K. Studies in Newtonian Flow. II. the Dependence of the Viscosity of Liquids on Free-Space. *J. Appl. Phys.* **1951**, *22*, 1471–1475.
26. Ferry, J.D. Viscoelastic properties of polymers. 3rd ed. New York: John Wiley & Sons; **1980**.
27. Pohl, K. Adams, J. Johannsmann, D. Correlation between Particle Deformation Kinetics and Polymer Interdiffusion Kinetics in Drying Latex Films. *Langmuir* **2013**, *29*, 11317−11321.

Appendix A: Determination of $f_{w,o}$ through the Gravimetric Method

The latex 3K-0.17 is taken as an example to illustrate the determination of $f_{w,o}$ by the gravimetric method. During the calculation, the solid contents of the latex before (SC_p) and after (SC_{p+o}) the incorporation of oligomers are defined as the mass of solid over the mass of latex dispersion. The calculation of the solid content requires to measure the masses ($m_{latex,p}$ or $m_{latex,p+o}$) of the latex dispersions before lyophilization and the masses ($m_{solid,p}$ or $m_{solid,p+o}$) of solids after lyophilization.

$$SC_p = \frac{m_{solid,p}}{m_{latex,p}} \tag{A.1}$$

$$SC_{p+o} = \frac{m_{solid,p+o}}{m_{latex,p+o}} \tag{A.2}$$

Then, the pure masses of polymer (m_p) and oligomer (m_o) whose expressions are given in Equations A.3 and A.4 are obtained by subtracting from $m_{solid,p}$ and $m_{solid,p+o}$ the mass of AOT ($m_{AOT}(s)$ or $m_{AOT}(o)$) and APS ($m_{APS}(s)$ or $m_{APS}(o)$) present in the volume withdrawn from the emulsion polymerization mixture to obtain latex particles with a given $f_{w,o}$ value. In Equations A.3 and A.4, *s* and *o* represent the stages where the seed and oligomers are prepared during the emulsion polymerization, respectively.

$$m_p = SC_p \times m_{latex,p+o} - m_{AOT}(s) - m_{APS}(s) \tag{A.3}$$

$$m_o = m_{solid,p+o} - m_{latex,p+o} \times SC_p - m_{AOT}(o) - m_{APS}(o) \tag{A.4}$$

The weight fraction ($f_{w,o}$) is then obtained as shown in Equation A.5.

$$f_{w,o} = \frac{m_o}{m_p + m_o} \tag{A.5}$$

Appendix B: Details about the Films

Table B.1. Details about the Seed-3K film (350 kD).

T=67 °C			
t_{an} (min)	I_E/I_M (a.u.)	f_m	D(nm^{2}s^{-1})
0	0.120	0.00	\
15	0.105	0.17	0.038
30	0.102	0.20	0.027
60	0.100	0.23	0.018
120	0.096	0.27	0.013
257	0.091	0.32	0.008
∞	0.029	1.00	\

T=77 °C			
t_{an} (min)	I_E/I_M (a.u.)	f_m	D(nm^{2}s^{-1})
0	0.117	0.00	\
15	0.098	0.21	0.063
30	0.094	0.26	0.047
60	0.090	0.31	0.034
120	0.088	0.33	0.020
257	0.081	0.41	0.014
∞	0.029	1.00	\

T=86 °C			
t_{an} (min)	I_E/I_M (a.u.)	f_m	D(nm^{2}s^{-1})
0	0.115	0.00	\
7	0.091	0.28	0.240
15	0.086	0.34	0.163
30	0.081	0.40	0.116
60	0.075	0.47	0.083
120	0.070	0.53	0.055
240	0.066	0.57	0.034
464	0.062	0.62	0.021
∞	0.029	1.00	\

T=97 °C			
t_{an} (min)	I_E/I_M (a.u.)	f_m	D(nm^{2}s^{-1})
0	0.114	0.00	\
7	0.081	0.39	0.482
15	0.074	0.47	0.329
30	0.071	0.51	0.204
60	0.066	0.57	0.131
120	0.062	0.62	0.082
240	0.058	0.65	0.048
464	0.056	0.69	0.028
∞	0.029	1.00	\

T=109 °C			
t_{an} (min)	I_E/I_M (a.u.)	f_m	D(nm^{2}s^{-1})
0	0.118	0.00	\
7	0.070	0.54	1.004
15	0.065	0.60	0.617
30	0.060	0.65	0.379
60	0.056	0.70	0.235
120	0.054	0.72	0.131
∞	0.029	1.00	\

T=119 °C			
t_{an} (min)	I_E/I_M (a.u.)	f_m	D(nm^{2}s^{-1})
0	0.113	0.00	\
7	0.061	0.62	1.401
15	0.055	0.69	0.913
30	0.051	0.74	0.564
60	0.047	0.79	0.353
120	0.043	0.84	0.231
240	0.042	0.85	0.129
∞	0.029	1.00	\

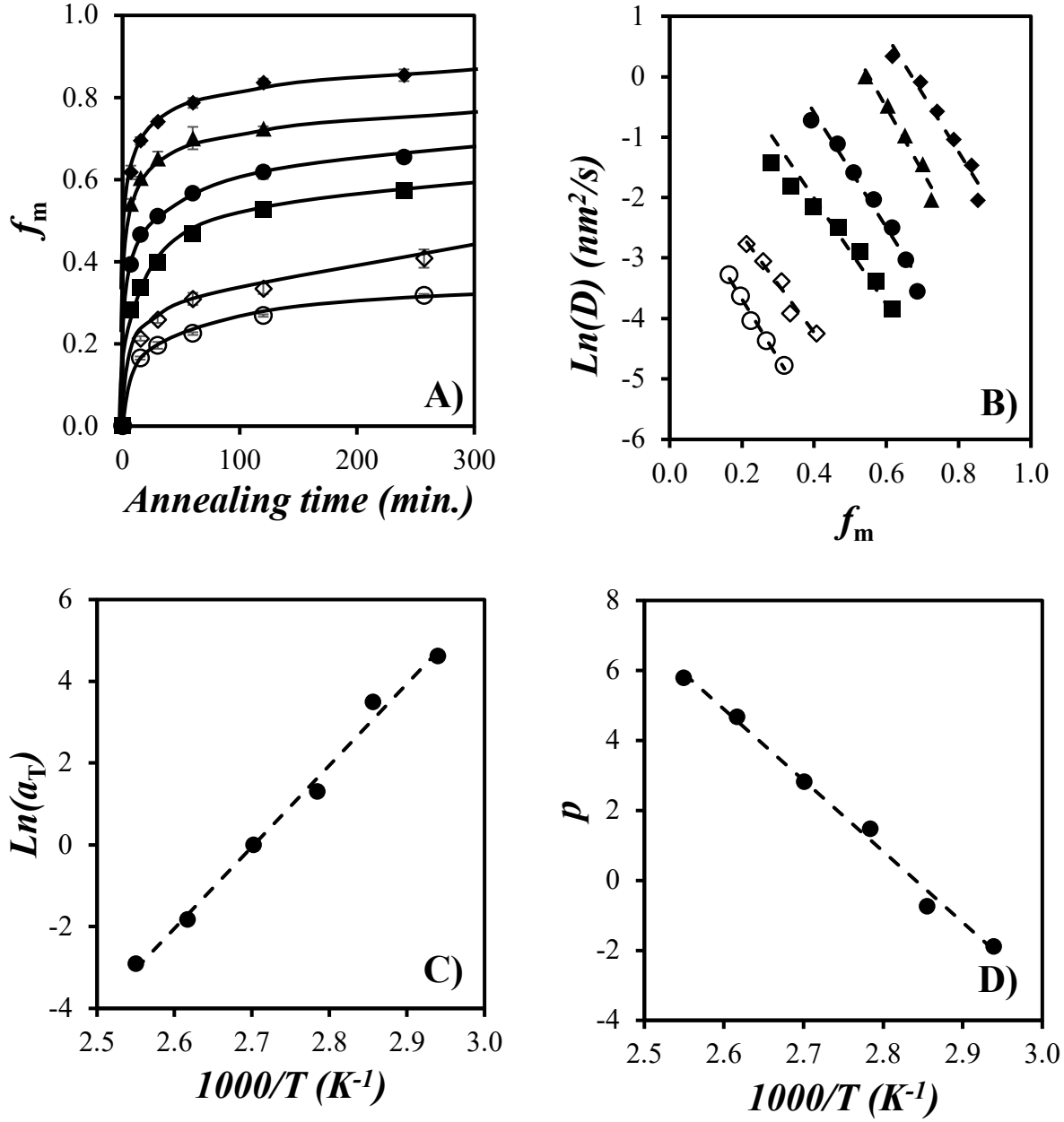

Figure B.1. Plot of (A) f_m as a function of annealing time and (B) D as a function of f_m for films prepared with the seed (350 kD) film annealed at 67 ˚C (○), 77 ˚C (Δ), 86 ˚C (■), 97 ˚C (●), 109 ˚C (▲), and 119 ˚C (♦); (C) Arrhenius plot of ln(a_T) as a function of 1/T; and (D) the intercept p value as a function of 1/T.

Table B.2. Details about the 3K-0.12 film.

T=63 °C			
t_{an} (min)	I_E/I_M (a.u.)	f_m	D(nm^{2}s^{-1})
0	0.104	0.00	\
7	0.064	0.54	1.101
15	0.061	0.57	0.607
30	0.057	0.63	0.383
53	0.053	0.69	0.285
87	0.049	0.73	0.213
137	0.046	0.77	0.164
∞	0.030	1.00	\

T=75 °C			
t_{an} (min)	I_E/I_M (a.u.)	f_m	D(nm^{2}s^{-1})
0	0.104	0.00	\
7	0.081	0.31	0.335
15	0.080	0.32	0.168
30	0.076	0.38	0.118
53	0.073	0.42	0.081
87	0.070	0.47	0.064
137	0.068	0.49	0.045
∞	0.030	1.00	\

T=86 °C			
t_{an} (min)	I_E/I_M (a.u.)	f_m	D(nm^{2}s^{-1})
0	0.103	0.00	\
7	0.072	0.42	0.636
15	0.069	0.47	0.374
30	0.066	0.51	0.224
53	0.063	0.55	0.157
87	0.060	0.58	0.110
137	0.059	0.61	0.077
∞	0.030	1.00	\

T=88 °C			
t_{an} (min)	I_E/I_M (a.u.)	f_m	D(nm^{2}s^{-1})
0	0.108	0.00	\
7	0.074	0.44	0.701
15	0.070	0.49	0.414
30	0.066	0.54	0.258
53	0.064	0.56	0.165
87	0.060	0.62	0.127
137	0.058	0.65	0.091
∞	0.030	1.00	\

T=95 °C			
t_{an} (min)	I_E/I_M (a.u.)	f_m	D(nm^{2}s^{-1})
0	0.104	0.00	\
7	0.064	0.54	1.101
15	0.061	0.57	0.607
30	0.057	0.63	0.383
53	0.053	0.69	0.285
87	0.049	0.73	0.213
137	0.046	0.77	0.164
∞	0.030	1.00	\

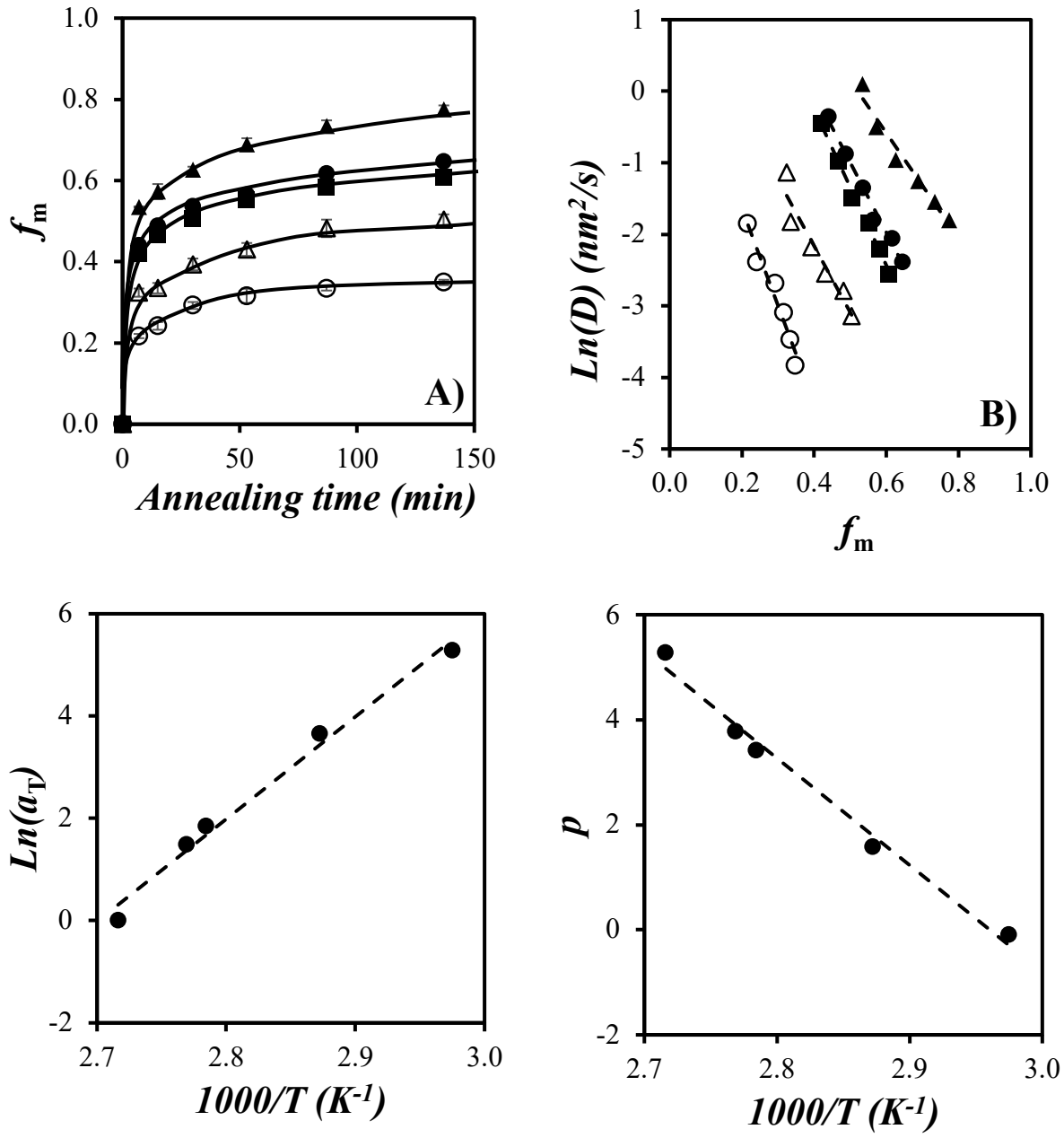

Figure B.2. Plot of (A) f_m as a function of annealing time and (B) D as a function of f_m for films prepared with the 3K-0.12 film annealed at 63 ˚C (○), 75 ˚C (Δ), 86 ˚C (■), 88 ˚C (●), 95 ˚C (▲); (C) Arrhenius plot of ln(a_T) as a function of 1/T; and (D) the intercept p value as a function of 1/T.

Table B.3. Details about the 3K-0.17 film.

T=63 °C			
t_{an} (min)	I_E/I_M (a.u.)	f_m	D(nm^{2}s^{-1})
0	0.105	0.00	\
7	0.087	0.24	0.200
15	0.083	0.29	0.135
30	0.080	0.34	0.091
53	0.078	0.36	0.060
87	0.077	0.38	0.041
137	0.075	0.40	0.029
∞	0.030	1.00	\

T=75 °C			
t_{an} (min)	I_E/I_M (a.u.)	f_m	D(nm^{2}s^{-1})
0	0.104	0.00	\
7	0.078	0.35	0.438
15	0.074	0.40	0.266
30	0.072	0.43	0.158
53	0.069	0.47	0.107
87	0.067	0.50	0.074
137	0.065	0.53	0.055
∞	0.030	1.00	\

T=86 °C			
t_{an} (min)	I_E/I_M (a.u.)	f_m	D(nm^{2}s^{-1})
0	0.104	0.00	\
7	0.068	0.48	0.868
15	0.066	0.51	0.459
30	0.063	0.55	0.277
53	0.061	0.58	0.181
87	0.058	0.62	0.130
137	0.055	0.66	0.097
∞	0.030	1.00	\

T=89 °C			
t_{an} (min)	I_E/I_M (a.u.)	f_m	D(nm^{2}s^{-1})
0	0.113	0.00	\
7	0.073	0.49	0.891
15	0.068	0.55	0.542
30	0.065	0.59	0.331
53	0.062	0.62	0.212
87	0.059	0.66	0.156
137	0.055	0.71	0.119
∞	0.032	1.00	\

T=95 °C			
t_{an} (min)	I_E/I_M (a.u.)	f_m	D(nm^{2}s^{-1})
0	0.102	0.00	\
7	0.062	0.56	1.253
15	0.058	0.62	0.749
30	0.053	0.68	0.486
53	0.050	0.73	0.342
87	0.047	0.77	0.255
137	0.044	0.81	0.199
∞	0.030	1.00	\

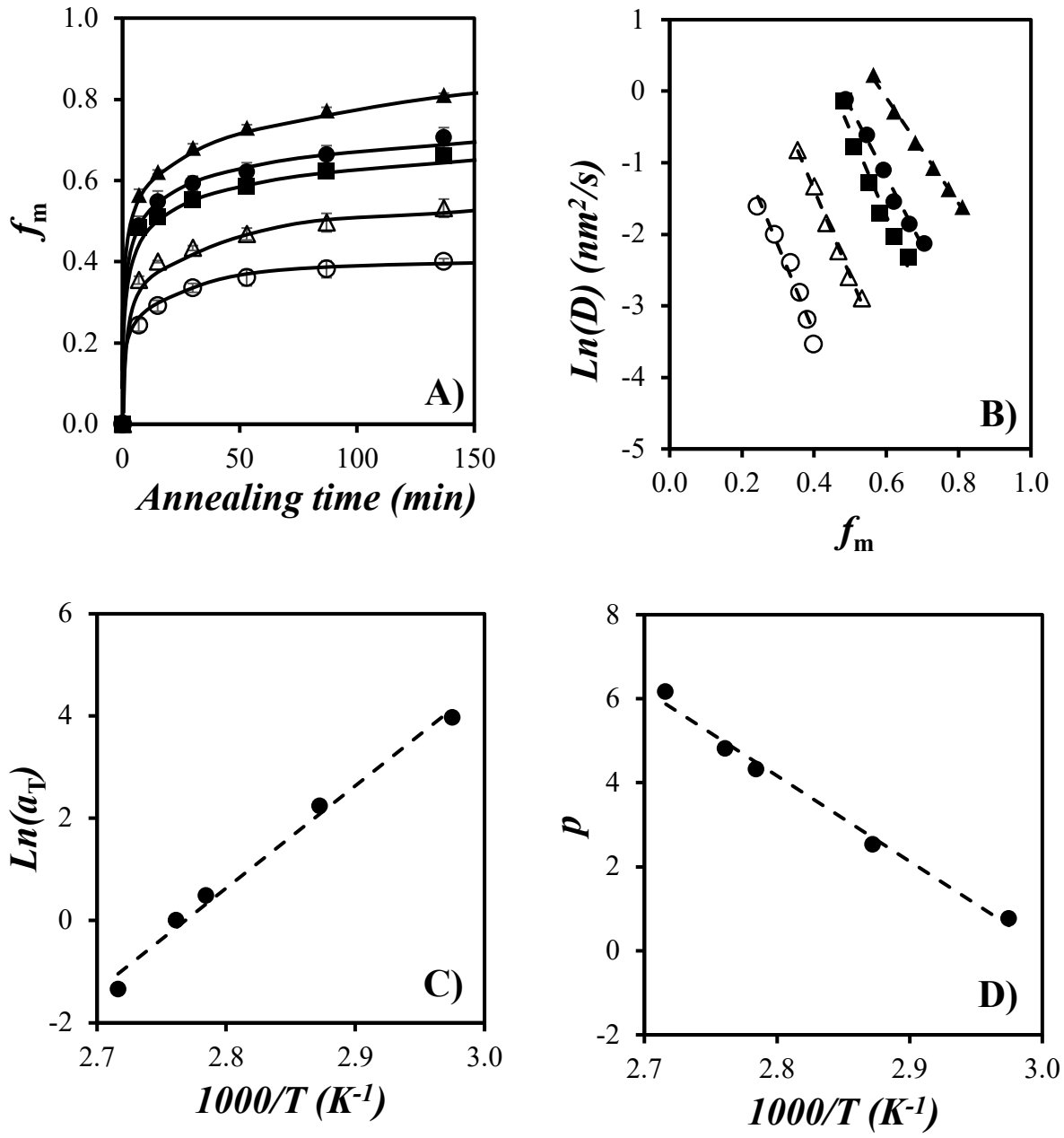

Figure B.3. Plot of (A) f_m as a function of annealing time and (B) D as a function of f_m for films prepared with the 3K-0.17 film annealed at 63 ˚C (○), 75 ˚C (Δ), 86 ˚C (■), 89 ˚C (●), 95 ˚C (▲); (C) Arrhenius plot of ln(a_T) as a function of 1/T; and (D) the intercept p value as a function of 1/T.

Table B.4. Details about the 3K-0.19 film.

T=66 °C			
t_{an} (min)	I_E/I_M (a.u.)	f_m	D(nm^{2}s^{-1})
0	0.104	0.00	\
7	0.084	0.28	0.272
15	0.080	0.34	0.183
30	0.077	0.37	0.110
53	0.074	0.41	0.081
87	0.071	0.45	0.059
137	0.071	0.46	0.040
∞	0.031	1.00	\

T=77 °C			
t_{an} (min)	I_E/I_M (a.u.)	f_m	D(nm^{2}s^{-1})
0	0.103	0.00	\
7	0.073	0.41	0.595
15	0.070	0.45	0.350
30	0.067	0.50	0.221
53	0.064	0.54	0.146
87	0.063	0.56	0.100
137	0.060	0.59	0.073
∞	0.031	1.00	\

T=86 °C			
t_{an} (min)	I_E/I_M (a.u.)	f_m	D(nm^{2}s^{-1})
0	0.102	0.00	\
7	0.066	0.51	1.001
15	0.062	0.56	0.583
30	0.061	0.57	0.304
53	0.057	0.63	0.224
87	0.055	0.66	0.151
137	0.053	0.69	0.113
∞	0.031	1.00	\

T=97 °C			
t_{an} (min)	I_E/I_M (a.u.)	f_m	D(nm^{2}s^{-1})
0	0.102	0.00	\
7	0.058	0.62	1.590
15	0.055	0.66	0.869
30	0.053	0.69	0.513
53	0.050	0.73	0.338
87	0.047	0.78	0.259
137	0.044	0.82	0.203
∞	0.031	1.00	\

T=103 °C			
t_{an} (min)	I_E/I_M (a.u.)	f_m	D(nm^{2}s^{-1})
0	0.101	0.00	\
7	0.046	0.79	3.520
15	0.044	0.82	1.926
30	0.041	0.86	1.203
53	0.039	0.90	0.898
87	0.036	0.93	0.769
137	0.035	0.95	0.683
∞	0.032	1.00	\

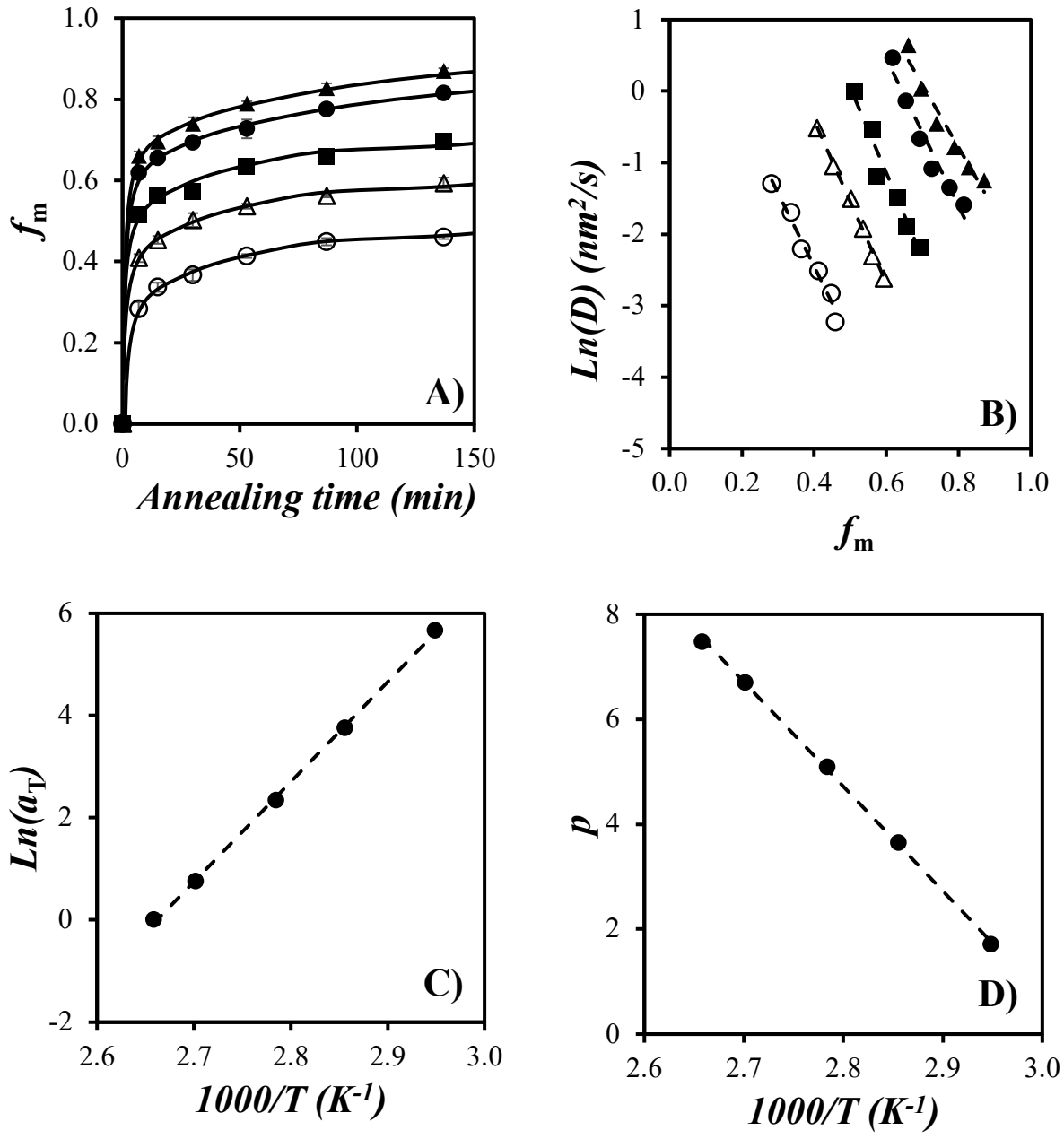

Figure B.4. Plot of (A) f_m as a function of annealing time and (B) D as a function of f_m for films prepared with the 3K-0.19 film annealed at 66 ˚C (○), 77 ˚C (Δ), 86 ˚C (■), 97 ˚C (●), 103 ˚C (▲); (C) Arrhenius plot of ln(a_T) as a function of 1/T; and (D) the intercept p value as a function of 1/T.

Table B.5. Details about the 3K-0.27 film.

T=66 °C			
t_{an} (min)	I_E/I_M (a.u.)	f_m	D(nm^{2}s^{-1})
0	0.100	0.00	\
7	0.075	0.36	0.444
15	0.071	0.42	0.292
30	0.066	0.49	0.207
53	0.064	0.52	0.137
87	0.061	0.56	0.100
137	0.060	0.58	0.070
∞	0.032	1.00	\

T=82 °C			
t_{an} (min)	I_E/I_M (a.u.)	f_m	D(nm^{2}s^{-1})
0	0.102	0.00	\
7	0.063	0.55	1.177
15	0.061	0.58	0.631
30	0.057	0.64	0.401
53	0.055	0.67	0.262
87	0.052	0.70	0.185
137	0.050	0.73	0.133
∞	0.032	1.00	\

T=86 °C			
t_{an} (min)	I_E/I_M (a.u.)	f_m	D(nm^{2}s^{-1})
0	0.102	0.00	\
7	0.057	0.63	1.672
15	0.055	0.66	0.901
30	0.051	0.72	0.581
53	0.050	0.74	0.360
87	0.049	0.75	0.225
137	0.047	0.78	0.168
∞	0.032	1.00	\

T=97 °C			
t_{an} (min)	I_E/I_M (a.u.)	f_m	D(nm^{2}s^{-1})
0	0.101	0.00	\
7	0.051	0.72	2.535
15	0.048	0.76	1.392
30	0.045	0.80	0.855
53	0.042	0.85	0.645
87	0.040	0.87	0.451
137	0.038	0.91	0.396
∞	0.032	1.00	\

T=103 °C			
t_{an} (min)	I_E/I_M (a.u.)	f_m	D(nm^{2}s^{-1})
0	0.101	0.00	\
7	0.046	0.79	3.520
15	0.044	0.82	1.926
30	0.041	0.86	1.203
53	0.039	0.90	0.898
87	0.036	0.93	0.769
137	0.035	0.95	0.683
∞	0.032	1.00	\

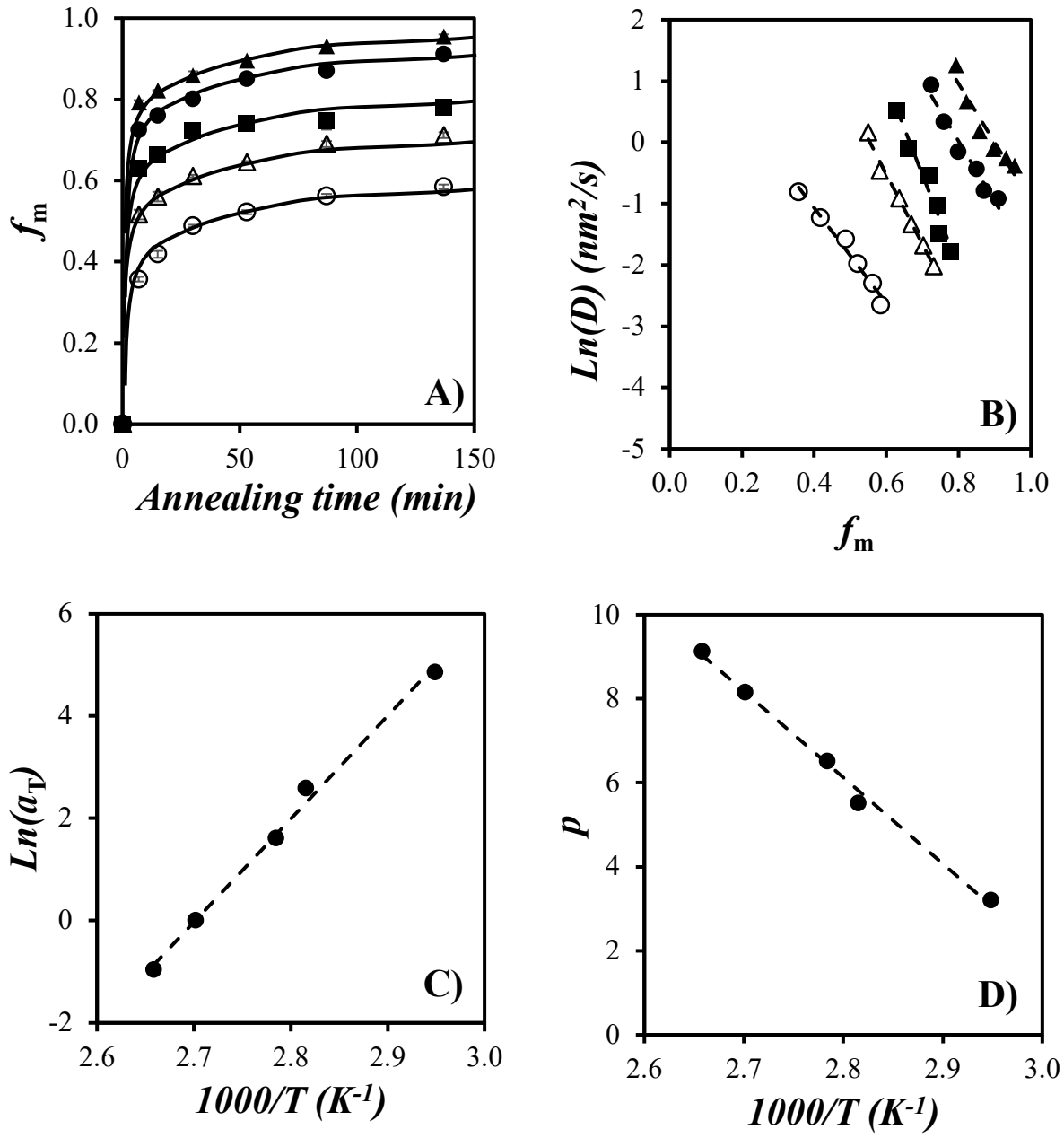

Figure B.5. Plot of (A) f_m as a function of annealing time and (B) D as a function of f_m for films prepared with the 3K-4 film annealed at 66 ˚C (○), 82 ˚C (Δ), 86 ˚C (■), 97 ˚C (●), 103 ˚C (▲); (C) Arrhenius plot of ln(a_T) as a function of 1/T; and (D) the intercept p value as a function of 1/T.

Table B.6. Details about the Seed-5K film (450 kD).

T=75 °C			
t_{an} (min)	I_E/I_M (a.u.)	f_m	D(nm^{2}s^{-1})
0	0.109	0.00	\
7	0.097	0.14	0.069
15	0.094	0.18	0.050
30	0.091	0.22	0.038
53	0.088	0.26	0.031
87	0.084	0.31	0.026
137	0.081	0.34	0.021
∞	0.029	1.00	\

T=79 °C			
t_{an} (min)	I_E/I_M (a.u.)	f_m	D(nm^{2}s^{-1})
0	0.103	0.00	\
7	0.088	0.20	0.139
15	0.084	0.25	0.097
30	0.080	0.31	0.077
53	0.077	0.35	0.055
87	0.074	0.38	0.042
137	0.072	0.42	0.032
∞	0.029	1.00	\

T=81 °C			
t_{an} (min)	I_E/I_M (a.u.)	f_m	D(nm^{2}s^{-1})
0	0.107	0.00	\
7	0.090	0.22	0.167
15	0.087	0.26	0.108
30	0.082	0.32	0.085
53	0.078	0.37	0.065
87	0.074	0.43	0.053
137	0.070	0.47	0.042
∞	0.029	1.00	\

T=92 °C			
t_{an} (min)	I_E/I_M (a.u.)	f_m	D(nm^{2}s^{-1})
0	0.104	0.00	\
7	0.080	0.33	0.367
15	0.074	0.40	0.259
30	0.069	0.46	0.184
53	0.064	0.53	0.140
87	0.059	0.60	0.119
137	0.057	0.63	0.084
∞	0.029	1.00	\

T=96 °C			
t_{an} (min)	I_E/I_M (a.u.)	f_m	D(nm^{2}s^{-1})
0	0.106	0.00	\
7	0.077	0.38	0.497
15	0.070	0.46	0.354
30	0.065	0.53	0.247
53	0.060	0.59	0.188
87	0.056	0.64	0.139
137	0.053	0.68	0.105
∞	0.029	1.00	\

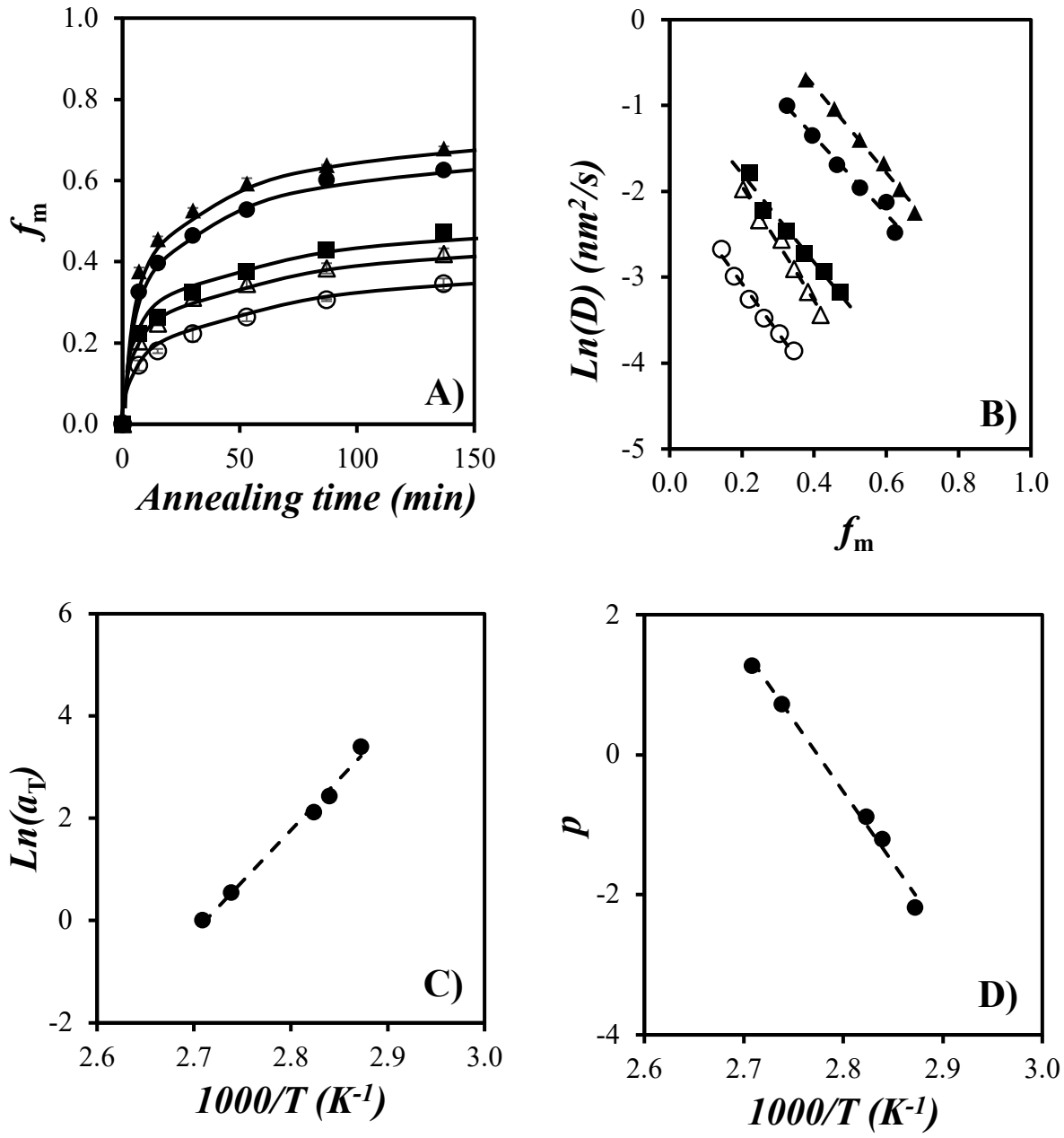

Figure B.6. Plot of (A) f_m as a function of annealing time and (B) D as a function of f_m for films prepared with the seed film (450 kD) annealed at 75 ˚C (○), 79 ˚C (Δ), 81 ˚C (■), 92 ˚C (●), 96 ˚C (▲); (C) Arrhenius plot of ln(a_T) as a function of 1/T; and (D) the intercept p value as a function of 1/T.

Table B.7. Details about the 5K-0.10 film.

T=71 °C			
t_{an} (min)	I_E/I_M (a.u.)	f_m	D(nm^{2}s^{-1})
0	0.113	0.00	\
7	0.100	0.16	0.087
15	0.096	0.21	0.067
30	0.092	0.26	0.053
53	0.085	0.34	0.052
87	0.083	0.37	0.038
137	0.080	0.40	0.029
∞	0.030	1.00	\

T=76 °C			
t_{an} (min)	I_E/I_M (a.u.)	f_m	D(nm^{2}s^{-1})
0	0.104	0.00	\
7	0.087	0.24	0.191
15	0.084	0.27	0.118
30	0.081	0.31	0.077
53	0.075	0.40	0.076
87	0.074	0.41	0.049
137	0.071	0.46	0.039
∞	0.030	1.00	\

T=81 °C			
t_{an} (min)	I_E/I_M (a.u.)	f_m	D(nm^{2}s^{-1})
0	0.117	0.00	\
7	0.092	0.30	0.302
15	0.087	0.35	0.199
30	0.082	0.41	0.138
53	0.076	0.48	0.114
87	0.072	0.52	0.084
137	0.068	0.57	0.066
∞	0.030	1.00	\

T=89 °C			
t_{an} (min)	I_E/I_M (a.u.)	f_m	D(nm^{2}s^{-1})
0	0.114	0.00	\
7	0.082	0.38	0.512
15	0.077	0.45	0.341
30	0.071	0.52	0.237
53	0.067	0.56	0.160
87	0.062	0.62	0.127
137	0.060	0.64	0.090
∞	0.030	1.00	\

T=96 °C			
t_{an} (min)	I_E/I_M (a.u.)	f_m	D(nm^{2}s^{-1})
0	0.113	0.00	\
7	0.069	0.54	1.116
15	0.065	0.59	0.654
30	0.059	0.65	0.430
53	0.055	0.70	0.299
87	0.052	0.74	0.222
137	0.050	0.77	0.160
∞	0.030	1.00	\

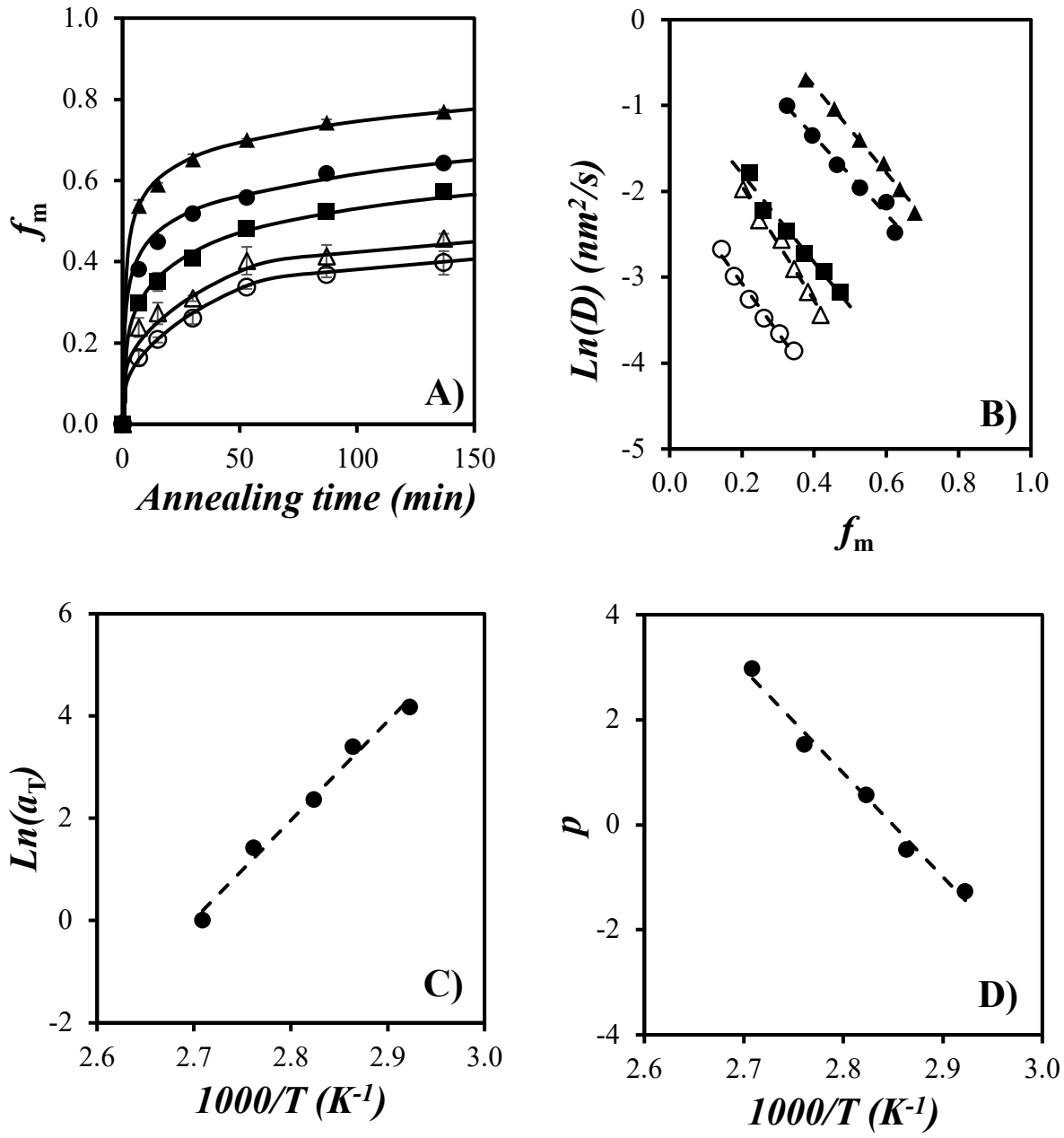

Figure B.7. Plot of (A) f_m as a function of annealing time and (B) D as a function of f_m for films prepared with the 5K-0.10 film annealed at 71 ˚C (○), 76 ˚C (Δ), 81 ˚C (■), 89 ˚C (●), 96 ˚C (▲); (C) Arrhenius plot of ln(a_T) as a function of 1/T; and (D) the intercept p value as a function of 1/T.

Table B.8. Details about the 5K-0.16 film.

T=72 °C			
t_{an} (min)	I_E/I_M (a.u.)	f_m	D(nm^{2}s^{-1})
0	0.117	0.00	\
7	0.097	0.23	0.170
15	0.094	0.27	0.112
30	0.089	0.32	0.084
53	0.083	0.40	0.074
87	0.079	0.44	0.056
137	0.077	0.46	0.039
∞	0.031	1.00	\

T=81 °C			
t_{an} (min)	I_E/I_M (a.u.)	f_m	D(nm^{2}s^{-1})
0	0.114	0.00	\
7	0.088	0.31	0.323
15	0.083	0.37	0.230
30	0.077	0.45	0.171
53	0.072	0.51	0.128
87	0.067	0.56	0.099
137	0.065	0.59	0.072
∞	0.031	1.00	\

T=84 °C			
t_{an} (min)	I_E/I_M (a.u.)	f_m	D(nm^{2}s^{-1})
0	0.110	0.00	\
7	0.078	0.41	0.596
15	0.073	0.47	0.371
30	0.069	0.52	0.238
53	0.065	0.56	0.165
87	0.063	0.59	0.112
137	0.062	0.61	0.079
∞	0.031	1.00	\

T=89 °C			
t_{an} (min)	I_E/I_M (a.u.)	f_m	D(nm^{2}s^{-1})
0	0.120	0.00	\
7	0.080	0.46	0.757
15	0.075	0.50	0.443
30	0.071	0.55	0.277
53	0.065	0.61	0.206
87	0.063	0.64	0.139
137	0.060	0.67	0.103
∞	0.031	1.00	\

T=96 °C			
t_{an} (min)	I_E/I_M (a.u.)	f_m	D(nm^{2}s^{-1})
0	0.113	0.00	\
7	0.068	0.55	1.177
15	0.063	0.61	0.719
30	0.057	0.69	0.495
53	0.054	0.72	0.334
87	0.050	0.76	0.244
137	0.048	0.79	0.179
∞	0.031	1.00	\

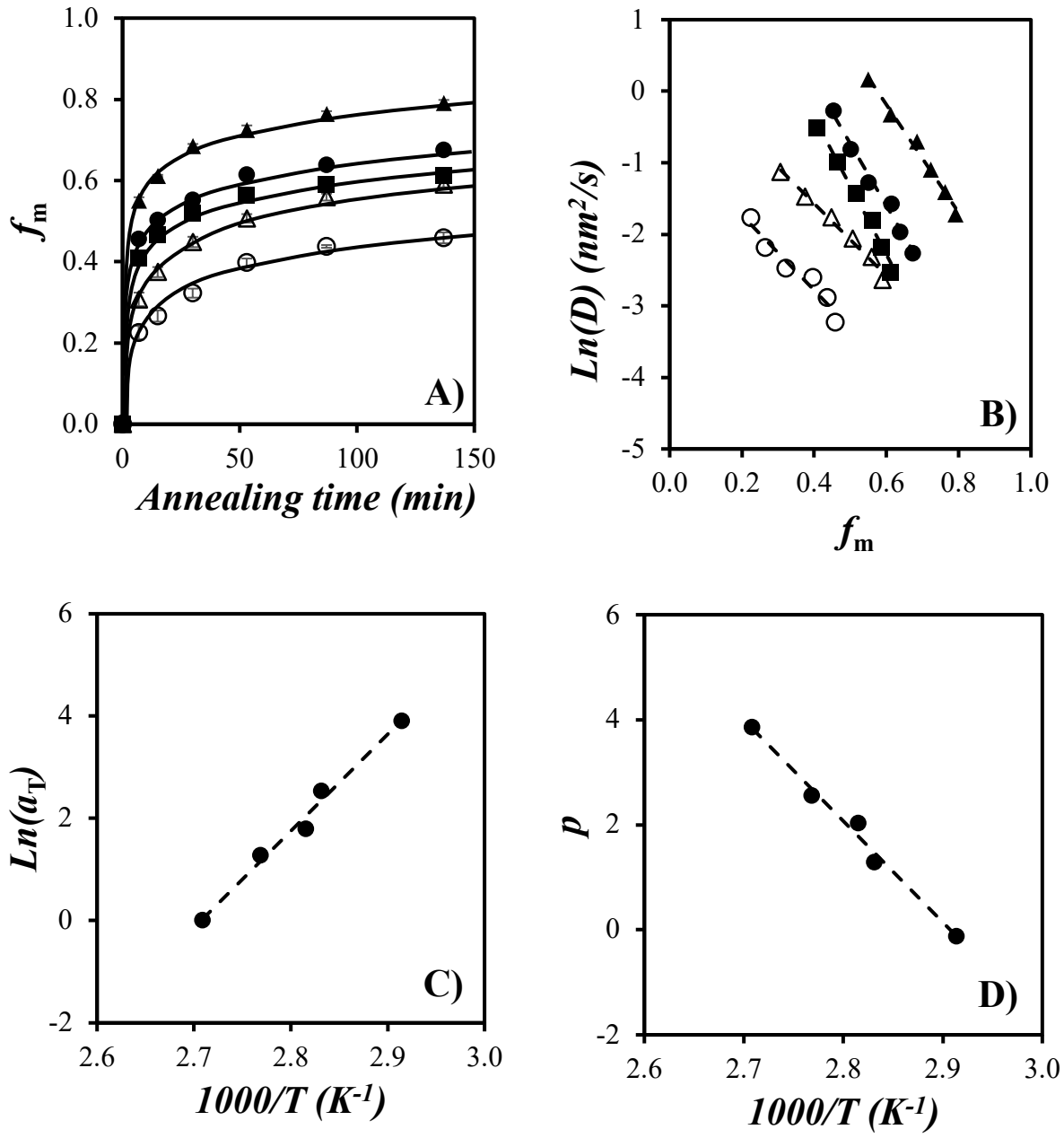

Figure B.8. Plot of (A) f_m as a function of annealing time and (B) D as a function of f_m for films prepared with the 5K-0.16 film annealed at 72 ˚C (○), 81 ˚C (Δ), 84 ˚C (■), 89 ˚C (●), 96 ˚C (▲); (C) Arrhenius plot of ln(a_T) as a function of 1/T; and (D) the intercept p value as a function of 1/T.

Table B.9. Details about the 5K-0.23 film.

T=72 °C			
t_{an} (min)	I_E/I_M (a.u.)	f_m	D(nm^{2}s^{-1})
0	0.111	0.00	\
7	0.091	0.26	0.222
15	0.088	0.29	0.132
30	0.082	0.36	0.107
53	0.077	0.43	0.088
87	0.073	0.48	0.070
137	0.070	0.52	0.052
∞	0.032	1.00	\

T=78 °C			
t_{an} (min)	I_E/I_M (a.u.)	f_m	D(nm^{2}s^{-1})
0	0.108	0.00	\
7	0.083	0.33	0.384
15	0.079	0.38	0.234
30	0.074	0.44	0.166
53	0.072	0.47	0.110
87	0.069	0.51	0.079
137	0.066	0.54	0.059
∞	0.032	1.00	\

T=81 °C			
t_{an} (min)	I_E/I_M (a.u.)	f_m	D(nm^{2}s^{-1})
0	0.113	0.00	\
7	0.081	0.39	0.545
15	0.076	0.46	0.359
30	0.069	0.55	0.271
53	0.064	0.60	0.193
87	0.060	0.65	0.146
137	0.058	0.68	0.105
∞	0.032	1.00	\

T=89 °C			
t_{an} (min)	I_E/I_M (a.u.)	f_m	D(nm^{2}s^{-1})
0	0.112	0.00	\
7	0.072	0.50	0.952
15	0.067	0.56	0.564
30	0.063	0.62	0.368
53	0.058	0.67	0.262
87	0.055	0.71	0.193
137	0.052	0.74	0.140
∞	0.032	1.00	\

T=96 °C			
t_{an} (min)	I_E/I_M (a.u.)	f_m	D(nm^{2}s^{-1})
0	0.112	0.00	\
7	0.063	0.61	1.524
15	0.059	0.66	0.870
30	0.052	0.74	0.643
53	0.048	0.80	0.482
87	0.046	0.82	0.335
137	0.043	0.86	0.258
∞	0.032	1.00	\

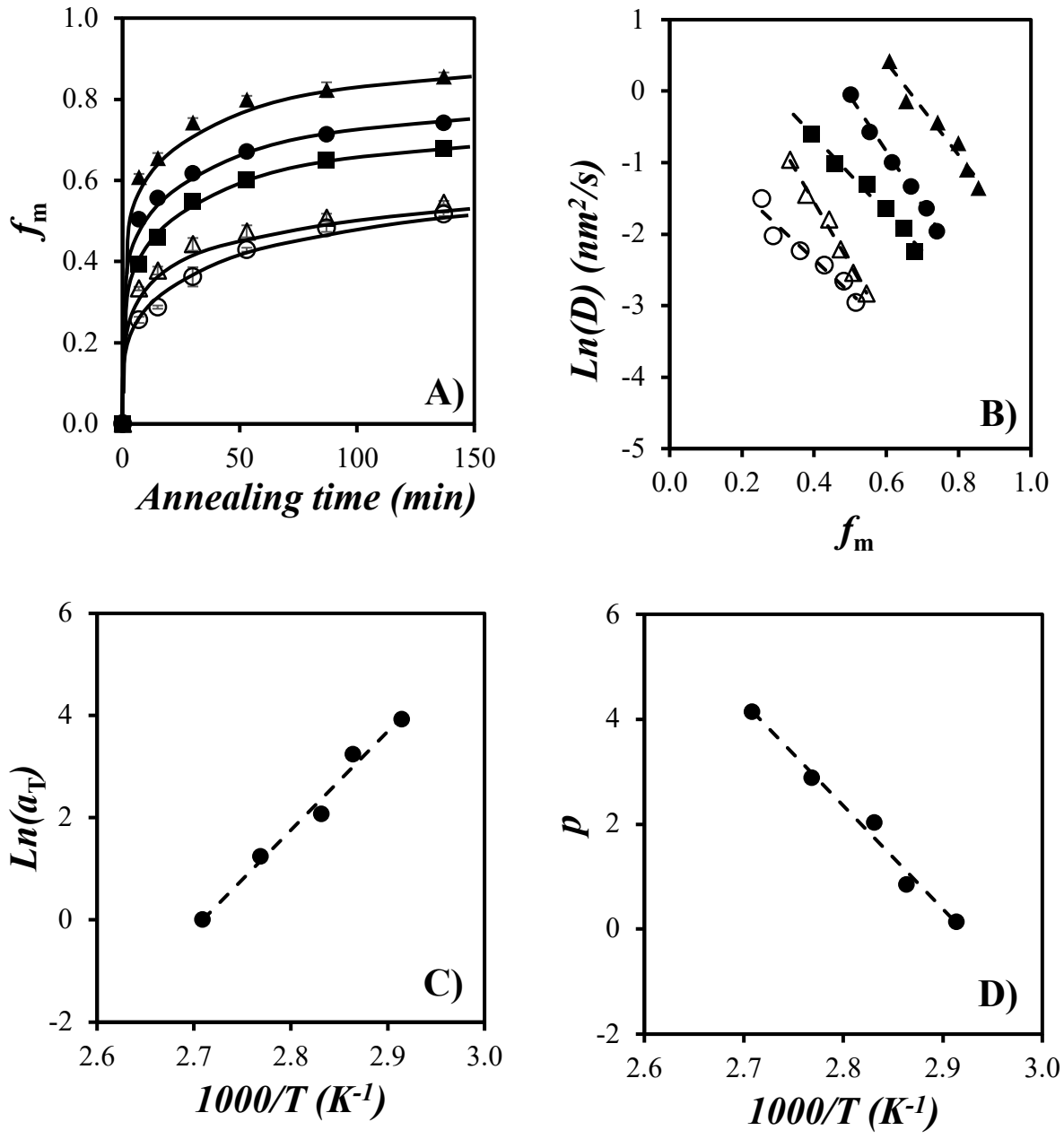

Figure B.9. Plot of (A) f_m as a function of annealing time and (B) D as a function of f_m for films prepared with the 5K-0.23 film annealed at 72 ˚C (○), 78 ˚C (Δ), 81 ˚C (■), 89 ˚C (●), 96 ˚C (▲); (C) Arrhenius plot of ln(a_T) as a function of 1/T; and (D) the intercept p value as a function of 1/T.

Appendix C: Master Curve – Optimization of Shift Factors with Respect to a Reference Data Set

This section considers a set of $0 \le i \le N$ data sets constituted of $1 \le j \le M$ $[x(i,j); y(i,j)]$ data points obtained under different conditions (temperature, oligomer content …) which can be shifted with respect to a reference data set ($i = 0$) by a factor $b(i)$ [$b(i=0) = 0$]. Shifting of the different data sets is expected to result in a linear master curve described by Equation A1.

$$y(i,j) = m \times x(i,j) + p \tag{C1}$$

The set of $b(i)$ shift factors with $0 < i \le N$ that would result in the tightest master curve (MC) should minimize the function (χ^2) given in Equation C2.

$$\chi^2 = \sum_{\substack{0<i\le N \\ 1\le j\le M}} \frac{[y(i,j) + b(i) - m \times x(i,j) - p]^2}{\sigma_{ij}^2} + \sum_{\substack{i=0 \\ 1\le j\le M}} \frac{[y(0,j) - m \times x(0,j) - p]^2}{\sigma_{0j}^2} \tag{C2}$$

There are $N + 2$ parameters to be optimized in Equation C2. They are the slope (m) and intercept (p) of the MC and the shift factors ($b(i)$ with $1 < i \le N$ since $b(0) = 0$ as the reference. Setting the derivative of χ^2 with respect to these $N + 2$ parameters to equal zero generates $N + 2$ equations that can be solved to find the $N + 2$ parameters.

Derivative with respect to the slope:

Setting $\partial\chi^2 / \partial m = 0$ yields Equation A3.

$$\sum_{\substack{0<i\le N \\ 1\le j\le M}} b(i) \frac{x(i,j)}{\sigma_{ij}^2} - m \sum_{\substack{0\le i\le N \\ 1\le j\le M}} \frac{x(i,j)^2}{\sigma_{ij}^2} - p \sum_{\substack{0\le i\le N \\ 1\le j\le M}} \frac{x(i,j)}{\sigma_{ij}^2} = - \sum_{\substack{0\le i\le N \\ 1\le j\le M}} \frac{x(i,j)y(i,j)}{\sigma_{ij}^2} \tag{C3}$$

Derivative with respect to the intercept:

Setting $\partial\chi^2 / \partial p = 0$ yields Equation C4.

$$\sum_{\substack{0<i\le N\\1\le j\le M}} \frac{b(i)}{\sigma_{ij}^2} - m\sum_{\substack{0\le i\le N\\1\le j\le M}} \frac{x(i,j)}{\sigma_{ij}^2} - p\sum_{\substack{0\le i\le N\\1\le j\le M}} \frac{1}{\sigma_{ij}^2} = -\sum_{\substack{0\le i\le N\\1\le j\le M}} \frac{y(i,j)}{\sigma_{ij}^2} \qquad \text{(C4)}$$

Derivative with respect to the shift factor $b(i)$:

Setting $\partial\chi^2/\partial b(i)=0$ for $i > 0$ yields Equation C5 for each i value.

$$b(i)\sum_{1\le j\le M} \frac{1}{\sigma_{ij}^2} - m\sum_{1\le j\le M} \frac{x(i,j)}{\sigma_{ij}^2} - p\sum_{1\le j\le M} \frac{1}{\sigma_{ij}^2} = -\sum_{1\le j\le M} \frac{y(i,j)}{\sigma_{ij}^2} \qquad \text{(C5)}$$

Equations C3 – C5 can be written under a matrix form as shown in Equation C6 where M is a $(N+2)\times(N+2)$ matrix and X and Y are vectors of dimension $N+2$. The expressions of M, X, and Y are given in Table C1.

$$M \times X = Y \qquad \text{(C6)}$$

Inversion of Equation C6 in MS excel yields the shift factors $b(i)$, the slope (m), and intercept (p) as shown in Equation C7.

$$X = M^{-1} \times Y \qquad \text{(C7)}$$

Table C1. Expression of the matrix M and vectors X and Y for $N = 3$.

X	Y	M
$\begin{pmatrix} b(1) \\ b(2) \\ b(3) \\ m \\ p \end{pmatrix}$	$\begin{pmatrix} -\sum\limits_{\substack{0\le i\le N \\ 1\le j\le M}} \dfrac{x(i,j)y(i,j)}{\sigma_{ij}^2} \\ -\sum\limits_{\substack{0\le i\le N \\ 1\le j\le M}} \dfrac{y(i,j)}{\sigma_{ij}^2} \\ -\sum\limits_{\substack{i=1 \\ 1\le j\le M}} \dfrac{y(1,j)}{\sigma_{1j}^2} \\ -\sum\limits_{\substack{i=2 \\ 1\le j\le M}} \dfrac{y(2,j)}{\sigma_{2j}^2} \\ -\sum\limits_{\substack{i=3 \\ 1\le j\le M}} \dfrac{y(3,j)}{\sigma_{3j}^2} \end{pmatrix}$	$\begin{pmatrix} \sum\limits_{\substack{i=1 \\ 1\le j\le M}} \dfrac{x(1,j)}{\sigma_{1j}^2} & \sum\limits_{\substack{i=2 \\ 1\le j\le M}} \dfrac{x(2,j)}{\sigma_{2j}^2} & \sum\limits_{\substack{i=3 \\ 1\le j\le M}} \dfrac{x(3,j)}{\sigma_{3j}^2} & -\sum\limits_{\substack{0\le i\le N \\ 1\le j\le M}} \dfrac{x(i,j)^2}{\sigma_{ij}^2} & -\sum\limits_{\substack{0\le i\le N \\ 1\le j\le M}} \dfrac{x(i,j)}{\sigma_{ij}^2} \\ \sum\limits_{\substack{i=1 \\ 1\le j\le M}} \dfrac{1}{\sigma_{1j}^2} & \sum\limits_{\substack{i=2 \\ 1\le j\le M}} \dfrac{1}{\sigma_{2j}^2} & \sum\limits_{\substack{i=3 \\ 1\le j\le M}} \dfrac{1}{\sigma_{3j}^2} & -\sum\limits_{\substack{0\le i\le N \\ 1\le j\le M}} \dfrac{x(i,j)}{\sigma_{ij}^2} & -\sum\limits_{\substack{0\le i\le N \\ 1\le j\le M}} \dfrac{1}{\sigma_{ij}^2} \\ \sum\limits_{\substack{i=1 \\ 1\le j\le M}} \dfrac{1}{\sigma_{1j}^2} & 0 & 0 & -\sum\limits_{\substack{i=1 \\ 1\le j\le M}} \dfrac{x(1,j)}{\sigma_{1j}^2} & -\sum\limits_{\substack{i=1 \\ 1\le j\le M}} \dfrac{1}{\sigma_{1j}^2} \\ 0 & \sum\limits_{\substack{i=2 \\ 1\le j\le M}} \dfrac{1}{\sigma_{2j}^2} & 0 & -\sum\limits_{\substack{i=2 \\ 1\le j\le M}} \dfrac{x(2,j)}{\sigma_{2j}^2} & -\sum\limits_{\substack{i=2 \\ 1\le j\le M}} \dfrac{1}{\sigma_{2j}^2} \\ 0 & 0 & \sum\limits_{\substack{i=3 \\ 1\le j\le M}} \dfrac{1}{\sigma_{3j}^2} & -\sum\limits_{\substack{i=3 \\ 1\le j\le M}} \dfrac{x(3,j)}{\sigma_{3j}^2} & -\sum\limits_{\substack{i=3 \\ 1\le j\le M}} \dfrac{1}{\sigma_{3j}^2} \end{pmatrix}$

Appendix D: Determination of the WLF Parameters c_1 and c_2 at any Reference Temperature

The WLF equation has been established at a reference temperature (T_{01}) for which $c_1(T_{01})$ and $c_2(T_{01})$ have been determined. We now want to obtain the WLF equation at another reference temperature (T_{02}) for which the WLF parameters $c_1(T_{02})$ and $c_2(T_{02})$ must be determined. We begin the derivation with the WLF equation shown in Equation D1 where $a_T(T_{01})$ represents the shift factor for the temperature T using the reference temperature T_{01}.

$$Ln[a_T(T_{01})] = Ln\left[\frac{\eta(T)}{\eta(T_{01})}\right] = -c_1(T_{01})\frac{T - T_{01}}{C_2(T_{01}) + T - T_{01}} \tag{D1}$$

The relationship between $a_T(T_{01})$ and $a_T(T_{02})$ is given in Equation D2.

$$Ln[a_T(T_{01})] = Ln\left[\frac{\eta(T)}{\eta(T_{02})}\frac{\eta(T_{02})}{\eta(T_1)}\right] = Ln\left[\frac{\eta(T)}{\eta(T_{02})}\right] + Ln\left[\frac{\eta(T_{02})}{\eta(T_{01})}\right] = Ln[a_T(T_{02})] + Ln[a_{T_{02}}(T_{01})] \tag{D2}$$

An expression of $Ln[a_T(T_{02})]$ can be obtained in Equation D3 by re-arranging Equation D2.

$$Ln[a_T(T_{02})] = Ln[a_T(T_{01})] - Ln[a_{T_{02}}(T_{01})] \tag{D3}$$

Using Equation C1, $Ln[a_T(T_{02})]$ in Equation D3 can be rewritten as Equation D4.

$$Ln[a_T(T_{02})] = -c_1(T_{01})\frac{T - T_{01}}{c_2(T_{01}) + T - T_{01}} + c_1(T_{01})\frac{T_{02} - T_{01}}{c_2(T_{01}) + T_{02} - T_{01}} \tag{D4}$$

Putting Equation D4 on a same denominator yields Equation D5.

$$Ln[a_T(T_{02})] = -c_1(T_{01})\frac{(T - T_{01})(C_2(T_{01}) + T_{02} - T_{01}) - (T_{02} - T_{01})(C_2(T_{01}) + T - T_{01})}{(C_2(T_{01}) + T - T_{01})((C_2(T_{01}) + T_{02} - T_{01}))} \tag{D5}$$

Equation D5 can be re-arranged to yield Equation D6.

$$Ln[a_T(T_{02})] = -\frac{c_1(T_{01})c_2(T_{01})}{c_2(T_{01}) + T_{02} - T_{01}} \times \frac{T - T_{02}}{[c_2(T_{01}) + T_{02} - T_{01}] + T - T_{02}} \tag{D6}$$

Using the expression of $c_1(T_{02})$ and $c_2(T_{02})$ in Equations D7 and D8, respectively, yields the WLF

equation given in Equation D9 at a reference temperature T_{02}.

$$c_1(T_{02}) = -\frac{c_1(T_{01})c_2(T_{01})}{c_2(T_{01}) + T_{02} - T_{01}} \tag{D7}$$

$$c_2(T_{02}) = c_2(T_{01}) + T_{02} - T_{01} \tag{D8}$$

$$Ln[a_T(T_{02})] = Ln\left[\frac{\eta(T)}{\eta(T_{02})}\right] = -c_1(T_{02})\frac{T - T_{02}}{C_2(T_{02}) + T - T_{02}} \tag{D9}$$

Appendix E: Master Curve – Optimization of the Shift Factors without a Reference Data Set

This derivation considers the case where a set of $1 \le i \le N$ data sets constituted of $1 \le j \le M$ [$x(i,j)$; $y(i,j)$] data points were obtained under different conditions (temperature, oligomer content …). Each data set can be fitted according to a straight line with a same slope (m) and an intercept ($p(i)$) whose value depends on the data set ($1 \le i \le N$). The dependency of $p(i)$ on i is known so that the intercept p can be predicted for any conditions (temperature, oligomer content …) where no experimental data is available. The different data sets can be shifted with a shift factor $b(i)$ with respect to a reference represented by a straight line of known slope (m) and intercept (p) but for which no data was recorded. Shifting of the different data sets is expected to result in a linear master curve described by Equation E1.

$$y(i,j) = m \times x(i,j) + p \tag{E1}$$

The set of $b(i)$ shift factors with $1 < i \le N$ that would result in the tightest master curve (MC) should minimize the function (χ^2) given in Equation E2.

$$\chi^2 = \sum_{\substack{1<i\le N \\ 0\le j\le M}} \frac{[y(i,j) + b(i) - m \times x(i,j) - p]^2}{\sigma_{ij}^2} \tag{E2}$$

There are $N + 1$ parameters to be optimized in Equation E2. They are the slope (m) of the MC and the shift factors ($b(i)$ with $1 \le i \le N$). Setting the derivative of χ^2 with respect to these $N + 1$ parameters to equal zero generates $N + 1$ equations that can be solved to find the $N + 1$ parameters.

Derivative with respect to the slope:

Setting $\partial\chi^2 / \partial m = 0$ yields Equation E3.

$$-\sum_{\substack{1\le i\le N\\1\le j\le M}} b(i)\frac{x(i,j)}{\sigma_{ij}^2}+m\sum_{\substack{1\le i\le N\\1\le j\le M}}\frac{x(i,j)^2}{\sigma_{ij}^2}+p\sum_{\substack{1\le i\le N\\1\le j\le M}}\frac{x(i,j)}{\sigma_{ij}^2}=\sum_{\substack{1\le i\le N\\1\le j\le M}}\frac{x(i,j)y(i,j)}{\sigma_{ij}^2} \qquad \text{(E3)}$$

Derivative with respect to the shift factor $b(i)$:

Setting $\partial\chi^2/\partial b(i)=0$ for $1 \le i$ yields Equation E4 for each i value.

$$-b(i)\sum_{0\le j\le M}\frac{1}{\sigma_{ij}^2}+m\sum_{0\le j\le M}\frac{x(i,j)}{\sigma_{ij}^2}+p\sum_{0\le j\le M}\frac{1}{\sigma_{ij}^2}=\sum_{0\le j\le M}\frac{y(i,j)}{\sigma_{ij}^2} \qquad \text{(E4)}$$

Equations E3 – E4 can be written under a matrix form as shown in Equation E5 where M is a $(N+1)\times(N+1)$ matrix and X and Y are vectors of dimension $N+1$. The expressions of M, X, and Y are given in Table E1.

$$M \times X = Y \qquad \text{(E5)}$$

Inversion of Equation E5 in MS excel yields the shift factors $b(i)$, the slope, and intercept as shown in Equation E6.

$$X = M^{-1} \times Y \qquad \text{(E6)}$$

Table E1. Expression of the matrix M and vectors X and Y for $N = 3$.

X	Y	M
$\begin{pmatrix} b(1) \\ b(2) \\ b(3) \\ m \end{pmatrix}$	$\begin{pmatrix} \sum\limits_{\substack{1\le i\le N \\ 1\le j\le M}} \frac{x(i,j)y(i,j)}{\sigma_{ij}^2} - p\sum\limits_{\substack{1\le i\le N \\ 1\le j\le M}} \frac{x(i,j)}{\sigma_{ij}^2} \\ \sum\limits_{\substack{i=1 \\ 1\le j\le M}} \frac{y(1,j)}{\sigma_{1j}^2} - p\sum\limits_{\substack{i=1 \\ 1\le j\le M}} \frac{1}{\sigma_{1j}^2} \\ \sum\limits_{\substack{i=2 \\ 1\le j\le M}} \frac{y(2,j)}{\sigma_{2j}^2} - p\sum\limits_{\substack{i=2 \\ 1\le j\le M}} \frac{1}{\sigma_{2j}^2} \\ \sum\limits_{\substack{i=3 \\ 1\le j\le M}} \frac{y(3,j)}{\sigma_{3j}^2} - p\sum\limits_{\substack{i=3 \\ 1\le j\le M}} \frac{1}{\sigma_{3j}^2} \end{pmatrix}$	$\begin{pmatrix} -\sum\limits_{\substack{i=1 \\ 1\le j\le M}} \frac{x(1,j)}{\sigma_{1j}^2} & -\sum\limits_{\substack{i=2 \\ 1\le j\le M}} \frac{x(2,j)}{\sigma_{2j}^2} & -\sum\limits_{\substack{i=3 \\ 1\le j\le M}} \frac{x(3,j)}{\sigma_{3j}^2} & \sum\limits_{\substack{1\le i\le N \\ 1\le j\le M}} \frac{x(i,j)^2}{\sigma_{ij}^2} \\ -\sum\limits_{\substack{i=1 \\ 1\le j\le M}} \frac{1}{\sigma_{1j}^2} & 0 & 0 & \sum\limits_{\substack{i=1 \\ 1\le j\le M}} \frac{x(1,j)}{\sigma_{1j}^2} \\ 0 & -\sum\limits_{\substack{i=2 \\ 1\le j\le M}} \frac{1}{\sigma_{2j}^2} & 0 & \sum\limits_{\substack{i=2 \\ 1\le j\le M}} \frac{x(2,j)}{\sigma_{2j}^2} \\ 0 & 0 & -\sum\limits_{\substack{i=3 \\ 1\le j\le M}} \frac{1}{\sigma_{3j}^2} & \sum\limits_{\substack{i=3 \\ 1\le j\le M}} \frac{x(3,j)}{\sigma_{3j}^2} \end{pmatrix}$